Dissertation

submitted to the
Combined Faculties for the Natural Sciences and for Mathematics
of the Ruperto-Carola University of Heidelberg, Germany
for the degree of
Doctor of Natural Sciences

presented by
Devina Mitra, M. Sc. (Biotechnology)
born in: Kolkata, India

Oral-examination: 19.02.2018

Investigating the role of alanine aminotransferase 2 in breast cancer

Referees: Prof. Dr. Stefan Wiemann

Prof. Dr. Rüdiger Hell

Declaration of Authorship

I hereby declare that the work presented in my thesis was carried out between June 2013 and November 2017 under the supervision of Prof. Dr. Stefan Wiemann in the group of Molecular Genome Analysis at the German Cancer Research Center (DKFZ, Heidelberg, Germany). If not stated otherwise and referenced within the text, the data described has been performed by myself and has not yet been presented as part of a university examination.

Heidelberg, _____

Devina Mitra.

Table of Contents

List of Figures

List of Tables

Summary

Uncontrolled proliferation is one of the characteristic hallmarks of cancer and underlines the aberrant nutrient cycling seen in tumors. Cancer cells, therefore, need to rewire their metabolic pathways to meet the biosynthetic and bioenergetics demands of rapid growth. Metabolic reprogramming is thus, crucial for oncogenesis. The 'Warburg effect' is the most commonly reported metabolic characteristic in tumors, where cancer cells consume high amounts of glucose which then get shunted mostly into lactate production. Glutamine addiction is commonly observed in several cancers making it the second most important carbon source which fuels the citric acid (TCA) cycle to provide both energy and biosynthetic precursors.

Breast cancer is a heterogeneous disease and despite successes in targeted therapy of certain subtypes, treatment still remains a clinical challenge. Investigating metabolic changes in breast cancer, therefore, provides an opportunity to overcome these therapeutic challenges. The aim of this project was to understand the mechanisms by which tumors efficiently utilize their carbon and nitrogen sources and to identify potential targets for future therapeutic interventions. To this end, I identified alanine aminotransferase 2(also known as glutamate pyruvate transaminase 2 or GPT2) as a highly deregulated enzyme in breast cancer patients who have a poor prognosis. GPT2 catalyzes the reversible reaction that generates alanine from glutamate and pyruvate which, in turn, are produced by glutaminolysis and glycolysis, respectively. I found RNAi and chemical inhibition of GPT2 to suppress proliferation of several breast cancer cell lines. MDA MB 468 cells, which produce the highest levels of GPT2 and alanine, show a decrease in the supply of TCA cycle intermediates as well as a reduction in glutamine uptake when alanine production is blocked. Furthermore, GPT2 inhibition rewires glucose carbon cycling in the cell lines resulting in increased glucose carbon flow into the TCA cycle. I found the expression of GPT2 in these cancer cells to be regulated by the transcription factors, c-Myc and ATF4. In conclusion, my results demonstrate the role of GPT2 in connecting glucose and glutamine anaplerosis, thereby driving carbon atoms into key biosynthetic pathways of cancer cells. This study underlines the importance of investigating the balance of nutrient cycling in cancer to identify potential targets for therapeutic intervention.

Zusammenfassung

Als Ursache von unkontrollierter Proliferation, die zu den Hauptmerkmalen von Krebs gehört, liegt häufig ein abnormaler Nährstoffzyklus der Tumorzellen zugrunde. Daher müssen Krebszellen ihre Stoffwechselsignalwege umprogrammieren um biosynthetische und bioenergetische Prozesse, die für ein schnelles Tumorwachstum benötigt werden, entsprechend anzupassen. Der „Warburg Effekt“ beschreibt metabolische Eigenschaften von Tumorzellen, welche ein hohes Maß an Glukose verbrauchen, das hauptsächlich in Laktat umgewandelt wird. Glutaminabhängigkeit wird bei vielen Krebsarten beobachtet und bildet die zweitwichtigste Kohlenstoffquelle, welche in den Citratzyklus einfließt um Energie und biosynthetische Vorläufermoleküle bereit zu stellen. Brustkrebs ist eine heterogene Krankheit und die Therapie verbleibt, unabhängig von therapeutischen Erfolgen in einzelnen Subtypen, herausfordernd. Ein Ansatz diese therapeutischen Maßnahmen gegen Brustkrebs zu verbessern liegt in der Erforschung metabolischer Veränderungen. Ein Ziel dieses Projektes war es die Mechanismen zu verstehen, mit welchen Tumore effizient Kohlenstoff- sowie Stickstoffquellen nutzen, um so potentielle Ziele für zukünftige therapeutische Interventionen zu entdecken. In Bezug auf diese Fragestellung identifizierte ich die Alanin Aminotransferase 2 (auch bekannt als Glutamat Pyruvat Transaminase 2 oder GPT2) als stark dereguliertes Enzym in Brustkrebspatienten mit schlechter Überlebenswahrscheinlichkeit. GPT2 katalysiert die reversible Reaktion, die Alanin aus Glutamat und Pyruvat produziert, welche entsprechend über Glutaminolyse und Glycolyse gewonnen werden. Mit RNAi und chemischer Inhibition von GPT2 konnte ich die Zellproliferation von diversen Brustkrebszelllinien unterdrücken. MDA MB 468 Zellen, die am meisten GPT2 und Alanin produzieren, zeigen, dass wenn die Alanin Produktion geblockt wird, eine Reduktion der Citratzyklus Zwischenprodukte sowie eine verminderte Glutaminaufnahme, stattfindet. Weiterhin führt GPT2 Inhibition zu einer Neustrukturierung des Glukose-Kohlenstoff-Zyklus in den Zelllinien und resultiert so in einem erhöhten Glukoseflux in den Citratzyklus. Die Expression von GPT2 in den verwendeten Brustkrebszellen konnte auf Regulation durch die Transkriptionsfaktoren c-Myc und ATF4 zurückgeführt werden.

Zusammengefasst zeigen meine Ergebnisse, dass GPT2 Glukose- und Glutaminanaplerose verbindet und so zu einer Bereitstellung von Kohlenstoffatomen für spezielle biosynthetische Signalwege der Krebszellen führt. Diese Studie betont die Wichtigkeit der Forschung an dem Gleichgewicht des Nährstoffzyklus von Brustkrebszellen, um so potentielle Ziele für therapeutische Interventionen zu entdecken.

1. Introduction

1.1 Cancer and its hallmarks

Cancer is a major public health concern worldwide which resulted in 8.8 million deaths in 2015. The American Cancer Society has predicted that, in 2017, there will be almost 1.7 million new cancer cases diagnosed and over 600,000 cancer related deaths in the United States alone (Siegel, Miller, & Jemal, 2017a) Cancer is a complex group of diseases, characterized by uncontrolled proliferation, which arises as a result of dynamic genomic changes. The discovery of mutations that lead to the dominant gain of function of oncogenes and recessive loss of function of tumor suppressor genes and the concomitant effect that these have on cell growth form the basis of our knowledge of tumorigenesis. Tumors commonly have a high number of mutations, including point mutations, copy number variations and changes in chromosome complement(Alexandrov et al., 2013). Relapses and metastases show further mutational dynamics(Yates et al., 2017).

Decades of research in cancer has led to the understanding that the conversion of a normal cell to its neoplastic counterpart is a multistep process. Each of these steps reflects genetic adaptations that lead to the final malignant form via several pre-malignant states. Parallels can be drawn between Darwinian evolution and tumorigenesis where each subsequent change results in conferring a growth advantage to the cells, finally leading to the formation of a tumor (FOULDS, 1954; Nowell, 1976).

In 2000, Weinberg and Hanahan proposed the hallmarks of cancer which are essentially characteristics gained by cancer cells during the process of tumorigenesis, enabling them to proliferate and metastasize efficiently. These include self-sufficiency in growth signals, insensitivity to growth inhibitory signals, evasion of programmed cell death (apoptosis), sustained angiogenesis and tissue invasion and metastasis. The hallmarks are enabled by genomic instability and mutations acquired by the cancer cells along with tumor promoting inflammation (Hanahan & Weinberg, 2000). In 2011, the same authors updated the list of hallmarks as a result of progress made in research to include inflammation and genome instability The other new hallmark is reprogramming of energy metabolism (Hanahan &

Weinberg, 2011). The unrestricted rates of proliferation seen in cancer cells make it necessary for them to rewire their metabolic pathways to optimize nutrient utilization and energy production to support cell growth. This field has garnered a lot of attention in the past decade which has resulted in several clinical trials. The hope is that by targeting metabolism of cancer cells one can target the core of the ability of tumors to rapidly proliferate.

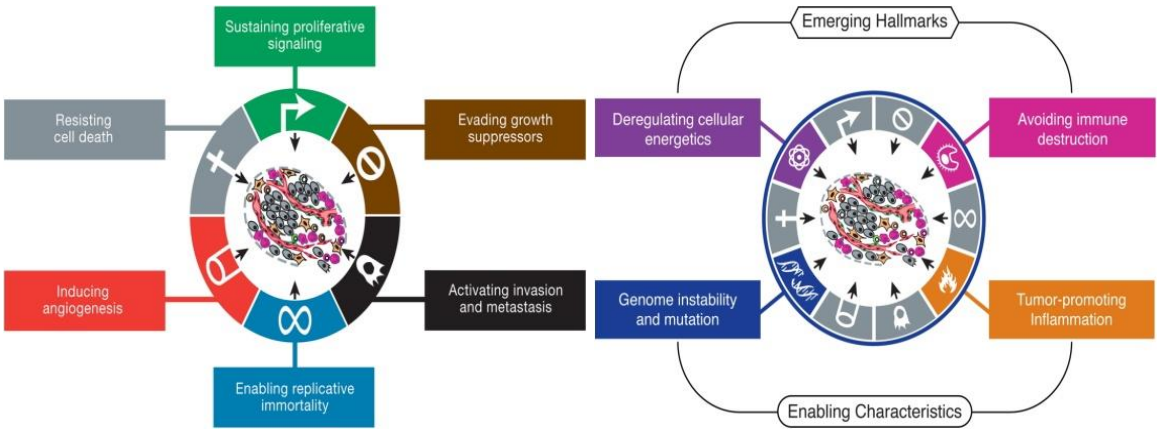

Figure 1: Hallmarks of Cancer, adapted from Hanahan and Weinberg, 2011 (Hanahan & Weinberg, 2011)

1.2 Breast Cancer

Breast cancer is the leading cause of cancer among women and the second most commonly occurring carcinoma worldwide. Although it can occur in both genders, the frequency is much higher in women and its incidence increases significantly with age. According to the American Cancer Society, in 2017, breast cancer is predicted to account for 30% of all new cancer cases and 14% of cancer related death among women(Siegel, Miller, & Jemal, 2017b). This translates to over 200,000 new cases and 40,000 deaths due to breast cancer.

Breast cancer is complex and heterogeneous; it is composed of several diseases with distinct histopathological and biological features which demand unique treatment strategies. Clinically, breast cancer is divided into 4 subtypes, Luminal A which is hormone receptor positive and heregulin 2 receptor (HER2, also known as ERBB2) negative, Luminal B which is also hormone receptor positive and HER2 positive or negative , HER2 amplified subtype and the triple negative subtype (which lack hormone and HER2 receptor)(Dai et al., 2015). These common immunohistochemistry markers along with clinical factors such as tumor grade, tumor size and nodal involvement are commonly used for tumor management and treatment strategies. However, the dawn of the omics era and evolution of high-throughput platforms such as microarrays and sequencing have made it possible stratify patients not only according to anatomical prognostic factors but also to intrinsic molecular characteristics, leading to better therapeutic strategies.

1.2.1 Molecular Subytpes of Cancer

In their pioneering work, Sorlie et al, identified five molecular subtypes of breast cancer with distinct clinical outcome (Sørlie et al., 2001). Subsequently, these five distinct subtypes have been identified by other groups using different gene signatures. For example, Hu et al, used a 306 gene signature to classify breast cancer into these subtypes (Z. Hu et al., 2006). Another study found a 50-gene classifier (PAM50, which contains mostly hormone receptor and proliferation related genes, and genes exhibiting myoepithelial and basal features) which has remarkable prognostic values for breast cancer (Parker et al., 2009).

Luminal

Luminal tumors (also known as ER positive cancers) which express hormone receptors are the most common subtype, accounting for nearly 70% of detected breast cancer. Luminal tumors can be further subdivided into luminal A and B. Very broadly, luminal A tumors are estrogen positive (ER+) (and/or progesterone positive (PR+)), HER2- and low Ki67, while Luminal B HER2+ are ER+ (and/or PR+) and HER2+ with low Ki67 and luminal B HER2- are ER+ (and/or PR+) and HER2- with high Ki67 (Dai et al., 2015). The luminal A subtype shows a higher expression of ER related genes and a lower expression of proliferation related genes. Luminal B subtype generally has a higher grade than the A subtype. Compared to the other subtypes of breast cancer the luminal subtypes have better prognosis. The luminal tumors are defined by their characteristic luminal expression signature. This includes *ESR1*, *GATA3*, *FOXA1*, *XBP1* and *MYB,* genes commonly involved in development, which are all highly expressed. Several genes are also frequently mutated in luminal cancers, for example *GATA1*, *FOXA1*, *RUNX1* which encode transcription factors involved in development (Cancer Genome Atlas Network, 2012). *PIK3CA*, which is also highly mutated in luminal cancer although it does not lead to pathway activation in luminal A cancers. *MAP3K1* and *MAP2K4* represent another class of genes commonly mutated in luminal tumors leading to inactivation of the p-38-JNK1 pathway (Cancer Genome Atlas Network, 2012) The tumor suppressor *TP53* has a higher frequency of mutations in luminal B (29%) than in luminal A (12%). This together with the analysis of another tumor suppressor, pRb activity show that tumors of the luminal A subtype retain TP53 and pRb activity while these genes are frequently mutated in the more aggressive Luminal B subtype. Additionally, luminal B subtypes show hyper activation of MYC and FOXM1, leading to higher proliferation rates (Cancer Genome Atlas Network, 2012).

HER2+

HER2+ subtype is defined by the overexpression of the HER2 amplicon and is identified by gene expression analysis and/or by immunostaining and FISH hybridization(Cancer Genome Atlas Network, 2012; Dai et al., 2015). However, not all clinically identified HER2 tumors show

overexpression at the transcriptional level leading to two subclasses of the HER2 subtype. One is HER2+ and expresses Her2E mRNA (around 50% of the tumors) and the other is HER2+ but essentially luminal(Cancer Genome Atlas Network, 2012). It has been observed that the HER2+/HER2E tumors have a dramatically higher expression of several receptor tyrosine kinases (RTKs) like FGFR4, EGFR, HER2, while the luminal/HER2+ tumors have a luminal expression signature. The HER2+/HER2E or ER negative subgroup also has a higher frequency for TP53 mutations whereas the luminal subtype is enriched for *GATA3* mutations. Additionally, the HER2+/HER2E subtype has high aneuploidy and DNA amplification of other genes such as, *FGFRs*, *EGFR* and genes involved in cell cycle *CDK4* and *CCND1*. HER2 overexpressing tumors are generally Grade 3 and have a poor prognosis(Cancer Genome Atlas Network, 2012).

Triple Negative

The triple negative subtype is devoid of any ER, PR and Her2 expression. The triple negative tumors are highly aggressive having the worst prognosis among the different breast cancer subtypes and are generally Grade 3 like the HER2 tumors. This subtype is characterized by germline and/or somatic *BRCA1* and *BRCA2* mutations, or mutations in other genes of the homologous end joining mechanism, as well as a high frequency of *TP53* mutation and loss of *RB1*. *PI3KCA* is also frequently mutated in these tumors, and the PI(3)K-AKT pathway is highly active probably due to the loss of tumor suppressors *PTEN* and *INPP4B* in addition to amplification of *PIK3CA*. The terms basal and triple-negative are often interchangeably used, however, 75% of TNBCs are basal, while the rest are of different subtypes. Lehmann *et al.*, originally divided triple negative breast cancer into 6 subtypes, 2 basal-like (BL1 and BL2), 1 immunomodulatory (IM), 1 mesenchymal (M), 1 mesenchymal stem-like (MSL) and 1 luminal androgen receptor (LAR) subtype(Lehmann et al., 2011). The BL1 subtype is enriched for cell cycle and cell division genes while BL2 is characterized by genes belonging to growth factor signaling and display features that have basal/myoepithelial origin. The IM subtype displays high expression of genes involved in the immune cell processes. The M subtype is enriched in genes involved in cell motility, ECM receptor interaction and cell differentiation pathways. The

MSL subtype is similar to the M subtype but is also enriched in genes involved in growth factor signaling and has low expression of claudin 3,4,7. Finally, the LAR subtype is ER- but has a luminal gene expression signature. As some of the expression of genes in these specimens were discovered to be from tumor infiltrating cells and the tumor stroma, the classification was later refined to 4 subtypes, namely BL1, BL2 M and LAR(Lehmann, Jovanovi, et al., 2016)

Sorlie et al also defined a fifth subgroup of breast cancer called normal breast-like which have high expression of several genes that are expressed in adipose and other non-epithelial tissues(Sørlie et al., 2001). They also display elevated expression of basal epithelial genes and low expression of luminal epithelial genes.

1.2.2 Therapy

Currently the standard treatment regimen for breast cancer is either surgery or radiotherapy. Depending on the type of breast cancer, patients may undergo additional treatment. Some receive neo-adjuvant therapy to shrink the tumor before surgery, others may receive adjuvant therapy post-surgery to treat potential micro-metastases. Therapies include chemotherapy, endocrine therapy and targeted therapy.

Endocrine therapy remains the mainstay and the first line of therapy for hormone receptor positive breast cancers(Liedtke & Kolberg, 2016) . Established in 1970, tamoxifen, an ER antagonist, remains a viable option with patients responding up to 12-18 months and in some cases up to years. However, in recent years tamoxifen has been replaced by aromatase inhibitors, AI, (e.g. letrozole and anastrozole) in postmenopausal patients as the first line of therapy due to higher response rates(Wood, Smith, & Dowsett, 2003). However, several patients have de novo or acquire resistance to first line therapy, leading to relapse. In case of AI resistance, estrogen receptor antagonists (tamoxifen and fulvestrant) are used as second line of therapy(Chia et al., 2008).

Dysregulation of the cell cycle is a common phenomenon of breast cancer. *CDK4/6* and *CCND1* regulate the transition from G1 to S phase via phosphorylation of pRb and are, therefore,

important to the highly proliferative cancer cells(Weinberg, 1995). As a result of this, metastatic ER+ breast cancers often benefit from additional therapy with cell cycle inhibitors as do cancers resistant to endocrine therapy. In view of this, CDK4/6 inhibitors, palbociclib (Ibrance; Pfizer Inc), ribociclib (LEE011; Novartis) and abemaciclib (LY2835219; Lilly) are undergoing clinical development. Given that cyclin D1 is regulated by PI3K/AKT/mTOR pathway and that over 70% of breast cancer show activation of this pathway, inhibiting this pathway provides a potential option for therapy(Fu, Osborne, & Schiff, 2013; Pang et al., 2014). As a result of its crosstalk with estrogen receptor, this pathway has also been implicated in endocrine resistance, thereby providing an opportunity to overcome resistance(Fu et al., 2013). While therapies targeting PI3K are still in development, mTOR inhibitor, everolimus, is used in combination with steroidal aromatase inhibitor, exemestane, in cases of non-response to non-steroidal aromatase inhibitors(Liedtke & Kolberg, 2016). Luminal breast cancers may also be treated with antiangiogenic therapy including, bevacizumab, which is an antibody directed against the vascular endothelial growth factor (VEGF)(Bear et al., 2012; Liedtke & Kolberg, 2016). Other targets for therapy include AKT, using inhibitors of AKT and PARP for patients harboring pathogenic mutations in *BRCA1/BRCA2* or other genes involved in DNA damage response.

HER2+ breast cancers are highly aggressive and tend to have a poor prognosis. However, due to the presence of the highly druggable target HER2, it has been possible to effectively treat this disease. The development of trastuzumab, a humanized monoclonal antibody that targets the extracellular domain of the HER2 receptor, has increased the overall survival of HER2+ breast cancers(Slamon et al., 2001). In addition, pertuzumab which targets the HER2-HER3 dimer has been recently approved for first line therapy and this in combination with docetaxel(chemotherapeutic drug) and trastuzumab has been shown to dramatically improved overall survival (Baselga et al., 2012). TDM-1 (Trastuzumab etansine), antibody drug conjugate (ADC) of the cytotoxic DM-1 and trastuzumab has proved to be an effective therapy against HER2+ cancers(Verma et al., 2012). Besides HER2-targeted antibodies, small HER2-directed molecules have also proven to be efficacious treatments. An example of this is Lapatinib (targeting both HER1/EGFR and HER2) which is used as a later-line therapy in combination with chemotherapy(Geyer et al., 2006) .

Due to the lack of a druggable hormone or HER2 receptor, TNBC proves to be the most challenging subtype of breast cancer. Additionally, the presence of distinct subgroups within this subtype makes it difficult to develop a general therapy for this subtype. Currently, TNBCs are heavily dependent on chemotherapy. Due to the common occurrence of *BRCA1/2* mutations, patients suffering from TNBCs benefit from taxane and platinum salts. In addition to this, PARP inhibitors, which can prevent DNA damage repair in cells, are commonly used for treatment of *BRCA1/2* mutated TNBC (Farmer et al., 2005). Increasing evidence suggests that tumors with strong lymphocytic infiltration can benefit from immune targeted agents which help to expose tumors cells to the immune system. Programmed cell death protein (PD-1) and its two ligands, PD-L1 and PD-L2 are currently being investigated as potential therapeutic targets. Phase I clinical trial of PD-1 inhibitor pembrolizumab has been a success with TNBC patients(Nanda et al., 2016).

Early detection and targeted therapy have greatly improved survival rates in breast cancer. Endocrine therapy and HER2 targeted therapy have been highly successful, however, recurrence and development of resistance still remains a problem. Furthermore, TNBCs still lack efficient therapy barring chemotherapy. This has led to the need for further molecular characterization of breast cancer. Recent studies show that cancers are also metabolic diseases(Pavlova & Thompson, 2016). The high rates of cell division demand metabolic reprogramming within the tumors. Therefore, targeting metabolism provides a promising therapeutic window, especially for tumors that cannot be otherwise treated effectively.

1.3 Cancer Metabolism

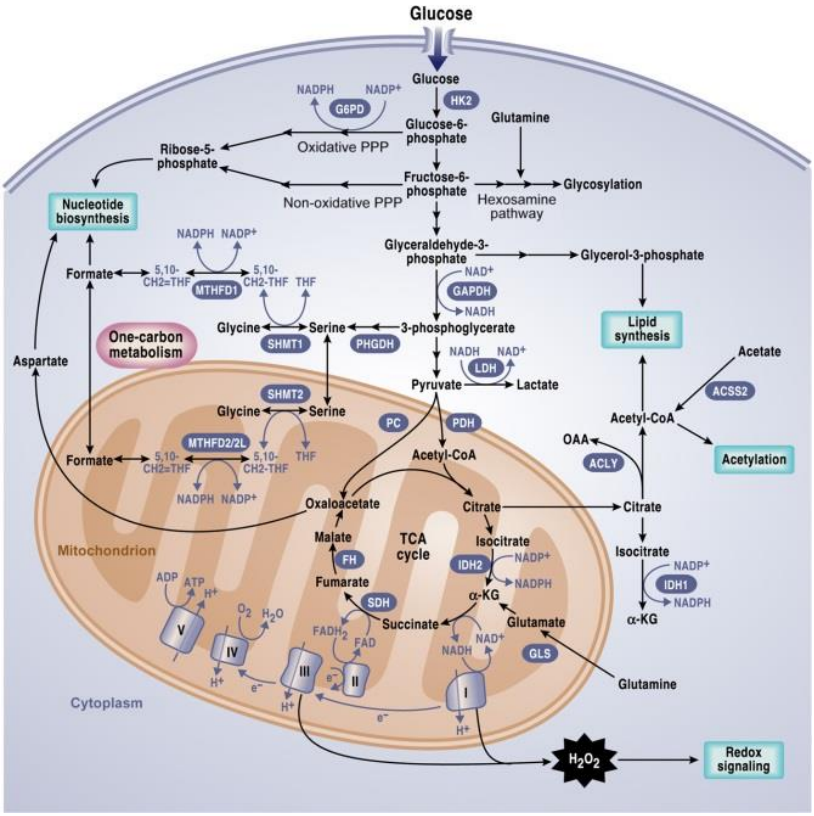

Figure 2: Metabolic pathways involved in tumorigenesis. Adapted from Berardinis and Chandel 2016(R. J. Deberardinis & Chandel, n.d.)

Metabolic reprogramming in cancer cells plays a crucial role in maintaining high levels of proliferation. Cellular metabolism is defined by three main tasks which are, to maintain energy reserves of the cell (via ATP and NADPH regeneration), biosynthesis of macromolecules required for cellular homeostasis and to maintain redox state of the cell. In order to fulfill these requirements, particularly fast growing cancer cells depend on efficient nutrient cycling. Metabolic rewiring is essential in order to maintain optimum levels of four major classes of macromolecules comprising carbohydrates, proteins, lipids and nucleic acids.

The association between cancer and metabolism dates back to nearly 100 years when Otto Warburg observed that cancer cells consume high amounts of glucose and instead of funneling it into the TCA cycle, it produces lactate via glycolysis(Warburg, 1927). In normal cells this occurs when the cells are under hypoxia but as this was observed in cancer cells even in the presence of oxygen it is called aerobic glycolysis or more famously the Warburg effect.

However, in the following years cancer research focused more on genetic alterations that are associated with tumorigenesis. This led to the identification of oncogenes and tumor suppressors that control growth factor signaling pathways leading to uncontrolled proliferation which remains a hallmark of cancer(Hanahan & Weinberg, 2000). However, in 1956, Otto Warburg claimed that "mutation and carcinogenic agents are not alternatives, but empty words, unless metabolically specified"(Warburg, 1956), thereby suggesting that despite the fact that several different factors can lead to different cancers, ultimately, they all lead to or depend on rewiring of metabolic pathways. In recent years, many studies have shown that these different signaling pathways indeed reprogram cellular metabolism via regulation of metabolic enzymes (Cairns, Harris, & Mak, 2011; Iurlaro, León-Annicchiarico, & Muñoz-Pinedo, 2014). Several metabolic enzymes are also amplified or mutated during tumorigenesis(L. Dang et al., 2009; Martín-Rufián et al., 2014). These findings together with the observations that cancer metabolism can influence other hallmarks of cancer has led to the inclusion of cancer bioenergetics into the hallmarks of cancer(Hanahan & Weinberg, 2011) and has brought tumor metabolism into the forefront of cancer research(Pavlova & Thompson, 2016). The fact that cancer cells rely heavily on efficient nutrient utilization provides an opportunity to find therapeutic targets especially for those cancers which are otherwise unresponsive to present therapies.

1.3.1 Warburg Effect and Glycolysis

Aerobic glycolysis remains one of the most significant characteristics of tumor metabolism. In his seminal work, Warburg observed that ascites cancer cells and tumor slices have a high uptake of glucose which, irrespective of the presence of oxygen, is converted into lactate via pyruvate(Warburg, 1927). Subsequently, this phenomenon has been observed in several cancers including breast cancer(Gatenby & Gillies, 2004). Glucose is transported into the cell via glucose transporter proteins (GLUT), of which 14 isoforms have been identified. While the different isoforms may have different expression levels in many cancers, GLUT1 seems to be predominant in cancer with high rates of glycolysis(Carvalho et al., 2011). In breast cancer, the HER2+ and TNBC subtypes, which have the worst prognosis, have high levels of glycolysis and

TNBCs show the highest expression of GLUT1 compared to other subtypes of breast cancer(Choi, Jung, & Koo, 2013; Pinheiro et al., 2011). In fact, targeting GLUT1 in breast cancer cells induces autophagy via AMPK-mTORC1 signaling(Fumarola et al., 2013). Hexokinase 2, the first regulatory enzyme in the glycolytic pathway, is activated in several cancers and can be targeted to slow down proliferation in cancer cells(Hennipman, van Oirschot, Smits, Rijksen, & Staal, 1988). Tumor specific expression of phosphofructokinase 2 (PFK2), which regulates intracellular levels of the glycolytic intermediate fructose-1,6-bisphosphate, has made it a potential therapeutic target(Atsumi et al., 2002; Telang et al., 2006). Pyruvate kinase (PK) is the rate limiting enzyme of glycolysis catalyzing the final reaction converting phosphoenolpyruvate to pyruvate generating ATP in the process. The splice variant PKM2 is predominantly expressed in tumor cells, but is inhibited by tyrosine kinases which are active in most cancer cells(Christofk, Vander Heiden, Harris, et al., 2008; Christofk, Vander Heiden, Wu, Asara, & Cantley, 2008). This low activity of PKM2 is essential for growth of tumor cells as it creates a buildup of glycolytic intermediates that serve as precursors for biosynthesis of macromolecules such as nucleotides and amino acids and generation of NADPH.

Lactate dehydrogenase (LDH) which catalyzes the interconversion of pyruvate to lactate has been implicated in oncogenesis. LDHA is the most common isoform of this enzyme that is upregulated in cancers and is being investigated as a target for highly glycolytic cancers(Miao, Sheng, Sun, Liu, & Huang, 2013; Xie et al., 2014). In breast cancers upregulation of ERBB2 leads to an increased expression of LDHA which promotes glycolysis and proliferation(Y. H. Zhao et al., 2009). Lactate produced by cancer cells is secreted into the surrounding of the tumor via monocarboxylate transporters (MCT). It has been shown that impaired function of these transporters can affect tumorigenesis, thereby suggesting that efficient secretion of lactate is important for the tumors(Dimmer, Friedrich, Lang, Deitmer, & Bröer, 2000). Notably, cancer cells use lactate to feed neighboring cells that are more oxidative to support its own growth and survival(Vegran, Boidot, Michiels, Sonveaux, & Feron, 2011).

In normal cells, the mitochondria function as the powerhouses of the cell, where oxidative phosphorylation and the electron transport chain are utilized to produce ATP in order to meet

the bioenergetic needs. Therefore, the propensity of cancer cells to use aerobic glycolysis as the major pathway for glucose metabolism over the energetically rich oxidative phosphorylation pathway still remains a paradox (Ralph J. DeBerardinis, Lum, Hatzivassiliou, & Thompson, 2008). However, plenty of evidence suggests that glycolysis gives the cancer cells a growth advantage. It provides intermediates for macromolecule synthesis which contributes to the biomass of the cell(Hay, 2016). Glycolysis via the pentose phosphate pathway produces sugars and NADPH that support nucleotide synthesis and reductive biosynthesis respectively. It also supports hexosamine and glycogen synthesis. Moreover, glycolysis increases serine biosynthesis which is essential for tumorigenesis. Serine supports one carbon metabolism via glycine production, leading to nucleotide biosynthesis, methylation and production of NADPH. Serine is also a source for amino acid, protein and glutathione replenishment of cancer cells(M. Yang & Vousden, 2016). Phosphoglycerate dehydrogenase (PHGDH) which catalyzes the first committed step in the biosynthesis of serine and is also the branching point from glycolysis, is amplified in 6% of breast cancers and 40% of melanomas(Ralph J DeBerardinis, 2011; Locasale et al., 2011; Possemato et al., 2011a). Possemato et al showed that 70% of ER negative breast cancers have elevated levels of PHGDH protein which when targeted by RNA interference lead to a significant decrease in cell proliferation(Possemato et al., 2011a).The high rates of glycolysis in tumors outpace oxidative phosphorylation which may lead to the accumulation of pyruvate. This is prevented by diverting excess pyruvate to lactate production. Furthermore, although the ATP yield per glucose via glycolysis is low, if the glycolytic rate is sufficiently high the percentage of cellular ATP contributed by glycolysis is more than oxidative phoshorylation(GUPPY, GREINER, & BRAND, 1993).

Warburg hypothesized that cancer cells divert glucose from the oxidative phosphorylation and produce lactate due to defective mitochondria. However, over the years this theory has been disproved and it has been shown that the mitochondria are indeed active in tumors and mitochondrial metabolism is important for tumorigenesis(Tan et al., 2015). Pyruvate, produced by glycolysis can feed into the TCA cycle via two reactions that are catalyzed by pyruvate dehydrogenase (PDH) and pyruvate carboxylase (PC). PDH produces acetyl coA which is then condensed with oxaloacetate (OAA) to produce citrate. PC on the other hand directly produces

OAA from pyruvate. Recently it was observed that both PDH and PC are essential for KRAS-driven lung tumors(Davidson et al., 2016) and that PC has a role in breast cancer-derived lung metastasis(Christen et al., 2016). Moreover, inhibiting glycolytic ATP production via deletion of *PKM2* does not affect tumorigenesis, thereby, suggesting that the major role of glycolysis is not to supply ATP to the cell (Ralph J. DeBerardinis & Chandel, 2016; Israelsen et al., 2013). Taken together these studies show that the TCA cycle is indeed active and is a major source of ATP also in cancer cells and that glucose also feeds into this pathway. In rare cases, however, the TCA cycle genes are mutated and can function as tumor suppressors. This is seen in cancers which have deletions in TCA cycle genes including succinate dehydrogenase (*SDH*) and fumarate hydratase (*FH*). *SDH* mutations are found in familial paraganglioma(Astuti et al., 2001; Baysal et al., 2000; Müller & Niemann, 2000) while FH mutations can result in uterine fibroids, leiomyoma and papillary renal cell cancer(Tomlinson et al., 2002). SDH and FH mutations lead to the accumulation of succinate and fumarate respectively, which can promote tumorigenesis (Sullivan, Gui, & Heiden, 2016). Both these metabolites have been implicated in epigenetic modifications leading to DNA and histone hypermethylation and activation of hypoxic signaling(Gimenez-Roqueplo et al., 2002; Hoekstra et al., 2015; Isaacs et al., 2005; Killian et al., 2013; Letouzé et al., 2013; Pollard et al., 2005). In contrast to this, only 3% of breast cancers show loss of SDHA or SDHB expression, while HER2+ breast cancers show high levels of SDHA expression(S. Kim, Kim, Jung, & Koo, 2013). A study in a Finnish population has shown that FH mutation is not associated with a predisposition to familial breast cancer(Kiuru et al., 2005). Furthermore, reports have shown that breast cancers are not associated with promoter methylation in *SDH* and *FH* genes(K. T. Huang, Dobrovic, Fox, Huang -KatieHuang, & Dobrovic -AlexanderDobrovic, n.d.). In addition to loss of *FH* and *SDH*, mutations in TCA cycle genes can result in neomorphic activity in cancers. The most prominent example of this are the isocitrate dehyrogenase (IDH1and 2) enzymes which are frequently mutated in glioma, chondrosarcoma, cholangiocarcinoma ad acute myeloid leukaemia (AML)(O. Clark, Yen, & Mellinghoff, 2016; Figueroa et al., 2010; Yan et al., 2009). While the wild type forms of these enzymes catalyze the reversible conversion of isocitrate to α-ketoglutarate (α-KG), the mutant forms convert α-KG to 2-hydroxyglutarate (2-HG) via oxidation of NADPH to NADP+(S. Gross et al., 2010). 2-HG can be

degraded by D2HGDH, however, its activity is insufficient for the high rate of production seen in these cancers (Sullivan et al., 2016). This results in high levels of 2-HG in cancers which leads to CpG island and histone hypermethylation(Figueroa et al., 2010). c-Myc-driven breast tumors, mostly of basal and mesenchymal origin, show 100 fold higher levels of 2-HG compared to other breast cancers leading to elevated levels of DNA methylation and are associated with poor prognosis(Terunuma et al., 2014). Therefore, cancer cells maintain an active TCA cycle in order to sustain both their biosynthetic and bioenergetic needs.

1.3.2 Glutamine addiction

An important carbon source for the TCA cycle in cancers is glutamine. Glutamine is the most abundant amino acid present in blood and tissues and is the second highest consumed nutrient by the cancer cells after glucose. It complements the glycolytic pathway by proving carbon to replenish the TCA cycle(R. Deberardinis & Cheng, 2009). Glutamine is thus a crucial anaplerotic source for cancer cells. It is not only an important carbon donor but also provides nitrogen for de novo biosynthesis of various nitrogenous metabolites required for tumor growth. Glutamine addiction in cancer cells was first observed by Harry Eagle in HeLa cells in the 1950s(Eagle, 1955). In later years this was also observed in Ehrlich ascites carcinomas, hepatomas and carcinomas(Márquez, Sánchez-Jiménez, Medina, Quesada, & de Castro, 1989; Sauer, Stayman, & Dauchy, 1982). In fact, several studies have shown that depletion of glutamine from the tumor microevironment is higher than in normal tissues(Márquez et al., 1989; Yuneva et al., 2012). Successful detection of glutamine in tumors using 18F-labeled glutamine in preclinical and early clinical studies(Lieberman et al., 2011; Venneti et al., 2015), provides a solution for cases where glucose tracing is not possible due to high glucose utilization in normal tissues, e.g. the brain. Glutamine restriction has been shown to restrict growth of most cancer cells including those of breast, thereby displaying what is commonly known as glutamine addiction. As is seen with glucose, tumor cells tend to take up glutamine at a much higher rate than their normal counterpart. In order to overcome the poor vascularization within tumors tumor cells express high levels of transporters thereby behaving like a ‘Glutamine trap’(Souba, 1993).

Glutamine uptake by cancer cells is mediated by amino acid transporters such as solute-linked carrier family A1 member 5 (SLC1A5) (also known as ASCT2) which is over expressed in several cancers and has been shown to be critical for tumor survival (Hassanein et al., 2013). High expression as well as increased activity of ASCT2 is critical for cell proliferation in triple negative breast cancer cells(van Geldermalsen et al., 2015a). Moreover, ASCT2 has been shown as an independent prognostic marker for survival in breast cancer(Bernhardt et al., 2017). There is also evidence that glutamine uptake is not only important for supporting the biosynthetic need of the cells but is also exported out in exchange for essential amino acids via the bidirectional amino acid transporter SLC7A5 (also called LAT1)(Nicklin et al., 2009).

Glutamine is utilized in roughly two ways in the cells. Firstly, its γ-nitrogen is used for nucleotide and hexosamine synthesis which supports cancer cell growth(David R Wise & Thompson, 2010). Secondly, α-nitrogen and carbon skeleton are used for NEAA synthesis and TCA cycle. Glutamine is the main nitrogen donor for the synthesis of NEAA in the cells. In a first step glutamine is converted to glutamate via the phosphate dependent glutaminase which removes an amide group as ammonia. Glutaminase has been observed to be highly expressed in tumors and cancer cell lines and limiting its activity causes growth arrest in tumor cells and xenografts (Lobo et al., 2000; Gao et al., 2009). In triple negative breast cancer cells, glutaminase activity regulates glutamine and oxygen consumption, glutamate production and levels of TCA cycle intermediates(M. I. Gross et al., 2014). The glutamate generated by glutaminase contains a sizeable pool of α (amino) nitrogen which is then distributed to different non-essential amino acids via transaminase reactions, namely alanine and aspartate transaminases (in details in the next section). Reactions catalyzed by transaminases and glutamate dehydrogenase (via liberation of ammonia) convert glutamate from glutamine into α-KG a key metabolic intermediate of the TCA cycle. PHGDH, the first enzyme in serine synthesis is also involved in supplying glutamine derived α-KG to the TCA cycle(Possemato et al., 2011b). In addition to being a TCA cycle metabolite, α-KG also functions as cofactor for various dioxygenases including prolyl hydroxylases, histone demethylases, and 5-methylcytosine hydroxylases(Zdzisińska, Żurek, & Kandefer-Szerszeń, 2017). Glutamine derived α-KG can be used to drive the TCA cycle or can contribute to lipid biosynthesis by a process called reductive carboxylation. Reductive

carboxylation or reversal of TCA cycle is a process by which α-KG is converted to citrate via IDH and it exits the mitochondria to be used for lipid biosynthesis(Metallo et al., 2011; Mullen et al., 2011; D. R. Wise et al., 2011). Reductive carboxylation was first observed as a method to synthesize lipids in normal brown fat cells, however, later it was shown as a mechanism to generate lipids in hypoxic cancer cells(Yoo, Antoniewicz, Stephanopoulos, & Kelleher, 2008). Indeed under hypoxia, HIF1α activate pyruvate dehydrogenase kinase 1 (PDK1), an inhibitor of PDH, thereby blocking the entry of pyruvate into the TCA cycle and shunting it into lactate, a process known as anaerobic glycolysis, leading to a depletion of citrate pools. The same is also observed in hypoxic cancer cells, and gives rise to the need for glutamine to feed into the TCA cycle and for reductive carboxylation in order to maintain the lipid reserves of the cells(Fendt, Bell, Keibler, Olenchock, et al., 2013). Mitochondrial glutamine is also used for production of oncometabolite, 2-HG in breast cancer. Malic acid generated via glutaminolysis, is converted to lactic acid by malic enzyme thereby generating carbon dioxide, pyruvate and NADPH. NADPH generated by production of lactic acid is the used by highly proliferative cells to sustain their demand for nucleotide and lipid synthesis and to maintain GSH in its reduced state (R. J. DeBerardinis et al., 2007; M. G. Vander Heiden, Cantley, & Thompson, 2009). Glutaminolysis can also be used to maintain glutathione pools, where glutamate is exported via the x-CT antiporter in exchange for cystine which is then used to generate glutathione (GSH). In a subset of triple negative breast tumors, which are glutamine auxotrophs and require glutamine to sustain their GSH pools, inhibition xCT antiporter abrogates tumor growth(Timmerman et al., 2013).

1.3.3 Transaminase reactions in Cancer

Alanine (GPT) and aspartate (AAT or GOT) aminotransferases lead to the production of alanine and aspartate respectively and are the two most important transaminases in cancer cells(L. Yang, Venneti, & Nagrath, 2017).

Aspartate transaminase derived aspartate is used for protein and nucleotide synthesis as well as ATP production via the aspartate malate shuttle. Aspartate is exported from the

mitochondria into the cytosol where it is converted to oxaloacetate which is then reduced to malate using NADH generated during glycolysis (thereby regenerating NAD+ for glycolysis). Malate is then transported into the mitochondria where it donates electrons to complex I of the electron transport chain, thereby generating ATP(Sullivan et al., 2015). Inhibition of GOT selectively suppresses proliferation of breast cancer cells but not normal mammary epithelial cells(Korangath et al., 2015; Thornburg et al., 2008). Aspartate is also used for asparagine synthesis in the cells. Asparagine supports proliferation under glutamine deprived or glutamine independent conditions. It also serves as an amino acid exchange factor, whereby it is exported to increase the uptake of other amino acids including serine. In addition to this, asparagine supports protein and nucleotide synthesis via regulation of mTORC1 activity(Krall, Xu, Graeber, Braas, & Christofk, 2016). Asparagine directly uses glutamine for its synthesis and is essential for cellular proliferation and in fact asparagine synthetase has been proposed as a potential biomarker for ovarian cancer(Lorenzi & Weinstein, 2009).

While the role of GOT has been clearly elucidated in cancers, GPT has emerged as a new target in cancers. Alanine is shown to be highly produced in patients including those with breast cancer(Budczies et al., 2012; Poschke, Mao, Kiessling, & de Boniface, 2013). Inhibition, of alanine aminotransferase like aspartate aminotransferase also impedes cell growth and survival(Beuster et al., 2011; Coloff et al., 2016; Hao et al., 2016). Aminooxyacetate which is a broad spectrum inhibitor of aminotransferases has been shown in several studies to suppress cell growth. In breast cancer cell lines, aminooxyacetate treatment increases the sub G1 population and leads to S-phase arrest(Korangath et al., 2015). Inhibition of aminotransferase results in decrease in amino acids which activates the ER stress pathway leading to cytotoxicity(Korangath et al., 2015). This highlights the importance of aminotransferases in breast cancer progression.

1.4 Regulation of Tumor metabolism

An important aspect of understanding the metabolic rewiring in cancer cells is to investigate the mechanism by which the metabolic pathways or individual enzymes are regulated. Cancer is driven by gain of function mutations in oncogenes and loss of tumor suppressors that enable the cells to proliferate rapidly. However, in recent years, it has become increasingly clear that cancer signaling pathways and the tumor microenvironment lead to rewiring of metabolic pathways in cancer cells. Moreover, these changes in metabolism are essential for sustaining the tumor progression that is propagated by these signaling pathways.

The oncogene *MYC* is amplified in several cancers, including breast, prostate, colon and bladder cancers and contributes to the cause of nearly 40% cancers(Deming, Nass, Dickson, & Trock, 2000). c-Myc is a transcription factor that has a central role in cancer progression. It regulates the expression of several cell cycle genes as well as those involved in mitochondrial biogenesis and stem cell maintenance. The last decade has seen c-Myc emerge into a master regulator of cancer cell metabolism(Chi V Dang, Le, & Gao, 2009; Miller, Thomas, Islam, Muench, & Sedoris, 2012; Wahlström & Henriksson, 2014). The first link between c-Myc and cancer metabolism was established when it was discovered that c-Myc regulates the expression of LDHA(Shim et al., 1997). c-Myc also promotes glycolysis via activation of glucose transporter, GLUT1 and other glycolytic genes such as hexokinase 2 (*HK2*), phosphofructokinase (*PFKM*), and enolase 1 (*ENO1*)(J. -w. Kim, Gao, Liu, Semenza, & Dang, 2007; Osthus et al., 2000). Therefore, under normoxic conditions c-Myc is believed to be one of the drivers of lactate production. Additionally, under hypoxic conditions, c-Myc collaborates with hypoxia inducible factor 1-alpha (HIF1a) to increase the activity of PDK1 which prevents the formation of acetyl CoA from pyruvate thereby promoting more lactate production(J. -w. Kim et al., 2007). However, under normoxic conditions c-Myc supports glucose oxidation via regulation of mitochondrial biogenesis. c-Myc also promotes RNA splicing to induce PKM2 expression which supports different biosynthetic pathways (David 2010). While c-Myc-induced glycolysis and glutaminolysis (in details later) promotes lipid biosynthesis, c-Myc can also directly induce fatty acid synthesis genes, *FASN* (fatty acid synthetase) and *SCD* (stearoyl-CoA desaturase) (Zeller et al. 2003; Loven et al. 2012).

c-Myc plays a major role in the energy metabolism of cancers via regulation of Glutamine metabolism(Chi V Dang et al., 2009). It has been found to increase the expression of Glutamine transporters ASCT2 (SLC1A5) and SLC7A5(Shajahan-Haq et al., 2014)(GAO 2009). In addition to this, c-Myc promotes expression of glutaminase (GLS1) via inhibition of microRNA-23A and microRNA-23B (Gao P, 2009). c-Myc induced GLS1 produces glutamate from glutamine, which can then drive the TCA cycle via production of α-KG. It has been shown that c-Myc driven glutamine uptake and glutaminolysis lead to glutamine addiction in cancer cells(David R Wise et al., 2008). Elevated glutamine metabolism by c-Myc leads to an upregulation of other amino acid pathways which are directly or indirectly fed by nitrogen from glutamine. A study in breast cancer shows that cancer cells are sensitive to a broad spectrum inhibitor of aminotransferase in a Myc dependent fashion. However, c-Myc has not been directly linked to the expression of these aminotransferase genes(Korangath et al., 2015). c-Myc is also involved in the serine and one carbon metabolism via regulation of enzymes PHGDH and PSAT (involved in serine metabolism, described earlier) and SHMT2 which converts serine to glycine, leading to nucleotide synthesis(Nikiforov et al., 2002; Sun et al., 2015).

One of the main mechanisms by which c-Myc regulates cell cycle is via induction of genes involved in cell cycle, *E2F* and *CDK*, and by inactivation of the tumor suppressor *RB1* thereby allowing cells to enter into the S phase(C. V. Dang, 2013). c-Myc and E2F coordinate together to activate genes involved in DNA replication and nucleotide metabolism (Rempel et al. 2009, Zeller et al. 2006). Interestingly, loss of *RB1*, which frequently occurs in cancers, promotes glutamine metabolism. It has been observed that *RB1* knockout cells have elevated expression of ASCT2 and GLS and show an increase in carbon flow from glutamine into the TCA cycle(Nicolay & Dyson, 2013; M. Reynolds et al., 2013). *RB1* is also involved in antioxidation and its loss leads to the accumulation of ROS in cancer cells. Similarly, TP53, another well-known tumor suppressor, induces the expression of GLS2 which promotes de novo synthesis of GSH which also controls the redox potential of the cells (Suzuki, S. et al., 2010). However, the primary function of TP53 is to induce cell cycle arrest and apoptosis in case of DNA damage which leads to a buildup of ROS. Recent studies have shown that p53 is also involved in glucose and energy metabolism(Chen & Russo, 2012). TP53 also activates PTEN which inhibits PI3K-AKT

pathway which is known to activate glycolysis and mTOR signaling. mTOR signaling is essential in integrating growth signals and nutrient availability which influences cell metabolism and it activates HIF1a to stimulate further metabolic changes (details below).

There are several other oncogenes which have been shown to regulate cancer metabolism. Prominent among these are mutant *KRAS*, which has been found in pancreatic, colon and lung cancers and also found in breast cancers. *KRAS* carrying activating mutations has been shown to regulate anabolic glucose metabolism as well as reprogram glutamine metabolism (Son et al., 2013a; Ying et al., 2012). *EGFR* which is frequently mutated in breast and lung cancer has been shown to regulate glycolysis in triple negative breast cancer cells (Lim et al., 2016) and fatty acid synthesis in glioma and has also been implicated in sensitivity to glutamine inhibition in lung cancer (Momcilovic et al., 2017).

Besides the genetic landscape of cancer cells, the tumor microenvironment also regulates tumor metabolism. The availability of nutrients, pH of the surrounding and oxygenation of the tumor are important factors controlled by the microenvironment that regulate cellular metabolism(Cairns et al., 2011). AMP-activated protein kinase (AMPK) functions as a metabolic checkpoint, which regulates metabolic pathways under stress including those imposed by the microenvironment. Under periods of stress and energy deficit, LKB1, a serine threonine kinase, activates AMPK and drives the cells towards a more oxidative metabolic pathway. Therefore, it is not surprising to see that *LKB1* is mutated in several cancers, including non-small cell lung cancer and breast cancer(Avizienyte et al., 1999; Ji et al., 2007), and others show a suppression of AMPK signaling(X. Huang et al., 2008; Xiang, Saha, Wen, Ruderman, & Luo, 2004). As an mTOR and HIF1α inhibitor, loss of AMPK activity leads to a more glycolytic phenotype in cancer cells(Carretero et al., 2007; Luo, Zang, & Guo, 2010).

As a result of irregular tumor vasculature, parts of the tumor are inconsistently oxygenated and receive insufficient nutrients, resulting in hypoxia and stress in these sections of the tumor. Low oxygen levels lead to stabilization of HIF1α(Keith, Johnson, & Simon, 2011; Wang, Jiang, Rue, & Semenza, 1995). As mentioned earlier, HIF1α can also be activated by mTOR signaling and ROS levels in cancer cells. HIF1α elevates glycolysis in the cells and inhibits mitochondrial respiration

(Denko N.C. 2008). HIF1α also cooperates with c-Myc to activate PDK1 and induce lactate production(Kim et al., 2007). HIF1α also regulates TCA cycle genes to support cancer cell growth (Wise et al., 2011). HIF is a heterodimer made up of two subunits HIF1α and HIF1β. The HIF1α subunit levels are controlled by oxygen levels and, during hypoxia, HIF1α levels are elevated via stabilization of the protein(Keith et al., 2011; Wang et al., 1995). While most of the metabolic changes seen under hypoxia are attributed directly to HIF1α, little is known about the metabolic role HIF1β (ARNT), which is stabily expressed in the cells.

Extreme hypoxia (<0.02% O_2) leads to endoplasmic reticulum (ER) stress and unfolded protein response (UPR) in cells, resulting in further metabolic adaptation that enable the cells to survive. For example, activating transcription factor 4 (*ATF4*) is a stress responsive gene which is activated in response to conditions of stress, including hypoxia, ER stress, amino acid deprivation, oxidative stress and growth factor heregulin (Cullinan & Diehl, 2006; Harding et al., 2003; Salgado, Metón, Anemaet, & Baanante, 2014a). ATF4 in turn regulates metabolism to protect the cells from stress and ensure sufficient supply of amino acids. In a study conducted in liver cells induction of stress lead to an increase in expression of alanine aminotransferase 2 by ATF4 (Salgado et al., 2014a).

Tumorigenesis is multistep process orchestrated by changes in cell signaling networks that promote rapid cell proliferation. In order to maintain these high levels of proliferation, signaling pathways and transcription networks rewire metabolic activities of the cells. However, connections between signaling and tumor metabolism are complex and are still not well understood. While some potential focal points for these connections have been discovered it is difficult to find one master regulator as these associations are temporally and spatially regulated. Moreover, integrating data from metabolic and proteomic (or genetic) pathway analysis is a challenge and requires further development. Nevertheless, determining the regulation of metabolic pathways by signaling molecules will be beneficial in the quest to find more effective targets for cancer therapy.

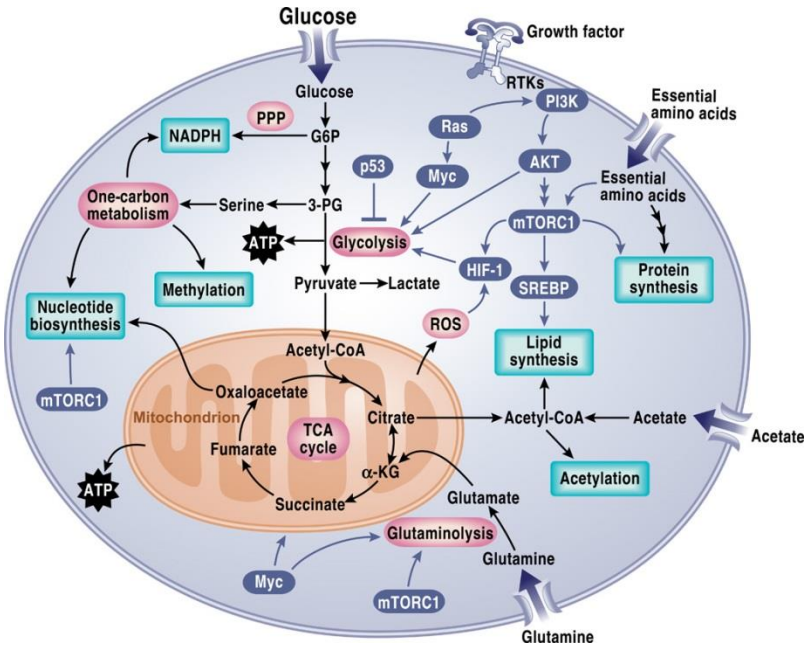

Figure 3: Transcription factors and signaling molecules involve in the regulation of cancer metabolism. Adapted from Berardinis and Chandel, 2016(R. J. Deberardinis & Chandel, n.d.)

1.5 Tumor Metabolism: Imaging and Therapeutics

Understanding the metabolic landscape of cancer provides new opportunities for tumor imaging, biomarker discovery and treatment strategies.

The last three decades have seen a surge in imaging of metabolic phenotypes of cancer cells. The most commonly used technique is positron imaging tomography (PET). Combined with a low-dose CT scan, PET imaging helps generate a three-dimensional image of the tumor. First discovered in the 1980s(Som et al., 1980), 18F-labelled fluorodeoxyglucose(FDG) is taken up by glucose transporters in the cells but unlike glucose it is phosphorylated to FDG-6 phosphate and cannot be metabolized further. Low levels of emission from FDG-6 phosphate are used as a measure for glucose consumption by the cells. This method is used to image breast, lung, head and neck, lymphoma, and sarcoma(Bar-Shalom et al., 2003). Although this technique is useful to detect the progression of the disease and efficacy of treatment, it is limited by the differential ability of cancers to take up FDG(Schirrmeister et al., 2001). This has led to the development of other tracers which can track other metabolic pathways in cancer cells, some

of them include ^{18}F-*N*-(methyl-(2-fluoroethyl)-1H-[1, 2, 3]triazole-4-yl)glucosamine ([^{18}F] NFTG), which is incorporated into glycogen and can be used to measure gluconeogenesis in the cells(Cheng et al., 2012). The glutamine analog, g [^{18}F] -(*2S,4R*)4-fluoroglutamine, is used to measure glutamine uptake in cells(Lieberman et al., 2011). Other pathways detected by this technique include, fatty acid metabolism using, [^{11}C] acetate-PET(Jadvar, 2011), glutamate metabolism via (S)-4-(3-[18F]Fluoropropyl)-L-glutamic acid (FSPG), which is a glutamate analogue(Baek et al., 2012) and amino acid metabolism with ^{11}C methionine (MET-PET)(Glaudemans et al., 2013). In addition to PET, magnetic resonance spectroscopic imaging (MRSI) has been used to monitor choline and NAD+ levels in tumors. Another method known as chemical exchange saturation transfer (CEST) has been shown to detect non labeled glucose uptake in the cells(Chan et al., 2012). Recent studies have shown the benefits of using dynamic nuclear polarization (a form of hyperpolarize MRI) in probing metabolic heterogeneity in cancer cells. Conversion of hyperpolarized pyruvate and glucose to lactate have been used in studies with tumor patients and models with promising results(Nelson et al., 2013; Rodrigues et al., 2013). While these techniques maybe powerful tools for cancer detection, they require further translational studies to prove their efficacy and ability to deal with the metabolic heterogeneity which is present with the tumor microenvironment. Furthermore, while the advantages of developing these techniques are undeniable, there is a need to develop more non-invasive methods for detection.

Metabolic pathways are crucial for the proliferation of cancer cells thereby presenting a new vulnerability. The question remains whether, these potential targets can be translated into successful treatment strategies. So far, several new drug targets which target either the uptake of nutrients or biosynthesis of macromolecules have been identified. However, the success rate has not been very satisfactory (Table 1). Targeting glucose uptake or the Warburg effect via targeting LDH or PDH has led to limited success. Nevertheless, there are several other targets in preclinical or clinical stages of development, which could result in effect cancer therapies. Drugs targeting *IDH* mutations, for example, have been successful in hematological cancers(Tateishi et al., 2015). Glutamine metabolism is another promising target for cancers that are dependent on glutamine. Currently, there are clinical trials being conducted with CB-

839 which a GLS1 inhibitor. Other drugs targeting different amino acid metabolic pathways are under preclinical investigation. The hope is that some of these can be translated into effective treatment strategies. There are of course several challenges; first of all, most metabolic pathways are redundant, and targeting one pathway may lead to usage of another pathway, therefore combinatorial therapies need to be developed. Also, similar to chemotherapy, which targets growing cells, metabolic pathways are used by all metabolically active cells and targeting them could lead to severe side effects, especially liver toxicity. Moreover, metabolic heterogeneity within the tumor as a result of the presence of different cell types presents a formidable challenge to efficacious therapy. However, a deeper understanding of the metabolic vulnerabilities of the cells and better metabolic stratification of patients will lead to successful therapy regimes.

Target pathway and Protein	Drugs	Development Stage
Glycolysis		
Glucose Transporter 1 (GLUT1)	WZB117, SILIBININ and RNAi	Preclinical studies
Hexokinases	2-DG, Ionidamine, 3-bromopyruvic acid and methyl jasmonate	Preclinical and clinical studies
Phospho-fructokinase 2 (isoform PFKFB3)	PFK158	Preclinical studies
Pyruvate Kinase isoform M2 (PKM2)	TLN-232 and RNAi	Preclinical and phase II clinical studies
Lactate Dehydrogenase A (LDHA)	GNE-140, FX11, galloflavin and RNAi	Preclinical studies
MCT1 and MCT4	AZD3965 and AZ93	AZD3965 in clinical development
TCA cycle		
Pyruvate dehydrogenase kinase 1 (PDK1)	Dichloroacetate (DCA) and RNAi	Approved for treatment of lactic acidosis. In phase I clinical trials
Pyruvate carboxylase	RNAi	Preclinical studies
α-ketoglutarate dehydrogenase	CPI-613	Preclinical and clinical studies
Isocitrate dehydrogenases	AG-120, AG-221, AG-881, and RNAi	Preclinical and clinical studies
Oxidative Phosphorylation		

Mitochondrial membrane potential	MKT-077	Clinical studies
Mitochondrial complex I	Metformin, phenformin	Phase III Clinical Trials
Mitochondrial complex III	Arsenic trioxide	Preclinical and clinical studies
Glutamine Metabolism		
Glutaminase (GLS1)	CB-839, BPTES and RNAi	Preclinical and clinical studies
Amino acid Metabolism		
Asparagine availability	L-Asparginase	Approved as anticancer agent
Arginine availability	PEG-BCT-100 (ADI-PEG20) AEB-1102	Clinical development: phase II clinical trials
Phosphoglycerate dehydrogenase (PHGDH)	RNAi	Preclinical studies Approved
Lipid synthesis		
Fatty acid synthase (FASN)	TVB-2640	Preclinical studies
ATP citrate lyase (ACL)	Hydroxycitrate	Preclinical studies
Acetyl-CoA carboxylase (ACC)	NDI-010976	Preclinical studies and clinical studies
Choline kinase	TCD-717, CK37, MN58b, RSM932A, and RNAi	TCD-717 is in clinical development
Nucleic Acid Metabolism		
Dihydrofolate reductase	Methotrexate, pemetrexed, and pralatrexate	Approved as anticancer agents
Thymidylate synthase	5-Fluorouracil	Approved as anticancer agents
Adenine/adenosine deaminase	Pentostatin	Approved as anticancer agents
DNA polymerase/ ribonucleotide reductase	Gemcitabine, Cytarabine and Fludarabine	Approved as anticancer agents

Table 1: Selected metabolic targets under different stages of development. Adapted from Outschoorn et al, 2016(Martinez-Outschoorn, Peiris-Pagés, Pestell, Sotgia, & Lisanti, 2016) and Heiden and DeBerardinis 2017(Matthew G Vander Heiden & DeBerardinis, 2017)

2. Aims

Breast cancer is a broad spectrum of diseases affecting the mammary gland. This diversity is due the high variability in the genomic and microenvironmental landscape of the tumors. Therefore, it is reasonable to assume that metabolism is also variable within breast cancer. However, reprogramming of metabolic pathways itself is a common phenomenon of nearly all breast cancers. While glycolysis remains the mainstay of this rewiring, most breast cancer cells also depend on alternative sources of carbon, including amino acids, especially glutamine, which can also be important sources of nitrogen within the cells. Recent advances in this field have highlighted the importance of glutamine and other amino acids in tumor progression. Therefore, investigation of the cycling of carbon and nitrogen atoms in these pathways may provide an insight into the metabolic vulnerabilities of cancer cells which may then be utilized to target them.

The aim of this study was to investigate the role of amino acid metabolism in breast cancer progression *via*

1. Identifying activated amino acid metabolism pathways within different breast cancer cell lines using genomic, proteomic and metabolomic approaches.
2. Using RNAi and chemical inhibitors to perturb the identified pathways and study the effect on cell growth.
3. Elucidating metabolic mechanisms underlying the effect of identified pathways on the growth of cancer cells.
4. Exploring the role of transcription factors in the regulation of identified pathways.

3. Materials and Methods

3.1 Materials

3.1.1 Instruments

Aushon 2470 contact printer	Aushon BioSystems (Billerica, USA)
Biohit Proline multichannel pipette	Sartorius (Göttingen, Germany)
Cell counter CASY	Roche Innovatis AG (Bielefeld, Germany)
Cell culture hood HERA Safe	Thermo Fisher Scientific (Waltham, USA)
Cell culture incubator	Heraeus (Hanau, Germany)
Centrifuges	Eppendorf AG (Hamburg, Germany)
Extracellular flow bioanalyzer (Seahorse XF96)	Agilent Technologies (Santa Clara USA)
Flow Cytometer FACS Calibur	Becton Dickinson (New Jersey, USA)
Gel documentation system	Herolab GmbH (Wiesloch, Germany)
Infinite M200 microplate reader	Tecan Group (Männedorf, Switzerland)
Molecular Devices Microscope IXM XLS	Molecular Devices (Sunnyvale, USA)
Nanodrop ND-1000 spectrophotometer	Thermo Fisher Scientific (Waltham, USA)
Odyssey Infrared Imaging System	Li-Cor Biosciences GmbH (Bad Homburg, Germany)
Pipetboy acu pipette	INTEGRA Biosciences (Fernwald, Germany)
Pipetman® pipette	Gilson (Limburg, Germany)
Protein Gel Apparatus MiniProtean II	Bio-Rad (Hercules, USA)
Sentrix Human HT-12 v4 BeadArrays	Illumina (San Diego, USA)
Spectrophotometer Nano Drop nd-1000	Thermo Fisher Scientific (Waltham, USA)
SW41 Ti Rotor and Tubes	Beckman Coulter (Brea, USA)
Thermocycler	Applied Biosystems (Foster City, USA)
Titramax 100 rocking platform	Heidolph (Schwabach, Germany)
Trans-Blot SD Semi-Dry Electrophoretic Transfer	Bio-Rad (Hercules, USA)
Tube Rotator	VWR (Darmstadt, Germany)

Ultracentrifuge, Beckman L8-70M	Beckman Coulter (Brea, USA)
Vacuboy aspiration device	INTEGRA Biosciences (Fernwald, Germany)
Vortex mixer	neoLab (Heidelberg, Germany)
xCelligence Real-time cell analyzer (RTCA)	Roche Diagnostics (Mannheim, Germany)
HPLC	
GC MS	
Mass spectrometry	

3.1.2 Chemicals

Acrylamide/bisacrylamide 37.5:1	Carl Roth (Karlsruhe, Germany)
Ammoniumperoxodisulfate (APS)	Sigma-Aldrich (Saint-Louis, USA)
B-chloro-L-alanine	Sigma-Aldrich (Saint-Louis, USA)
CASYton	Roche Innovatis AG (Bielefeld, Germany)
cOmplete Mini Protease Inhibitor Cocktail	Roche Diagnostics (Mannheim, Germany)
Dimethylsulfoxide (DMSO)	Sigma-Aldrich (Saint-Louis, USA)
EDTA	Sigma-Aldrich (Saint-Louis, USA)
Ethanol	Sigma-Aldrich (Saint-Louis, USA)
Fast Green FCF	Carl Roth (Karlsruhe, Germany)
Hoechst 33258	Sigma (Krefeld, Germany)
Isopropanol	Greiner Bio-One International GmbH (Kremsmünster, Austria)
Metformin	Sigma-Aldrich (Saint-Louis, USA)
Methanol	Greiner Bio-One International GmbH (Kremsmünster, Austria)
M-PER mammalian protein extraction reagent	Thermo Fischer Scientific (Rockford, USA)
NaCl	VWR International (Darmstadt, Germany)
NaOH	Sigma-Aldrich (Saint-Louis, USA)
non-DEPC treated nuclease-free water	Ambion, Thermo Fisher Scientific

	(Waltham, USA)
PhosSTOP Phosphatase Inhibitor Cocktail	Roche Diagnostics (Mannheim, Germany)
Protein Marker Precision Plus Protein Dual Color	BioRad
Proteinase K	Sigma-Aldrich (Saint-Louis, USA)
RNAiMax Reagent	Invitrogen
Rockland Blocking Buffer	Rockland Immunochemicals Inc. (Limerick, USA)
Rotenone	Sigma-Aldrich (Saint-Louis, USA)
Roti®-Load 1, 4x sample loading buffer	Carl Roth (Karlsruhe, Germany)
SDS	Carl Roth (Karlsruhe, Germany)
siRNAs	Dharmacon, Thermo Fisher Scientific (Waltham, USA)
Sodium Citrate Tribasic Dihydrate	AppliChem (Darmstadt, Germany)
NaF	
Na2VO4	
TaqMan® Fast Universal PCR Master Mix (2x)	Applied Biosystems (Foster City, USA)
TEMED	Carl Roth (Karlsruhe, Germany)
Tricine	Carl Roth (Karlsruhe, Germany)
Tris HCl	Sigma-Aldrich (Saint-Louis, USA)
Tris-base	Sigma-Aldrich (Saint-Louis, USA)
Triton X-100	Sigma-Aldrich (Saint-Louis, USA)
Tunicamycin	Tocris Bioscience
Tween 20	Sigma-Aldrich (Saint-Louis, USA)

3.1.3 Assay Kits

ABSOLUTE qPCR Mix	Thermo Fisher Scientific (Waltham, USA)
BCA Protein Assay Kit PierceTM	Thermo Fisher Scientific (Waltham, USA)
cDNA Synthesis Kit	Thermo Fisher Scientific (Waltham, USA)
RNeasy Mini kit	Qiagen (Hilden, Germany)

qPCR MasterMix (RT-QP2X-03+NR)	Eurogentec (Lüttich, Belgium)
RevertAid™ H Minus First Strand cDNA synthesis kit	Fermentas, Thermo Fisher Scientific (Waltham, USA)
RNeasy Mini Kit	Qiagen (Hilden, Germany)
TaqMan® MicroRNA Assays	Applied Biosystems (Foster City, USA)
Universal Probe Library (UPL)	Roche Diagnostics (Mannheim, Germany)
Seahorse kits	Agilent Technologies (MA, USA)

3.1.4 Cell culture

All breast cancer cell lines were purchased from ATCC (LGC Standards GmbH, Wesel, Germany).

0.25% Trypsin EDTA Solution	Gibco BRL (New York, USA)
DMEM	Gibco BRL (New York, USA)
DMEM F12	Gibco BRL (New York, USA)
DMSO	PAN Biotech GmbH (Aidenbach, Germany)
DPBS	Gibco BRL (New York, USA)
Fetal Bovine Serum	Gibco BRL (New York, USA)
L-glutamine, 200mM	Gibco BRL (New York, USA)
OptiMEM	Gibco BRL (New York, USA)
RPMI 1640 (A10491-01)	Gibco BRL (New York, USA)
Sodium pyruvate, 100mM	Gibco BRL (New York, USA)

3.1.5 Glass and Plastic ware

1.5 mL micro centrifuge tube	Eppendorf AG (Hamburg, Germany)
10cm Ø Petri dish	Techno Plastic Products (TPP) AG (Trasadingen, Switzerland)
15mL conical tube	Becton Dickinson (New Jersey, USA)
2 mL micro centrifuge tube	Eppendorf AG (Hamburg, Germany)

50mL conical tube	Becton Dickinson (New Jersey, USA)
6-well plate, flat bottom, transparent	Nunc, Thermo Fisher Scientific (Waltham, USA)
96-well plate, flat bottom, transparent	Becton Dickinson (New Jersey, USA)
96-well plate, flat bottom, µCLEAR®, black	Greiner Bio-One International GmbH (Kremsmünster, Austria)
96-well plate, flat bottom, white	PerkinElmer (Waltham, USA)
Adhesive Optically Clear Plate Seal	Thermo Fisher Scientific (Waltham, USA)
AMICON® Ultra-4 filtration units	Merck Millipore (Darmstadt, Germany)
Cell Culture Flasks, T-25, T-75, T-175	Greiner Bio-One International GmbH (Kremsmünster, Austria)
Cell Scraper	Corning (Corning, USA)
Cry vials 1.8mL	Nunc, Thermo Fisher Scientific (Waltham, USA)
Filter tips, 10µL, 20µL, 100µL, 200µL, 1000µL	Neptune Scientific (San Diego, USA)
HumanHT-12 v4 BeadChips	Illumina (San Diego, USA)
Oncyte® Avid Nitrocellulose Film-Slide	Grace Bio-Labs (Bend, USA)
PCR strips	Steinbrenner Laborsysteme GmbH (Wiesenbach, Germany)
PVDF membrane Immobilon-P	Merck Millipore (Darmstadt, Germany)
RTCA E-plates	Roche Diagnostics (Mannheim, Germany)
Seahorse Microplates and cartidges	Agilent Biotechnologies (MA, USA)
Sentrix Human HT-12 v4 BeadArrays	Illumina (San Diego, USA)
Serological pipettes 2.5mL, 5mL, 10mL, 25mL, 50ml	Becton Dickinson (New Jersey, USA)
Trans-well system (5.0µm pore size)	Corning (Corning, USA)
Whatman 3 MM filter paper	GE Healthcare (Little Chalfont, United Kingdom)

3.1.6 Software

GraphPad Prism 5	GraphPad Software, Inc. (La Jolla, USA)
Image Studio	LI-COR Biosciences (Lincoln USA)
Inkscape	Software Freedom Conservancy, Inc. (NY USA)
Molecular Devices Analysis Software	Molecular Devices (Sunnyvale, USA)
Odyssey 2.1	LI-COR (Lincoln, USA)
Roche UPL Design Center	Roche Diagnostics (Mannheim, Germany)
SDS 2.2	Applied Biosystems (Foster City, USA)
Seahorse analyzer	Agilent Technologies (MA, USA)
xCelligence Real Time Cell Analyzer (RTCA) software 1.2	Roche Diagnostics (Mannheim, Germany)

3.1.7 Database

METABRIC mRNA data	https://www.synapse.org/#!Synapse:syn1688369/wiki/27311
TCGA mRNA data	TCGA_BRCA_exp_HiSeqV2-2015-02-24

3.1.8 Buffers and solutions

Lysis buffer for mammalian cells

MPER Buffer 10ml, 1tbl PhosSTOP Phosphatase Inhibitor, 1tbl Complete Mini Protease Inhibitor Cocktail, 10µl Na_2VO_4, 100µl NaF

4% SDS-PAGE stacking gel

1.33mL Acrylamide, 2.55mL 1M Tris pH 6.8, 100µl 10%SDS, 200µl 10%APS, 10µl TEMED, 6mL ddH2O

12.5 % SDS-PAGE separating gel

8.3 ml Acrylamide:Bis, 5 ml 4x separation gel buffer, 0.2 ml 10% SDS, 6.4 ml ddH2O, 100 µl 10% APS, 20 µl TEMED

SDS-PAGE running buffer

30.3 g Tris Base (0.25 M), 144.1 g Glycine (1.92 M), 0.1% SDS (w/v), add 1L dH2O

Western Blotting buffers

Cathode buffer: 40mM aminohexanoic acid, 20% ethanol (v/v)

Anode buffer I: 300mM Tris Base, 20% ethanol, and 500ml dH20

Anode buffer II: 25mM Tris Base, 20% ethanol, and 500ml dH20

Washing buffer: 0.1% Tween®20 in TBS (TBST)

Blocking buffer: 50% Rockland blocking buffer, 5Mm NaF, 1Mm Na_3VO_4

Secondary antibody buffer: Washing buffer + 0.02% SDS (w/v)

10X TBS

1.37M NaCl, 200mM Tris, pH 7.6

1x TBS

50mM Tris-HCl pH 7.4, 150mM NaCl

1X TBST

0.1% Tween 20 in 1x TBS

4x RPPA printing buffer

10% Glycerol, 4% SDS, 10mM DTT, 125mM Tris, pH 6.8

FCF staining solution

0.005% Fast Green FCF, 10% acetic acid, 30% ethanol

FCF destaining solution

10% acetic acid, 30% ethanol

3.1.9 Antibodies

Primary antibody

Protein name	Host	Product ID (Company)
beta-Actin	mouse	Actin (clone C4) (MP Biomedicals USA)
beta-Actin	rabbit	Actin 21-33 (Sigma Aldrich USA)
pAMPKa	rabbit	sc-33524 (Santa Cruz Biotechnology USA)
ARG2	rabbit	GTX118048 (Genetex USA)

ASS1	rabbit	HPA020896 (Sigma Aldrich USA)
Bcl2-L-4 (Bax)	mouse	2772 (Cell Signaling Technology USA)
GLS1	Rabbit	ab156876 (Abcam plc UK)
GPT2	Mouse	sc-398383 (Santa Cruz Biotechnology USA)
c-Myc	Rabbit	sc-764 (Santa Cruz Biotechnology USA)
Cleaved PARP	Rabbit	9541 (Cell Signaling Technology USA)
PC	Rabbit	HPA058765 (Atlas Antibodies)
PDH	Rabbit	3205 (Cell Signaling Technology USA)
pRPS6	Rabbit	4858 (Cell Signaling Technology USA)

3.1.10 siRNAs

siRNA	Annotation	Catalogue Number	Target Sequence
siGENOME Non-Targeting siRNA Pool #2	NTC	D-001206-14-05	UAAGGCUAUGAAGAGAUAC
			AUGUAUUGGCCUGUAUUAG
			AUGAACGUGAAUUGCUCAA
			UGGUUUACAUGUCGACUAA
ON-TARGETplus non-targeting Pool	siControl	D-001810-10	UGGUUUACAUGUCGACUAA
			UGGUUUACAUGUUGUGUGA
			UGGUUUACAUGUUUUCUGA
			UGGUUUACAUGUUUUCCUA
siGenome Set of 4 Upgrade siRNA GPT2	siGPT2	D-004173-01	UCAAAUGGCUCCAGACAUG
		D-004173-03	GUGAAAGACUUCCACAUCA
		D-004173-04	UCAAGAAGGUGCUGUACGA
		D-004173-18	GUGAAAAGGUUAAAUCGUA
siGenome Set of 4	siPC	D-008950-01	GAAAGCAGAUGAAGCCUAU

Upgrade siRNA PC		D-008950-03	GAGCUGAUGUGGUGGAUGU
		D-008950-18	GGAUAAUGCUUCCGCCUUC
		D-008950-19	UCUCUGAGCGAGCGGACUU

siRNA pools composed of four different siRNA sequences targeting *MYC* (Cat. No. M-003282-04) and *ATF4* (Cat No. M-005125-02) were picked from the human siRNA library of siGENOME (Dharmacon).

3.1.11 Primers

Gene	Primer Left	Primer Right	Probe #
ATF4	ggtcagtccctccaacaaca	ctatacccaacagggcatcc	88
GPT	gggaaggcacctaccacttc	ttggcatggaacctgctc	66
GPT2	ggatcttcattcctgccaaa	acatgtctggagccatttga	75
MYC	caccagcagcgactctga	gatccagactctgacctttgc	34
PUM1	tcacatggatcctcttcaagc	cctggagcagcagagatgtat	86

Methods

3.1.12 Cell Culture and Growth Conditions

All breast cancer cell lines were obtained from ATCC. Cell lines were regularly authenticated by multiplex cell line authentication (Multiplexion GmbH, Friedrichshafen, Germany) and tested for mycoplasma contamination. The cell lines were cultured in RPMI 1640 media with 10% FBS and incubated at 37^{o}C with 5% CO_2 in a humidified atmosphere. Cells were passaged approximately every 3 days under aseptic conditions in a laminar air-flow hood. Briefly, medium was aspirated from the flask and the cells were washed with PBS following which 0.25% trypsin-EDTA was added and the cells were returned to 37^{o}C. Once the cells detached, growth medium was added to neutralize the trypsin. The cells were counted using the CASY counter. For counting, 50µl of cell suspension was diluted in 10ml CASYton and counted automatically. Depending on their growth and cell size, 1-2 x 10^6 cells were seeded into a 75 cm^2 flask with a final volume of 15ml. Cells were used upto passage number 20 for experiments after which new cells were thawed.

To generate frozen cell stocks, the trypsinized cells were counted as described above and centrifuged at 1200 rpm for 5min. The resulting pellets were resuspended in freezing media (70% growth media, 20%FBS, 10%DMSO) to a concentration of 1 x 10^6 cells per ml media and aliquoted into 1.5ml cryovials, The cell suspension was slowly cooled down in an isopropanol bath at -80^{o}C for a minimum of 24h before transferring to a liquid nitrogen container for long term storage.

Frozen vials of cells were recovered by thawing quickly in a 37^{o}C water bath. The cell suspension was then pipette into a 75cm^2 culture flasks with pre-warmed growth medium. Cells were allowed to attach overnight before aspirating the medium and replacing it with fresh growth medium.

3.1.13 siRNAs and Transfections

Cells were seeded to a confluency of 80%. After overnight incubation, transfections were performed with RNAiMax® according to manufacturer's instructions. Unless otherwise stated, siRNAs were used at a final concentration of 10nM. The transfection protocols were independent of the plate type, only the volumes of reagents were different.

Plate Format	Vol. of OptMEM added (µl)	Vol. of RNAiMax added (µl)	Final concentration of siRNA(nM)	Total volume of transfection mix (µl)
96 well plate	19.2	0.3	10	20
6 well plate	231	3	10	240
10 cm dish	955	15	10	1000

Table 2: Volumes of reagents used for transfections

A pre-mix of RNAiMax and Opti-MEM was prepared, and in parallel siRNAs were diluted in Opti-MEM. The siRNA and RNAiMax pre-mix were mixed and incubated for 5min. During this incubation, media was aspirated from the cells and replaced with fresh growth media. Post incubation, the transfection mix was added to the cells. Cells were then incubated in 37^{o}C, 5% CO_2 humidified atmosphere for different time points depending on the assay being performed.

Knockdown efficiency was determined by qPCR and western blot techniques (described below).

3.1.14 Inhibitor Treatment

Cells were seeded to a confluency of 60%. After overnight incubation cells were treated with inhibitors diluted in growth media, water (DMSO for Rotenone) was used as control. Cells were incubated in 37^{o}C, 5% CO_2 humidified atmosphere for different time points depending on the assay being performed.

3.1.15 Analysis of RNA expression

3.1.15.1 mRNA isolation

mRNA was isolated using the "RNeasy Mini" Kit from Qiagen according to manufacturer's recommendations. Extracted RNA was eluted in 50µl of nuclease free water.

3.1.15.2 Quantitative RT PCR

Primers and probes were designed for Taqman® qRT-PCR using the Roche UPL Design Center (Refer to section 3.1.11 for Primer sequences and Probe numbers). For quantification, first 1ug of total RNA was reverse transcribed to cDNA using the RevertAid™ H minus First strand Kit.

For the Taqman assay the cDNA was first diluted to 2ng/µl. For each gene to be quantified a Mastermix was prepared consisting of 5.5µl 2x ABgene mastermix, 0.11µl forward primer, 0.11µl reverse primer and 0.11µl Taqman probe per well. 6µl of the Mastermix was pipetted with 5ul of cDNA into 384 well plates in triplicates.

A plate layout document was prepared using the SDS software and the PCR conditions were set as follows, 2min at 50^{o}C, 15min at 95^{o}C followed by 45 cycles of 15s at 95^{o}C and 60s at 60^{o} C. Raw data was analysed using the SDS software with the ΔΔCt method(Yuan, Reed, Chen, & Stewart, 2006). The Ct values were normalized to housekeeping gene *PUM1*.

3.1.15.3 Microarray

Genome-wide gene expression profiling is performed using HumanHT-12 v4 BeadChips (Illumina, San Diego, CA, USA). Raw probe intensities are back-ground corrected using negative control probes and a normal+exponential (normexp) convolution model. An offset value (16) is added to the data in order to prevent negative expressions in the background correction step. Data are then normalized via quantile normalization using the negative and positive probes(Shi, Oshlack, & Smyth, 2010) (Shi et al., 2010). Control probes are removed and intensities are log2

transformed after normalization. DKFZ microarray core facility performed sample preparation, RNA quality control and hybridization. Khalid Abnaof performed data normalization.

3.1.16 Protein Analysis

3.1.16.1 Western Blotting

3.2.5.1.1 Protein Isolation

After indicated times of incubation post transfection or inhibition, cell lysates were extracted. Cells were placed on ice, media was aspirated and cells were washed with ice cold PBS. Cells were lysed with M-PER lysis buffer (10ml MPER Buffer, 1x Complete Mini Protease Inhibitor Cocktail and 1x Phospho-Stop phosphatase Inhibitor) and detached and homogenized by scraping. The lysis reaction was collected in 1.5ml centrifuge tubes and incubated at 4^{o}C for 30min on a vertical rotor. The lysate was centrifuged at 13,000rpm for 10min and the supernatant was transferred to a fresh 1.5ml centrifuge tube. Lysates were stored at -80^{o}C.

3.2.5.1.2 Protein Quantification

Protein concentrations of the lysates were determined using the BCA™ protein assay kit. Protein concentrations were hence, determined by following the kit protocol. Briefly, BSA standards of different concentrations (2000µg/ml, 1500µg/ml, 1000µg/ml, 750µg/ml, 500µg/ml, 250µg/ml, 125µg/ml, 25µg/ml and 0µg/ml) were prepared according to the manufacturer's recommendations. All standards were diluted in PBS. 25µl of each standard was pipetted into a 96-well microplate in duplicates. 5µl of each sample was pipetted into the plate in duplicates as well. Hence, the dilution factor of samples compared to standards in 1:5.

BCA™ working reagent is prepared freshly for each assay by mixing Reagent A with Reagent be in a 50:1 ratio. The 200µl of the working reagent is then added to each well of the microplate.

The plate was protected from light and incubated at 37^{o}C for 30min. Thereafter, the absorbance at 562nm was measured on the TECAN infinite200 plate reader.

A standard curve was prepared after blank correcting the absorbance readings of the BSA standards and protein concentration of the samples were calculated from this curve. The obtained concentrations were then multiplied by 5 to account for the dilution factor.

Cell lysates for gel electrophoresis were then prepared for gel electrophoresis by mixing with protein loading buffer (4X RotiLoad) in a 1:4 dilution and heated to 95^{o}C for 5min for denaturation.

3.2.5.1.3 SDS PAGE

Gel electrophoresis is a method by which protein can be separated according to their size. In SDS PAGE (Sodium Dodecyl Sulphate Polyacrylamide Gel Electrophoresis) heat denatured proteins are coated with negatively charged SDS which therefore, migrate towards the cathode (irrespective of their intrinsic charge). The polyacrylamide gel serves as a sieve to retard the larger proteins while the smaller ones move faster and thus separates the different protein in the lysate spatially.

The gels for electrophoresis were prepared prior to the experiment. Depending on the size of the protein to be detected different % acrylamide running gels were cast. The running and stacking gels were prepared as indicated earlier. The running gel was prepared first and poured into the gel casting chamber upto 2.5cm of the chamber and covered with isopropanol. Once the gel polymerized the isopropanol was discard and 4% stacking gel was casted into the chamber and a comb was inserted to create wells where protein lysates could be loaded. After polymerization the gels were wrapped in wet paper towels and stored at 4^{o}C till they were used.

On the day of the experiment, the gels were loaded onto the running box clamp of the MiniProtean gel assembly (BioRad) and the clamp was placed into the gel box. The clamp and

the box were filled with 1X running buffer. The comb was then removed and the wells were loaded with 5µl molecular weight marker (Precision Plus Protein™ Dual Color Standard) and 20µg protein lysate. Electrophoresis was performed at 110V for 75min.

3.2.5.1.4 SemiDry Transfer

Blotting solutions were prepared according to the Section 3.1.8. Whatman filter papers and PVDF membranes (Millipore) were cut to a size of 6.5 x 9cm. The membranes were activated in ethanol and then soaked in Anode II blotting solution. For the transfer a sandwich was prepared with 4 filter papers soaked in Anode I solution, followed by 2 filter papers soaked in Anode II. The membrane was then placed and the gel was layered on top of the membrane carefully to avoid formation of bubbles. Finally, 6 filter papers soaked in Cathode solution were placed on top. The blotter was then assembled and run at 25V for 1h. After the transfer the membranes were blocked with blocking buffer (prepared as described in 3.1.8) for 1h at room temperature.

3.2.5.1.5 Antibody Incubation and Detection

After blocking, the membranes were incubated with primary antibodies (diluted in blocking buffer to concentrations indicated in table) overnight at 4^{o}C. After primary antibody incubation the membranes were washed 3X for 10min each with TBST (1X TBS with 0.1% Tween-20). The membranes were then incubated with secondary IRDye®680 or IRDye®800 conjugated antibodies (diluted in TBST to concentrations indicated in table) for 1h at room RT on a shaker. The membranes were washed again with TBST (3X for 10min each) and scanned and analyzed with the Odyssey® Infrared Imaging System. Local background corrections and β-actin normalization was performed for quantification.

3.1.16.2 RPPA

Another technique used for analysis of protein expression was Reverse Phase Protein Array (RPPA)(Paweletz et al., 2001).

In case of cell line samples, the lysates were harvested and protein concentration was determined as described above. In case of tumor specimens, the frozen samples were homogenized using a bead mill and tissue protein extraction reagent (50mM Tris, pH 8.5, 138mM NaCl, 2.7mM KCl, 1% Triton X-100). Protein concentration was determined in the same way as for the cell line samples, i.e., with the BCA kit.

Tumor and cell line lysates were adjusted to a total protein concentration of 2 µg/µl. Samples were mixed with 4 x RPPA printing buffer (10% glycerol, 4% SDS, 10 mM DTT, 125 mM Tris–HCl, pH 6.8) and denatured at 95°C for 5min. The lysates were then pipetted into 348-well plates and centrifuged for 2min at 200 x g. As internal controls a dilution series of tumor samples/cell line pools were created. All samples were printed as technical triplicates on Oncyte® Avid Nitrocellulose Film-Slides using a Aushon 2470 contact printer equipped with 185 µm solid pins (1.6nl sample per spot, average spot diameter 250µm). The humidity during the printing run was kept constant at 80%. Slides were stored after the print run at -20°C with desiccant. After spotting the slides were blocked for 2h at room temperature with blocking buffer (TBS (50%, v / v with 5mM NaF and 1mM Na3VO4).

Post blocking, the arrays were incubated with target-specific primary antibodies at 4°C overnight. Representative subarrays were incubated without primary antibody and served as “blank” control. After incubation the slides were washed 4 x 5min with TBST and subsequently incubated with Alexa Fluor® 680 F(ab')2 fragments of goat anti-mouse IgG or anti-rabbit IgG in 1:12000 dilution for 1h at RT in dark. Slides were again washed 4 x 5min with TBST followed by two final washing steps with ultra-pure water for 5min. The slides were then air dried and imaged. Every ninth slide of each run was stained using Fast Green FCF protein dye for total protein quantification and was used for normalization. The slides were scanned with an excitation wavelength of 685nm and a resolution of 21 µm with the Odyssey® Infrared Imaging System and the resulting TIFF images (16 bit) were used for further analysis.

Signal intensities of individual spots were quantified using GenePixPro 7.0 software. The acquired TIFF image of each slide and gene pix array list file (generated by the printer to map the sample location on the slide) was matched into a gene pix result file. At this step, a visual inspection of each spot was performed and slides without uniform background signal were excluded from further analysis. RPPA raw data preprocessing and quality control were performed using the *RPPanalyzer* R-package (Mannsperger, Gade, Henjes, Beissbarth, & Korf, 2010). The gene pix result files as well as sample and antibody information text files were required for further raw data analysis. The raw signal intensities of the control samples were plotted against the respective total protein concentration. Only data of antibodies showing a linear correlation between target signal intensity and protein concentration were used for further analysis. Next, target signals were normalized to the total protein amount per spot via Fast Green FCF control. After median calculation of technical replicates, normalized target signal intensities were plotted against the signal intensities obtained by incubation of primary antibody controls (blank signal).

Untreated cell line data generation and raw data processing was done by Stephan Bernhardt, PhD student, Division of Molecular Genome Analysis.

Experiments with siRNA and inhibitor treatments were done by me as described above (Section 3.2.2 and 3.2.3), including protein harvest and protein concentration determination. Sample preparation for RPPA was done with the help of Stephan Bernhardt. Antibody incubation and imaging of slides were done by Stephan Bernhardt and me. Machine running and raw data processing was done by Stephan Bernhardt.

RPPA of tumor specimens was done by Stephan Bernhardt and the normalized protein data was further analyzed by collaboration partners at the Institute of Physics at the Freiburg Institute for Advanced Studies (Freiburg, Germany). Details of dataset generation and analysis can be found in the thesis of Stephan Bernhardt and the subsequent publication(Bernhardt et al., 2017). Briefly, for statistical analysis, different groups were compared using the Kruskal-Wallis Rank Sum Test(Kruskal & Wallis, 1952) and p values were adjusted using Benjamini-Hochberg procedure(Benjamini & Hochberg, 1995).

3.1.16.3 Mass Spectrometry

3.2.5.3.1 Sample preparation

Cells were washed once with PBS, scratched, collected and transferred into a 1.5 ml Eppi. Sample was centrifuged at max. speed at 4°C, supernatant was removed, pellet snap-frozen and stored at -20 °C until further processing. Cells were lysed by adding 300 µl of 8M Urea buffer (8 M Urea, 100 mM TrisHCl, pH 8.5) followed by sonification and centrifugation for 5 min at max. speed at 4 °C . Protein content was determined using the BCA Protein Assay Kit (Pierce, Thermo Scientific). Prior to digestion the denaturation and alkylation of proteins were performed by treating samples with 2 mM DTT (30 min at 25°C), followed by 11 mM iodoacetamide (20 min at room temperature in the dark).100 µg of protein were digested according using Lys-C (Wako, 1:40, w/w, overnight under gentle shaking, 30°C) and immobilized trypsin beads (Applied Biosystem, 1:80, w/w, 4 hrs under rotation, 30°C). Lys-C digestions product were diluted four times with 50 mM ammonium bicarbonate before continuing the tryptic digestion that was stopped through acidification with 5 µL of triflouracetic acid. Fifteen µg of each resulting peptide mixture were then desalted on Stage Tip (Rappsilber et.al., 2007), the eluates dried and reconstituted to 15 µL in 0.5% acetic acid.

3.2.5.3.2 LC-MS analysis

5 microliters of each sample were injected in duplicate on a LC-MS/MS system (NanoLC 400 [Eksigent] coupled to Q Exactive Plus [Thermo]), using a 240 minutes gradient ranging from 5% to 40% of solvent B (80% acetonitrile, 0.1 % formic acid; solvent A= 5 % acetonitrile, 0.1 % formic acid). For the chromatographic separation 100 cm long MonoCap C18 HighResolution 2000 (GL Sciences) was used.

The nanospray source was operated with spay voltage of 2.4 kV and ion transfer tube temperature of 260 °C. Data were acquired in data dependent mode, with a top10 method (one survey MS scan with resolution 70,000 at m/z 200, followed by up to 10 MS/MS scans on the

most intense ions, intensity threshold 5,000). Once selected for fragmentation, ions were excluded from further selection for 45 seconds, in order to increase new sequencing events.

3.2.5.3.3 Data analysis

Raw data were analyzed using the MaxQuant proteomics pipeline (v1.5.3.30) and the built in the Andromeda search engine (Cox, Neuhauser et al. 2011) with the human Uniprot database. Carbamidomethylation of cysteines was chosen as fixed modification, oxidation of methionine and acetylation of N-terminus were chosen as variable modifications. The search engine peptide assignments were filtered at 1% FDR and the feature match between runs was enabled; other parameters were left as default. Raw data analysis was performed by Nadine Royla.

Data dependent acquisition (DDA) in label-free quantification (LFQ) of peptides abundances in mass-spectrometry (MS) has stochastic precursor selection and low sampling efficiency (Cotte-Rodriguez, Miao, Zhang, & Chen, 2013; Matthiesen & Bunkenborg, 2013). This intrinsic feature of mass-spectrometry technology poses the problem that protein expression is sometimes not fully quantifiable, i.e. signals are not determined for those peptides whose abundance have not reached the detection limits. This was particularly the case in our study of high throughput protein expression in different cell-lines (MDA-MB231, MDA-MB468 and MCF7). Many proteins were not expressed across the samples in the data. This implies that conventional t-test based approaches cannot be applied directly to test of differentially expressed proteins between different cell-lines. A common way to treat these undetermined features is by excluding them from the analysis (Noble & MacCoss, 2012). However, the expressions of these features might not be missing in all conditions or all replicates of a condition.

In order to account for this issue we developed the *double detection* procedure, which comprises a detection step *detection test* as first step and in the second step a subsequent moderated t-test based approach is used either via the “limma” method.

First Step: The *detection test* is a one-sided t-test to investigate whether expression values of a particular feature in a given sample group are statistically significant higher than a defined threshold, meaning there is a significant detected protein expression. The threshold was set to the average of the minimum observable expression value per sample in a given experimental condition (here cell-line). Formally, this means testing for the null hypothesis:

$H0 : Arg\_Avr(Ct)c,m > Arg\_Avr(min(Ct)c)$, where *m* denote features and the conditions *c* are factor combinations of cell-line type and replicates factors. The *detection test* aims to filter out features that are undetectable in a given sample group. Thus, it ensures the applicability of t-test based significance tests in the subsequent step.

Second Step: The *Moderated test* Features, which passed the detection test are checked for their differential expression using the "limma" method utilizing empirical Bayes (G. Smyth, 2005; G. K. Smyth, 2004). However, many features did not pass the *detection test*. The number of which varies between ~700 and ~800 depending on the cell-lines under comparison. These features can be very informative, particularly when they pass the *detection test* in one condition in a comparison and measured in more than one peptide in each replicate of that condition. However, they cannot be tested in the second step properly. In order to get useful information from these few features we computed a quasi- log fold change by imposing the missing values to be the equal to $Arg\_Avr(min(Ct)c)$ -1. Data analysis was done by Dr. Khalid Abnaof.

3.1.17 Functional assays

3.1.17.1 Cell Counting Assay

Cell growth under different treatment (siRNA, inhibitor and media) conditions were analyzed with a microscopy based nuclei counting method. Cells were seeded in clear-bottomed 96 well black plates and after overnight incubation they were transfected with siRNA or treated with inhibitors. At different time points DNA was stained with intercalating dye Hoechst-33258 (1:1000 dilution in growth media) for 45min. Subsequently, the plates were imaged with a molecular devices microscope IXM XLS. All nuclei were defined by Hoechst signals within a

certain size and intensity and were detected and counted by the Molecular Devices Software. The number obtained was considered as cell number.

3.1.17.2 RTCA-based Proliferation Assay

Cell proliferation rates were also determined with the xCelligence Real Time Cell Analyzer (RTCA). The RTCA system uses plates which are similar to the 96 well cell culture plates, but are in A 16 well format. The plates are provided with golden electrodes at the bottom which can sense changes in impedance caused by cell attachment. Increase in electrical impedance can be due to increase in the number of cells attaching to the surface or increase in the attachment ability of the cells.

For RTCA-based proliferation assays, RTCA E plates were used. Prior to seeding, background impedance was measured with 100µl media. For measurement of growth rates under different nutrient conditions, the cells were seeded directly in the indicated media and allowed to grow for 5 days. In case of transfection or inhibitor treatment, the day after seeding, the cells were treated with the respective conditions and allowed to grow for 72h. Cell Index values were recorded every 15 mins. The RTCA machine was kept in a 37^{o}C incubator with 5% CO_2 and a humidified atmosphere.

3.1.17.3 WST Cell Viability Assay

One of the methods to assess Cell viability was the WST-1 assay from Roche which measures the NADPH content of the cells. For this assay cells were seeded in transparent 96-well plates and after overnight incubation cells were treated with different media. 72h after media change, 10µl of WST-1 reagent was added to each well and absorbance was measured at 450nm using the TECAN infinite200. In order to perform background correction, WST-1 was also added to wells containing only media without cells and the absorbance values of these wells were subtracted from all others.

3.1.17.4 Cell Titer Glo Assay

Cell titer Glo assay from Promega was second assay used for measuring cell viability. This method detects the ATP in cells which is an indication of the metabolic activity. The incubation with the assay reagent results in lysis of the cells which can then release its ATP. Luciferin in the assay is catalyzed by UtraGlo® Luciferase and ATP to generate oxyluciferin which can be detected via Luminescence. The resulting signal serves as a quantification of ATP in the wells and thereby the metabolic activity of the cells in the well.

For this assay cells were seeded into opaque white 96-well plates and treated after overnight incubation with siRNA or inhibitor. The assay was performed 72h after treatment according to the manufacturer's recommendation. Luminescence was measured using the TECAN infinite200.

3.1.17.5 Alanine assay

Efficiency of the GPT2 inhibitor (BCLA) was determined by measuring the alanine levels in the supernatant after inhibitor treatment. Alanine assay kit from Sigma was used for this. In this assay alanine is converted to pyruvate which can be detected by fluorescence. The experiment was setup as follows; cells were seeded to 80% confluency in 6-well plates. The following day growth media was replaced by fresh growth media supplemented with inhibitor (water in control wells). After 24h of treatment spent media was collected in 1.5ml centrifuge tube and frozen in -80^{o} C. Cells were counted using the CASY counter and cell numbers were used for normalization. The spent media was thawed, quickly spun down to remove debris and floating cells and diluted 1:10. 5µl of the diluted media was used for the assay. Using the manufacturer's recommendation alanine was detected in the media using fluorescence detection which was measured with TECAN infinite200.

3.1.18 Determination of metabolite levels via HPLC

Aliquots of flash-frozen cell culture supernatants were used for absolute quantification of amino acid, cation, organic acid and sugar content each.

To analyze the content of amino acids, 10 µl supernatant was mixed with 290 µl cold 0.1M HCl. Insoluble material and proteins were precipitated by centrifugation for 10min at 25.000g. 5µl of the resulting supernatant were quantified after specific labeling with the fluorescence dye AccQ-Tag™ (Waters) according to the manufacturers protocol. The resulting derivatives were separated by reversed phase chromatography on an Acquity BEH C18 column (150mm x 2.1mm, 1.7µm, Waters) connected to an Acquity H-class UPLC system and quantified by fluorescence detection (Acquity FLR detector, Waters, excitation: 250nm, emission: 395nm) using ultrapure standards (Sigma). The column was heated to 42 °C and equilibrated with 5 column volumes of buffer A (140 mM sodium acetate pH 6.3, 7 mM triethanolamine) at a flow rate of 0.45 ml min^{-1}. Baseline separation of amino acid derivates was achieved by increasing the concentration of acetonitrile (B) in buffer A as follows: 1 min 8% B, 7 min 9% B, 7.3 min 15% B, 12.2 min 18% B, 16.3 min 40% B, 18.5 min 80% B, hold for 3 min, and return to 8% B in 3 min. Data acquisition and processing was performed with the Empower3 software suite (Waters).

For determination of organic acids, cations and sugars, supernatants were diluted with ultra-pure water before analysis. For sugar determination, samples were diluted 1/1000, for organic acids and cations a 1/30 dilution was used. Organic acids were separated using an IonPac AS11-HC (2mm, ThermoScientific) column connected to an ICS-5000 system (ThermoScientific) and quantified by conductivity detection after cation suppression (ASRS-300 2mm, suppressor current 95-120 mA). Prior separation, the column was heated to 30°C and equilibrated with 5 column volumes of solvent A (ultra-pure water) at a flow rate of 0.38ml min^{-1}. Separation of anions and organic acids was achieved by increasing the concentration of solvent B (100mM NaOH) in buffer A as follows: 8min 4% B, 18min 18% B, 25min 19 % B, 43min 30% B, 53min 62% B, 53.1min 80% B for 6min, and return to 4% B in 11min.

Cations were separated using an IonPac CS16 (2mm, ThermoScientific) column connected to an ICS-1000 system (ThermoScientific) and also quantified by conductivity detection after anion suppression (CERS-500 2mm, suppressor current 43 mA). Prior separation, the column was heated to 43°C and equilibrated with 10 column volumes of 30mM methanesulfonic acid at a flow rate of 0.36ml min^{-1}. Cations were eluted using an isocratic run for 27min. Soluble sugars

were separated on a CarboPac PA1 column (ThermoScientific) connected to the ICS-5000 system and quantified by pulsed amperometric detection (HPAEC-PAD). Column temperature was kept constant at 25°C and equilibrated with five column volumes of solvent A (ultra-pure water) at a flow rate of 1ml min^{-1}. Baseline separation of carbohydrates was achieved by increasing the concentration of solvent B (300mM NaOH) in solvent A as follows: From 0 to 25 min 7.4% B, followed by a gradient to 100% B within 12min, hold for 8min at 100% B, return to 7.4% B and equilibration of the column for 12min. Data acquisition and quantification was performed with Chromeleon 7 (ThermoScientific).

Sample preparation and raw data analysis was done at the Metabolomics Core Technology Platform of the Excellence Cluster CellNetworks by Dr. Gernot Poschet.

3.1.19 Labelling experiments

In order to investigate the utilization of carbon atoms (derived from one of the main nutrients namely Glucose) by different metabolic pathways under different conditions and in different cell lines, media supplemented with stable isotope labeled glucose was used. While stationary labelling is obtained by longer labeling time, the Kempa Lab at BIMSB, Berlin have developed a method called pulsed Stable Isotope Resolved Isotopic Metabolomics (pSIRM) with shorter labelling times in order to determine fate of nutrients and metabolic dynamics in a time resolved manner(Pietzke & Kempa, 2014). In order to track the fate of carbon atoms of glucose in the TCA cycle and adjacent pathways the label was applied for 30mins to the cells. All the labelling experiments were performed by me in Stefan Kempa's lab in collaboration with Nadine Royla, PhD student, AG Kempa.

3.2.8.1 Cell culture

For each cell line (MCF-7, MDAMB231, MDA MB 468) cells were plated with a beforehand determined cell number to reach a similar confluency after 48h of incubation. The GPT2 inhibitor was applied 24h after plating for another 24h. Four hours prior to harvest, 1 ml of

media was collected to determine all secreted metabolites and remaining media was renewed. Cell culture media was replaced by media containing ^{13}C-glucose (Campro Scientific, Berlin, Germany). After incubation of 30min adherent cells were quickly flushed with wash buffer (140mM NaCl, 5 mM HEPES, pH 7.4, and supplemented with major carbon sources) to remove extracellular metabolites, but not the main carbon sources. Immediately, cells were quenched with 5 mL ice-cold 50% methanol (suppl. with cinnamic acid (final concentration: 2 µg/ml)). The cells were scratched, collected and transferred into a 15-ml falcon, and stored as well as the media samples at -20°C until proceeding with metabolite extraction.

3.2.8.2 Intracellular extraction

One milliliter chloroform was added to 5 ml of methanolic cell extracts, shaken for 60min at 4°C, and centrifuged at maximum speed for 15min at 4°C for phase separation (methanol-chloroform-water extraction). Polar phases were collected. Each polar phase was splitted into two aliquots - one for direct infusion MS and one for GS-MS analysis in order to measure nucleotides and central carbon metabolites from the same sample - and dried under vacuum. The cell extracts were stored at −20°C until preparation of GC-MS analysis or direct infusion MS analysis.

3.2.8.3 Extracellular extraction

One milliliter of methanol-chloroform-water (5:2:1, v/v/v, suppl. with cinnamic acid (final concentration: 2 µg/ml)) was added to 50 µL of media samples, shaken for 30 min at 4°C. 500 µL of H_2O were added and samples were centrifuged at maximum speed for 15 min at 4°C for phase separation. Two times 500 µL of polar phase were collected and dried under vacuum. The extracellular extracts were stored at −20°C until preparation of GC-MS analysis.

3.2.8.4 GC-MS analysis

A quantification dilution series was treated in parallel with extracts. Derivatization was carried out as described with modifications (Kempa et. al., 2007). Dried cell extracts were dissolved in 20 µL of methoxyamine hydrochloride solution (Sigma, 40 mg/mL in pyridine (Roth)) and incubated for 60min at 30°C with constant shaking followed by the addition of 80 µL of N-methyl-N-[trimethylsilyl]trifluoroacetamide (MSTFA; Machery-Nagel, Dueren, Germany) and incubation at 37°C for 90min. The extracts were centrifuged for 10min at 10,000 × g, and aliquots of 30 µL were transferred into glass vials (Th. Geyer, Berlin, Germany) for gas chromatography-mass spectrometry (GC-MS) measurement.

Metabolite analysis was performed on a gas chromatography coupled to time of flight mass spectrometer (Pegasus III- TOF-MS-System, LECO Corp., St. Joseph,MI, USA), complemented with an auto-sampler (MultiPurpose Sampler 2 XL, Gerstel, Mülheim an der Ruhr, Germany). The samples were injected in split mode (split 1:5, injection volume 1 µL) in a temperature-controlled injector (CAS4, Gerstel) with a baffled glass liner (Gerstel). The following temperature program was applied during sample injection: initial temperature of 80°C for 30 s followed by a ramp with 12°C/min to 120°C and a second ramp with 7°C/min to 300°C and final hold for 2 min. Gas chromatographic separation was performed on an Agilent 6890 N (Agilent, Santa Clara, CA, USA), equipped with a VF-5 ms column of 30-m length, 250-µm inner diameter, and 0.25-µm film thickness (Varian, Palo Alto, CA, USA). Helium was used as carrier gas with a flow rate of 1.2 mL/min. Gas chromatography was performed with the following temperature gradient: 2-min heating at 70°C, first temperature gradient with 5°C/min up to 120°C and hold for 30 s; subsequently, a second temperature increase of 7°C/min up to 350°C with a hold time of 2 min. The spectra were recorded in a mass range of 60 to 600 U with 20 spectra/s at a detector voltage of 1650 V.

The GC-MS chromatograms were processed with the ChromaTOF software (LECO). Mass spectra data were extracted using the software tool MetMax (http://gmd.mpimp-golm.mpg.de/apps/metmax/) or the in-house software Maui-VIA (Kuich et. al., 2014). Mass isotope distribution of unlabeled metabolites were used to determine the ^{13}C-glucose derived

stable isotope incorporation of ^{13}C in metabolites of interest. Absolute quantities were determined by the examination of the peak area in the GC-MS-derived chromatograms and their comparison to quantification standards. Acquired data were normalized to the internal standard cinnamic acid, the sum of area per sample and cell count.

Cell culture, inhibitor treatment, labeling, sample extraction and preparation were done by Nadine Royla and me. Data analysis was done by Nadine Royla.

3.1.20 Seahorse Experiments

In order to see the effector of the GPT2 inhibitor on mitochondrial respiration of the cells the Seahorse Bioanalyzer and XF cell mitostress kit from Agilent was used and Oxygen consumption rate (OCR) was measured by the seahorse bioanalyzer. The cell mitostress kit can be used to measure key parameters of mitochondrial function via determination of the oxygen consumption rate of the cells via serial injection of different compounds. Oligomycin, ATP synthase (complex V) inhibitor, is first injected leading to a decrease in OCR which corresponds to the mictochondrial respiration associated with cellular ATP production. The next compound to be injected is Carbonyl cyanide-4 (trifluoromethoxy) phenylhydrazone (FCCP). FCCP is an uncoupling agent that collapses the proton gradient and disrupts the mitchondrial membrane potential. This leads to an increase in oxygen consumption by complex IV as the electron flow through the ETC is uninhibited. The increase in OCR can be used to calculate the spare respiratory capacity of the cells. Finally, a mix of rotenone (complex I inhibitor) and antimycin A (complex II inhibitor is injected into the cells to completely shut down the respiration, the remaining oxygen consumption gives a measure of the non-mitochondrial respiration of the cells.

Seahorse analysis was performed according to the manufacturer's recommendations. Briefly, cells were seeded as a uniform monolayer to a confluency of 80% in seahorse 96-well microplates. The following day, the cells were treated with inhibitor as indicated earlier. The same day the sensor cartridges were hydrated with a calibrant and incubated overnight in a non CO_2 incubator. The next day after 24h incubation with inhibitor the media was changed to

seahorse assay media with inhibitor and incubated for 45min in a non CO_2 incubator. The cartridge plate was then loaded with different reagents of the mitostress kit, namely, Oligomycin, FCCP and Antimycin/Rotenone A and calibrated in the Seahorse bioanalyzer. After calibration the calibrant plate was replaced by the cell plate and the mitostress test was performed. Obtained data from the bioanalyzer was analyzed using the Wave 2.0 software. After the mitrostress test sulforhodamine staining was done on the cell plate to determine protein concentration. These values were then used for normalizing the Seahorse data. Prof. Dr. Stephan Herzig kindly allowed the use of the Seahorse Bioanalyzer belonging to his group at Heidelberg University Hospital.

3.1.21 Dataset Analysis

Publicly available METABRIC and TCGA datasets were downloaded from the website given in Section 3.1.7. METABRIC data comprised of mRNA expression microarray and clinical data of nearly 2000 patients with a follow up of 20 years. Box plots are represented as $\log_2$ transformed gene expression data. Kaplan-Meier method was used to generate survival curves(Kaplan & Meier, 1958.). 25% of the patients with the highest and lowest expression *GPT2* were used to generate survival curves. TCGA data comprises of RNA-sequencing and clinical data of nearly 1200 patients. Box plots were generated using gene expression data represented as $\log_2$ (x+1) rsem.

3.1.22 Statistical Analysis

Unless otherwise mentioned, data are presented as mean ± SD and statistical analyses were performed by unpaired two-tailed Student's t-test and p-values <0.05 were considered statistically significant. P values <0.05, <0.01 and <0.001 are indicated with one, two and three asterisks respectively.

3.1.23 Graphical Illustrations

All graphs were generated using the GraphPad Prism Software and illustrated via Inkscape v 0.91

4. Results

4.1 Metabolic characterization of Breast cancer cell lines

To study the role of metabolic pathways in breast cancer cells, 3 different model breast cancer cell lines were chosen. Two were triple negative breast cancer (TNBC) cell lines, MDA MB 468 and MDA MB 231. The third was a luminal cell line, namely MCF7. All three cell lines have been shown to have active glutamine metabolism(Korangath et al., 2015; Lampa et al., 2017). MDA MB 468 cells were moderately dependent on glutamine (Figure 1a, d) while, MDA MB 231 cells were observed to be a glutamine addicted cell line (Figure 4b, e), MCF7 represents a less aggressive subtype of breast cancer was still dependent on glutamine for growth (Figure 4 c, f). Proliferation slowed down in all 3 cell lines under glutamine starvation conditions, however, glucose deprivation had a stronger effect on cell survival (Figure 4 a-f). The doubling times were calculated for each cell line, MDA MB 468 was the slowest while MDA MB 231 was the fastest growing cell line (Figure 4h).

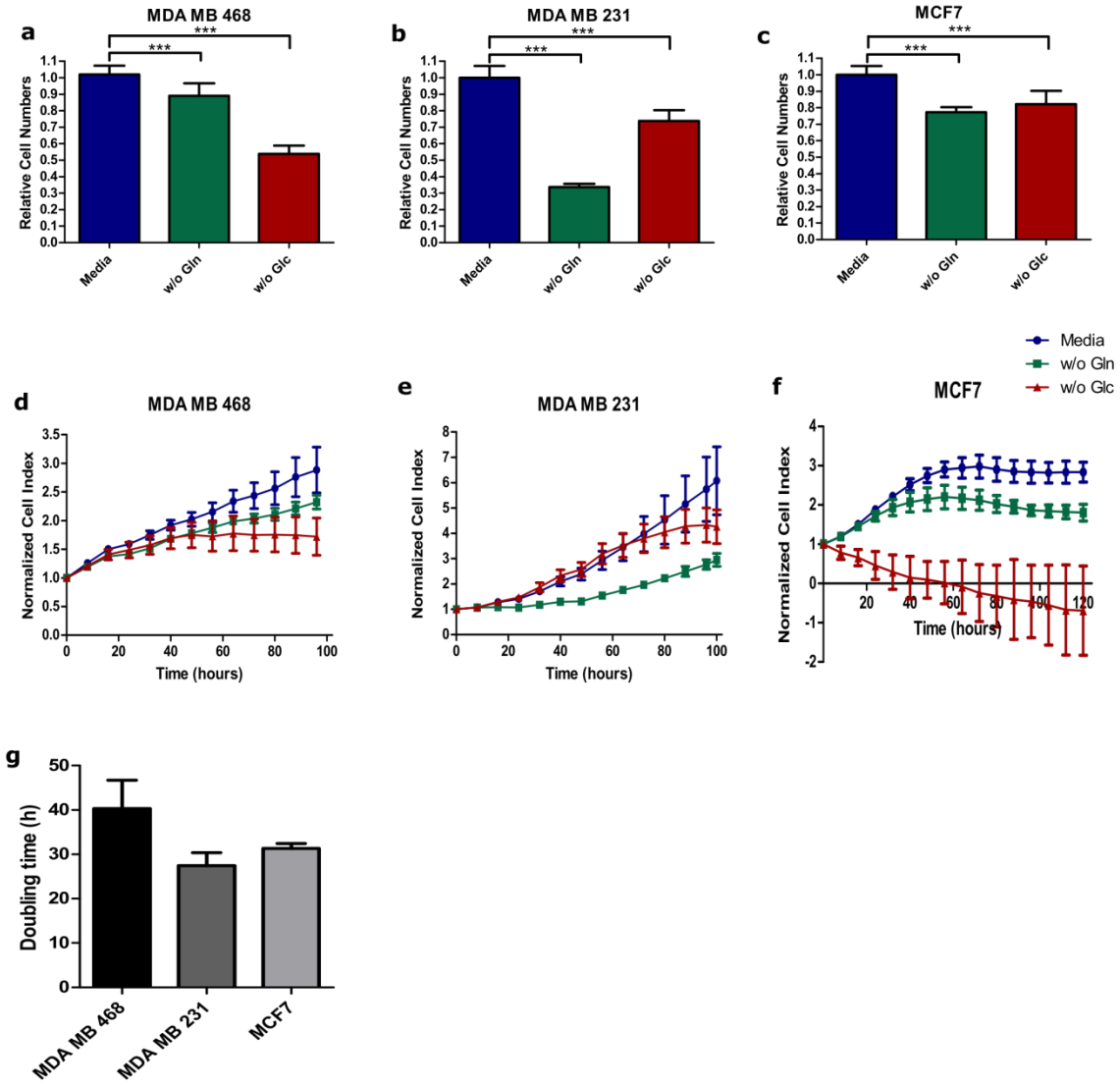

Figure 4: Metabolic characterization of cancer cells. a-c, Microscopy based nuclei counting of cells grown without glutamine or glucose for 72h. All values are represented as relative values normalized to media values. (d-f) Cells were grown without glutamine or glucose and cell density was measured over time with the real time cell analyzer (RTCA). (g) Doubling times of the different cell lines in cell culture. Data are presented as mean ± SD. For nuclei count n=2(each with 6 technical replicates), for real time cell analyzer, n=1 (with 4 technical replicates), for doubling time n=3 (each with 6 technical replicates). *** represents $p < 0.001$.

In order to understand the nutrient dependencies of cancer cells in more detail, consumption of key carbon sources, glucose and glutamine were measured (Figure 5 a, b). MDA MB 468 consumed the highest amount of glutamine and glucose, signifying that both these pathways are active in the cells. This was further validated by the high secretion of ammonia and lactate, which are major products of glutaminolysis and glycolysis, respectively (Figure 5 c, d). Metabolites were quantified at the Metabolomics Core Technology Platform (MCTP) by Dr. Gernot Poschet.

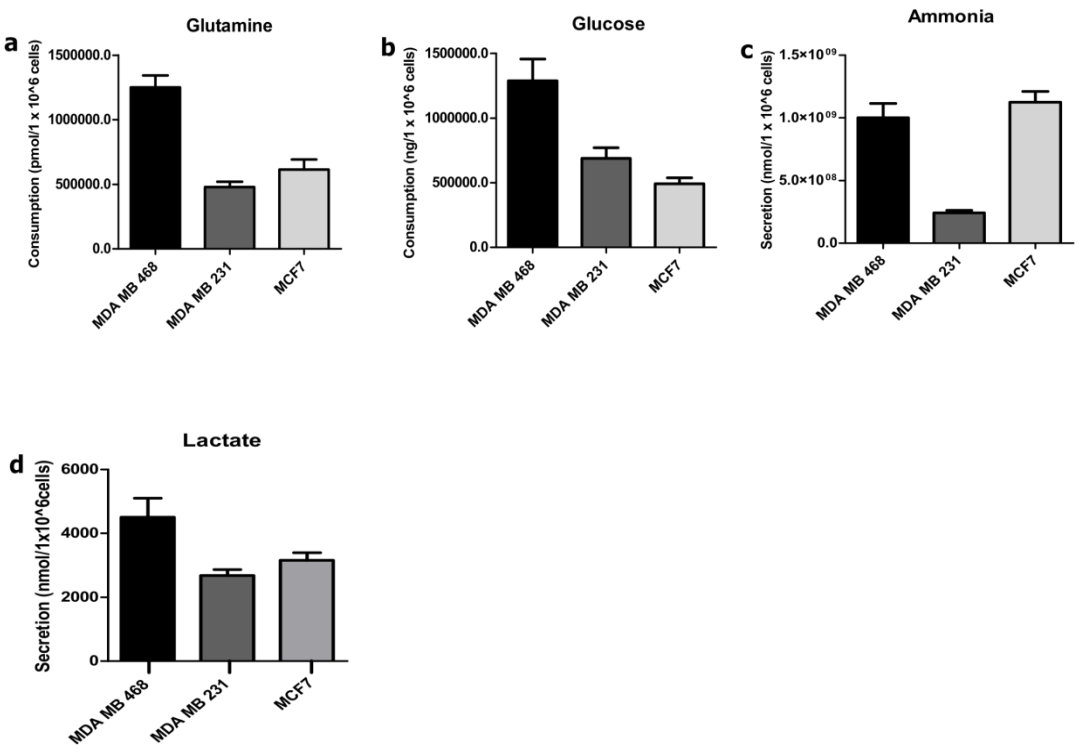

Figure 5: Metabolic characterization of cancer cells. Cells were grown in growth media for 48h and spent media were used to measure metabolites. HPLC was used to measure glutamine (a) and glucose (b) consumption as well as ammonia secretion (c). GC-MS was used to measure lactate secretion (d). Data are presented as mean ± SD. n=3

At the protein level, expression of enzymes involved in different metabolic pathways was quantified by mass spectrometry (Figure 6). Interestingly, MDA MB 231 showed higher expression of glycolysis/ gluconeogenesis enzymes, while glutaminolysis enzymes were highly expressed in both MDA MB 468 and MDA MB 231 (Figure 6 a, c). The TCA cycle enzymes were highest in MCF7 (Figure 6b), this was also confirmed by quantification of the TCA intermediates within the cells (Supplementary Table 1). The oxidative phosphorylation pathway was also most elevated in MCF7, followed by MDA MB 468 (Figure 6d). Blank boxes in the heatmap indicate that the respective protein was not detected. To understand whether this was due to the technique used, as in some cases the protein was detected in one or more of the replicates, other techniques were used. In a different experiment, a subset of the proteins was tested with RPPA, and it was found that ASS1, GPT2 and GLS could be detected in all three cell lines (Figure 6 e, f and 7c). Using a microarray all the other undetected proteins were found to be expressed at the mRNA level protein expression was not further tested (Supplementary Table 2). Mass spectrometry and raw data analysis was done by Nadine Royla (BIMSB). Differential expression analysis for mass spectrometry data was performed by Dr. Khalid Abnaof (DKFZ) and can be found in Supplementary Table 3. RPPA was performed by Stephan Bernhardt (DKFZ). Microarray was done by DKFZ microarray core facility and data normalization was performed by Dr. Khalid Abnaof.

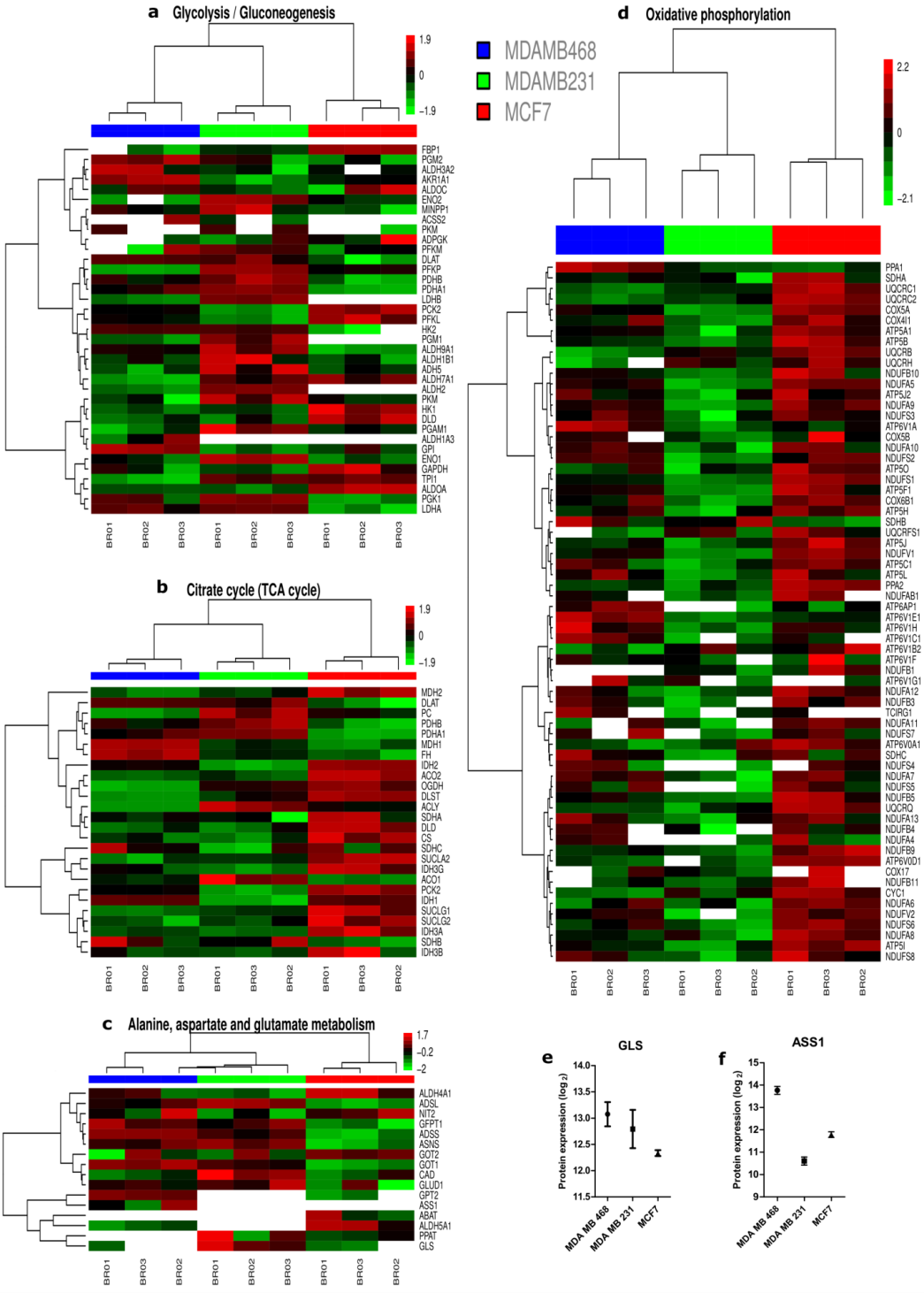

Figure 6: Proteomic characterization of cancer cells. (a-d) Heatmaps show the levels of different proteins belonging to key metabolic pathways in the different cell lines measured by mass spectrometry. (e-f) Expression of a subset of enzymes not detected by mass spectrometry was confirmed by RPPA. Data in graphs are presented as mean ± SD, n=3

To validate metabolic pathways which are activated in these cells, amino acids were measured in the spent media from the cells. Interestingly, MDA MB 468 secreted the highest amount of alanine (Figure 7a), while other amino acids did not show similar levels of difference between cell lines (Supplementary table 4). This result was further consolidated by the fact that GPT2, which produces alanine from pyruvate, had the highest expression in MDA MB 468 at both mRNA and protein levels (Figure 7 b, c). mRNA of *GPT*, a liver specific isoform, was expressed much less in the cell lines (Figure 7b). To confirm that MDA MB 468 cells have an active GPT2 catalyzed pathway, media supplemented containing $^{13}C_6$ glucose was used to track the production of new alanine, and intracellular pools of alanine were also measured (Figure 7 d, e). Both experiments showed that MDA MB 468 produced high amounts of alanine compared to the other two cell lines. MCF7 also had a notably higher protein expression of GPT2 compared to MDA MB 231(Figure 7c). To confirm that this phenomenon is not restricted to a few cell lines, 13 different breast cancer cell lines were tested and it was found that the expression of GPT2 was diverse and did not conform to the molecular subtypes, however, that this pathway was active in many cell lines (Figure 7c). Alanine secretion quantification and raw data analysis was done by Dr. Gernot Poschet. The labeling and intracellular experiments were done together with Nadine Royla, who also did the analysis of the data. RPPA and raw data processing was done by Stephan Bernhardt.

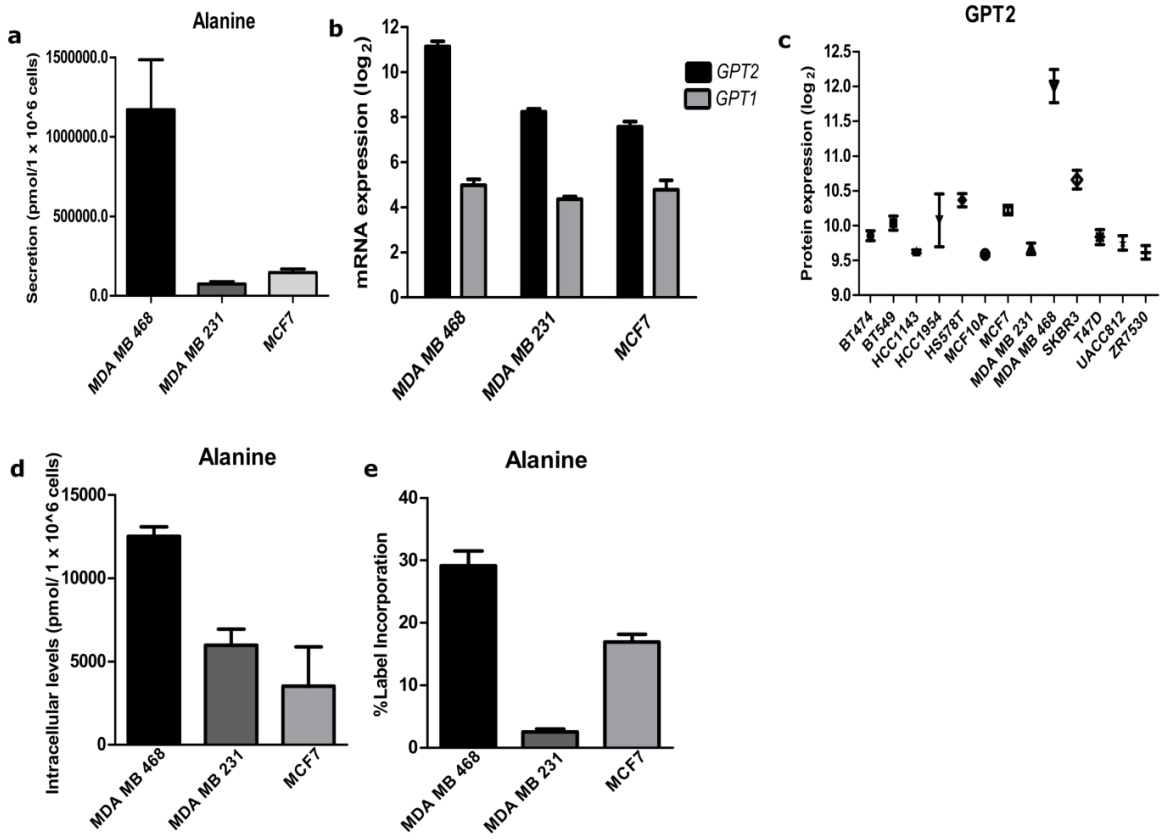

Figure 7: MDA MB 468 cells secrete high levels of alanine. (a) Alanine secretion in different cell lines, after 48h of growth, measured via HPLC. (b) *GPT2* and *GPT* mRNA expression levels in the different cell lines measured via microarray. (c) GPT2 protein levels in 13 different breast cancer cell lines measured via RPPA. (d) Intracellular alanine levels and % ^{13}C labelling in alanine after 30 mins of $^{13}C_6$ glucose media incubation. Data are presented as mean ± SD. n=3

4.2 GPT2 is crucial to cancer cell growth

4.2.1 Effect of GPT2 knockdown on cell growth

The high levels of alanine secretion and GPT2 expression in breast cancer cell lines indicate that this pathway is active and possibly important for the cancer cells. Therefore, it was hypothesized that this pathway would provide a growth advantage to the cells and in order to verify this, an RNAi approach was used. As a first step, cell viability was measured using the cell titer glo assay from Promega. This assay measures the ATP content of the cells and thereby

gives an indication of their metabolic activity. Using a pool of 4 siRNAs targeting GPT2, cell viability was measured 72h after transfection. MDA MB 468 cells (Figure 8a), which had the highest expression of GPT2 protein showed a significant decrease in cell viability. Hs578T, another TNBC cell line, (Figure 8b) which also had significantly higher GPT2 levels compared to the other tested cell lines (Figure 7c) showed a significant decrease in cell viability. MCF7 (Figure 8c) showed a small but significant decrease in cell viability. Interestingly, MDA MB 231 (Figure 8d) which had both low expression of GPT2 and little production of alanine showed a similar decrease in cell viability upon GPT2 knockdown as MDA MB 468. In contrast, T47D (Figure 8e), one of the cell lines which had the lowest expression of GPT2 (Figure 7c), did not show any decrease in cell viability in the RNAi experiment.

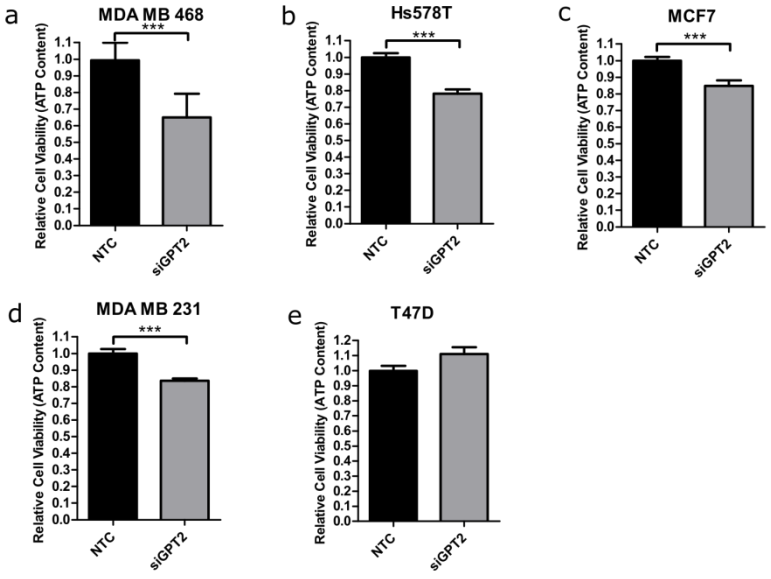

Figure 8: GPT2 knockdown affects cell viability. a-e, Cells were transfected with siGPT2 and cell viability was assessed after 72h with the cell titer glo assay. All values are represented as relative values normalized to non-targeting control siRNA (NTC). Data are presented as mean ± SD, *** represents $p < 0.001$. n=2 (each with 6 technical replicates)

As the cell viability assay did not take into account the number of cells in each well, further assays were required to validate these results. In order to check whether the decrease in

viability was a result of a decrease in cell numbers, microscopy based nuclei counting was done, after GPT2 knockdown, in the three cell lines of interest, namely, MDA MB 468, MDA MB 231 and MCF7. Using Hoechst nuclei staining the cell numbers were measured 72h post transfection. Knockdown of GPT2 significantly decreased cell numbers in MDA MB 468 (Figure 9a). Again, MDA MB 231, showed a similar decrease in cell numbers as compared to MDA MB 468 (Figure 9b). MCF7, however, did not show a decrease in cell numbers post knockdown (Figure 9c).

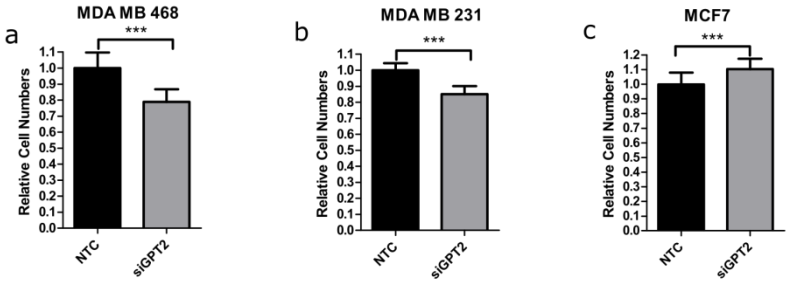

Figure 9: Knockdown of GPT2 decreases cell proliferation. Microscopy based nuclei counting of MDA MB 468 (a), MDA MB 231 (b) and MCF7 (c) 72h after transfection with siGPT2. All values were normalized to NTC. Data are presented as mean ± SD, n=3 (each with 6 technical replicates). *** represents $p < 0.001$.

To confirm these findings with a different method, real time cell analyzer (RTCA) technology was used and cell growth was measured over time. Cell Index measurements showed that GPT2 knockdown started to affect MDA MB 231 cells at an earlier time point compared to MDA MB 468 cells (Figure 10 a, b).

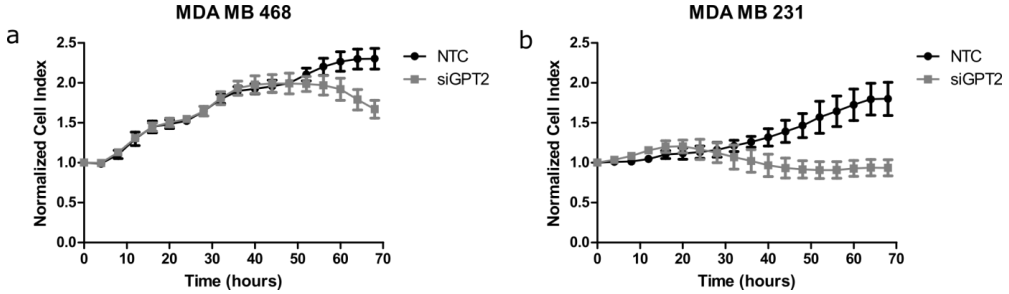

Figure 10: Effect of GPT2 knockdown on cell proliferation determined by RTCA based assay. Cells were transfected with siGPT2 and cell proliferation was measured over time with the real time cell analyzer (RTCA). Data are represented as mean ± SD of 4 technical replicates. Graphs are representative of n=2.

Deconvolution of the 4 siRNAs of the GPT2 pool revealed that all siRNAs show a strong decrease in GPT2 mRNA and protein levels (Figure 11, pool was also tested with RPPA, data not shown).

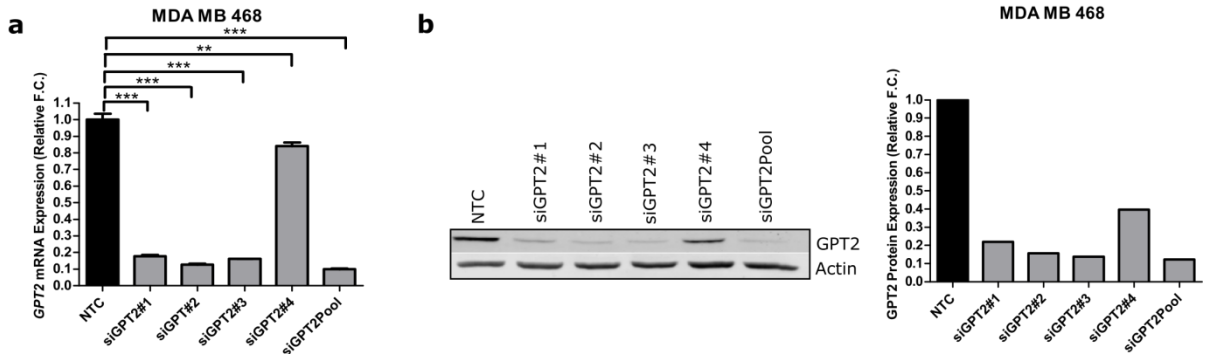

Figure 11: Knockdown efficiency and deconvolution of siGPT2 pool. Cells were transfected with siGPT2 (pool and individual). RNA and protein were harvested 72h after transfection and knockdown efficiency was determined by qPCR (a) and western blot (b) respectively. All values were normalized to NTC. For cell numbers, data are presented as mean ± SD, of 6 technical replicates). Values for mRNA expression were first normalized to *PUM1* levels and are presented as mean ± SD of 3 technical replicates. Protein expression values were first normalized to actin levels, n=1. *** represents $p < 0.001$, ** represents $p<0.01$, * represents $p<0.05$.

Next, phenotypic effect of the individual and pool GPT2 siRNAs was assessed. The different siRNAs affected cell growth variably, however, the pool behaved the same as 2 siRNAs (#1 and #3) which gave similar effect (Figure 12).

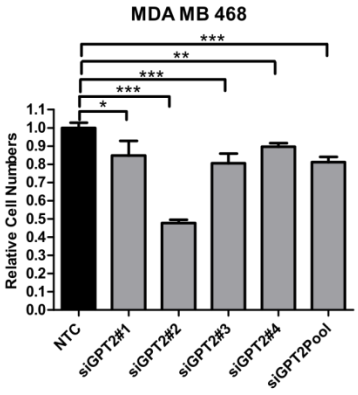

Figure 12: Deconvolution of siGPT2 pool. Cells were transfected with siGPT2 (pool and individual). Microscopy based nuclei counting of cells were done 72h after transfection with siGPT2. All values were normalized to NTC. Data are presented as mean ± SD, of 6 technical replicates. *** represents $p < 0.001$, ** represents $p<0.01$, * represents $p<0.05$.

Knockdown efficiency was also tested in the MDA MB 231 and MCF7. All cell lines showed >80% decrease in mRNA expression 72h post transfection of the GPT2 siRNA pool (Figure 13 a-d). Protein expression levels were also determined for MDA MB 231 and MCF7 and the siRNA decreased the expression of GPT2 in both cell lines (Figure 13 a, b). The decrease in GPT2 protein levels in MDA MB 231 was not as strong as in the other cell lines, this could be due to the fact that MDA MB 231 already has a low level of GPT2 expression under basal conditions and therefore the decrease is not accurately quantifiable.Hs578t and T47D also showed >80% decrease in GPT2 mRNA after transfection.

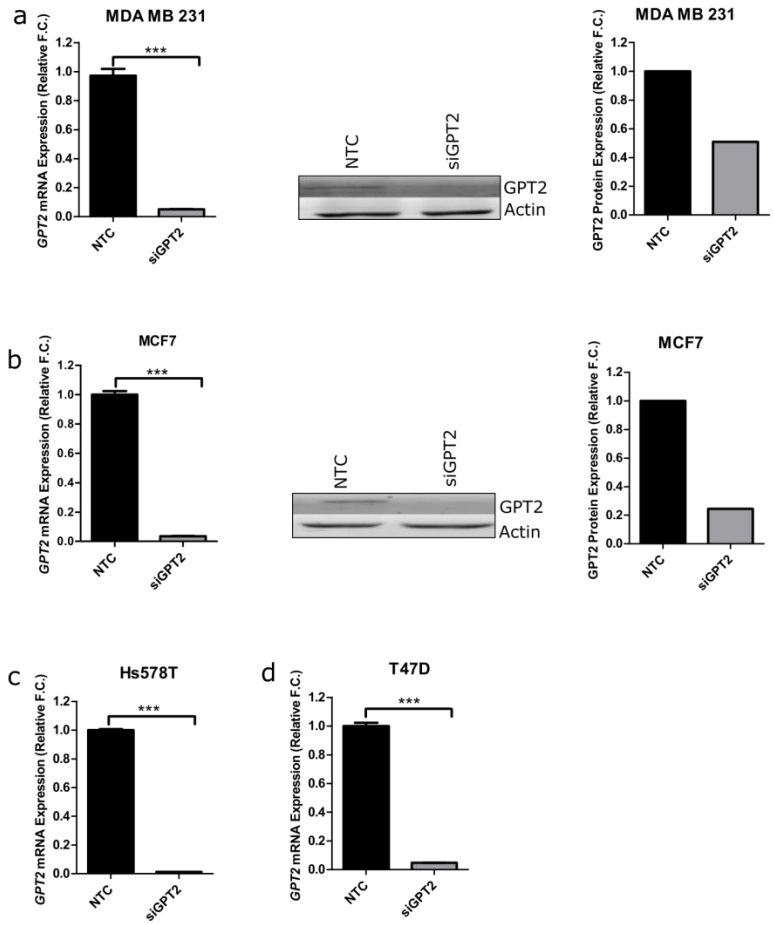

Figure 13: Knockdown efficiency of siGPT2. Cells were transfected with siGPT2 pool. RNA and protein were harvested 72h after transfection and knockdown efficiency was determined by qPCR and western blot respectively. All values were normalized to NTC. Values for mRNA expression were first normalized to *PUM1* levels and are presented as mean ± SD of 3 technical replicates. Protein expression values were first normalized to actin levels, n=1. . *** represents $p < 0.001$.

In order to confirm that the siRNA did not cross target GPT, GPT mRNA levels were measured after transfection, MDA MB 468 showed a slight decrease in GPT (Figure 14a), while in MCF7 the levels remained unchanged (Figure 14c). Interestingly, MDA MB 231 showed an increase in GPT expression (Figure 14b).

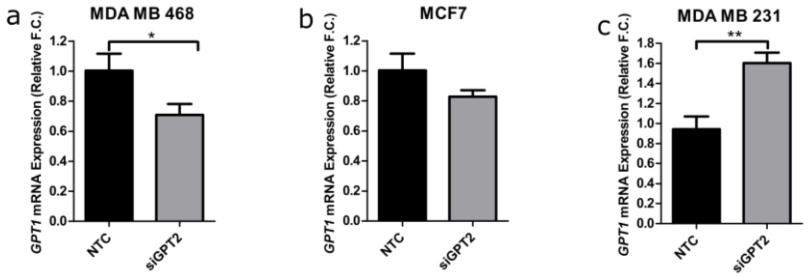

Figure 14: Off target effect of GPT2 siRNA on GPT1 gene expression. (a-c) Cells were transfected with siGPT2. RNA was harvested 72h after transfection and GPT1 levels were assessed by qPCR analysis. All values were normalized to NTC. Values for mRNA expression were first normalized to *PUM1* levels and then to non-targeting control and presented as mean ± SD of 3 technical replicates. ** represents $p<0.01$, * represents $p<0.05$.

In conclusion, knockdown of GPT2 showed significant decrease in cell growth in all cell lines with a high to moderate expression of GPT2. Contrary to expectations, MDA MB 231 showed a significant decrease in cell growth indicating that, despite low GPT2 protein levels and alanine being produced, this pathway is still essential for the growth of these cells.

4.2.2 GPT2 inhibition and cell growth

While RNAi is an efficient method to determine the effect of gene knockdown in cells, there are drawbacks to this method due to the fact that both gene specific and non-targeting controls can have off-target effects. In order to circumvent this and to prove that the effects seen with RNAi are independent of the off target effects siRNAs might have, a commercially available alanine aminotransferase inhibitor, β-chloro-L-alanine (BCLA) was used. BCLA can target both GPT isoforms, however, any possible cross reactivity was not relevant as GPT2 is more abundant than GPT in breast cancer and the focus was to block the interconversion of pyruvate to alanine.

Measurement of cell numbers 72h after inhibitor treatment showed a dose dependent effect of the inhibitor on cell growth and alanine secretion (Figure 15). While MDA MB 468 cell growth

and alanine secretion were considerably affected with 75µM inhibitor treatment (Figure 15 a, b), MDA MB 231 cells had the highest sensitivity and showed significant effects from 25µM (Figure 15a, d), MCF7 cell growth was least affected by the inhibitor with the highest effect at 100uM (Figure 15 a, c). Subsequent experiments were done with the indicated effective concentrations.

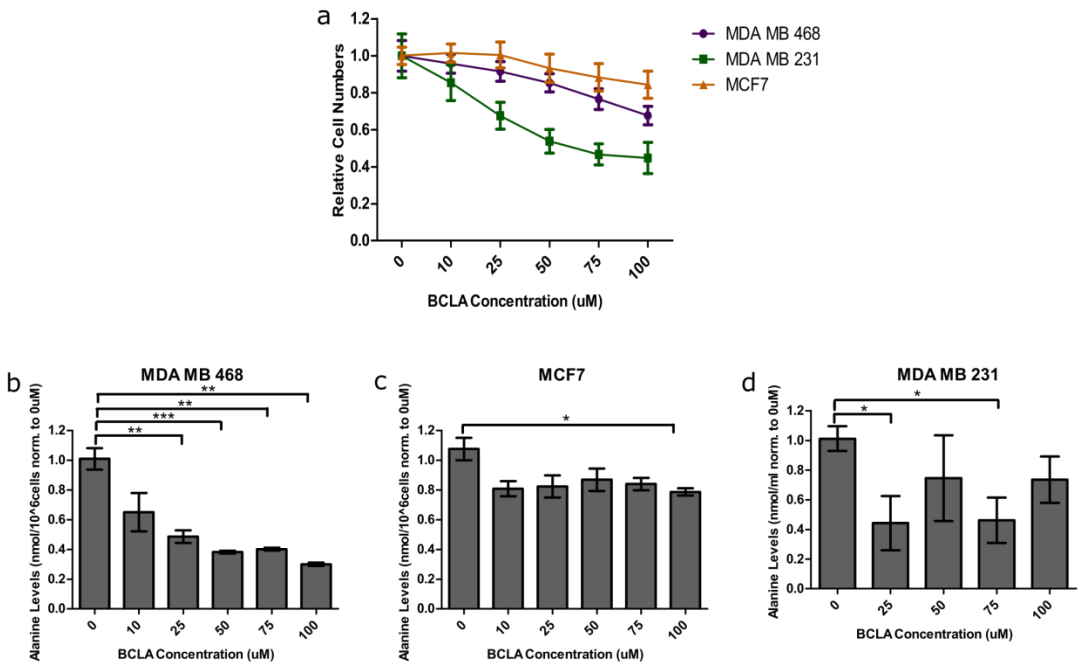

Figure 15: Alanine aminotransferase inhibitor reduces cell proliferation and alanine secretion. (a) Cells were treated with increasing concentration of alanine aminotransferase inhibitor and cell numbers were counted via microscopy after 72h. (b-d) Cells were treated with increasing concentration of BCLA, after 24h supernatants were collected and alanine was measured by the alanine assay kit. All data were normalized to untreated control (0). For cell numbers data are presented as mean ± SD, n=2 (6 technical replicates each). Alanine levels are presented as mean ± SEM, n=3. *** represents $p < 0.001$, ** represents $p<0.01$, * represents $p<0.05$.

These results were also confirmed with the RTCA analyzer, both MDA MB 468 and MDA MB 231 showed a strong decrease in cell growth after inhibitor treatment (Figure 16 a, b).

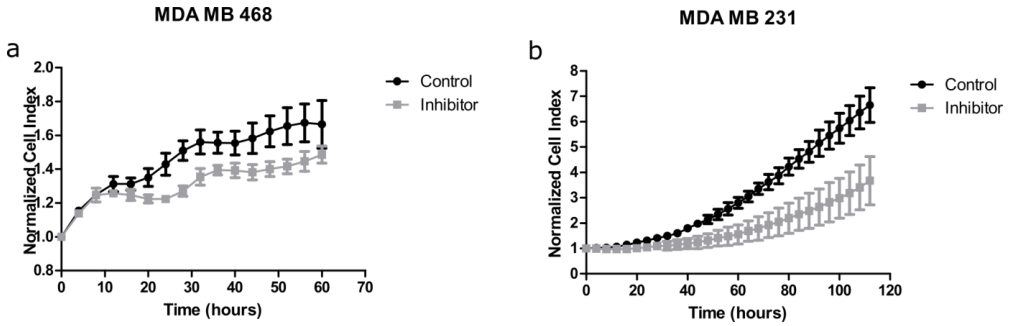

Figure 16: Effect of alanine aminotransferase inhibitor on cell proliferation determined by RTCA assay. Cells were treated with GPT2 inhibitor, BCLA (MDA MB 468: 75uM, MDA MB 231 25uM) and cell proliferation was measured over time with the real time cell analyzer (RTCA). Data are presented as mean ± SD. MDA MB 68 n=3 and MDA MB 231 n=4.

In order to confirm that the observed decrease in alanine levels in the media came from a blockage of the GPT2-catalyzed reaction, the cells were treated with the inhibitor for 24h and then incubated in inhibitor-containing media supplemented with $13C_6$ Glucose. Metabolite analysis after 30 minutes incubation with the labeled media showed almost complete abrogation in alanine production thereby proving that the inhibitor is efficacious in all three cell lines (Figure 17). The labeling experiment was done together with Nadine Royla, who also did the initial analysis of the data.

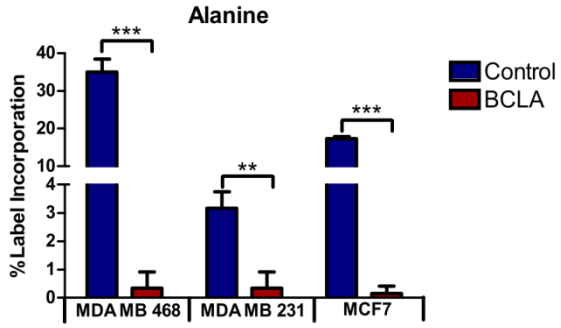

Figure 17: Efficiency of alanine transferase inhibitor. Cells were treated with GPT2 inhibitor, BCLA (MDA MB 468: 75uM, MDA MB 231: 25uM, MCF7:100uM) for 24h (with a media change after 20h). Cells were then incubated with media containing $^{13}C_6$ glucose for 30min and metabolites were extracted. % incorporation of glucose derived carbon-13 into alanine was measured by GC-MS. Data are presented as mean ± SD. n=3. *** represents $p < 0.001$, ** represents $p < 0.01$.

Therefore, two independent methods, namely RNAi of mRNA encoding GPT2 and targeting the activity of the protein, proved that GPT2 has an effect on cell proliferation and this pathway is essential for breast cancer cell growth.

4.3 Effect of GPT2 on cancer cell metabolism

4.3.1 Effect of GPT2 on extracellular metabolites

To determine whether the inhibition of GPT2 had a role in nutrient cycling in the cancer cells, the composition of the media surrounding the cells was analyzed. All 3 cell lines were treated with inhibitor or control (water) containing media. Spent media was collected after 20h of inhibitor treatment. Then, cell numbers were determined and used later as normalization control. Spent media was then treated as described in the methods. MDA MB 468 cells treated with inhibitor showed a significant decrease in glutamine consumption indicating that GPT2 plays an important role in glutaminolysis. Perturbation of GPT2 catalyzed pathway thus, seems to block an essential route of nitrogen cycling thereby forcing the cells to consume less glutamine (Figure 18a, first panel). In contrast, MDA MB 231 and MCF7 did not show any significant changes in glutamine consumption upon inhibitor treatment (Figure 18, c, first panel). Glucose, the other important carbon source of the cells indeed showed some changes (Figure 18 a-c, second panel). Inhibitor-treated MDA MB 468 cells showed a slight albeit significant increase in glucose consumption, whereas MDA MB 231 showed a significant decrease and MCF7 did not show any changes. To further confirm the effect of GPT2 inhibition on glycolysis, lactate secretion was measured. None of the cells showed a change in lactate

secretion confirming that the glycolytic pathway remains unchanged in these cells (Figure 18 a-c, third panel). Glutamine was measured via HPLC by Dr. Gernot Poschet and glucose and lactate were measured via GC-MS together with Nadine Royla. Both performed extraction and initial data processing of the respective chromatograms.

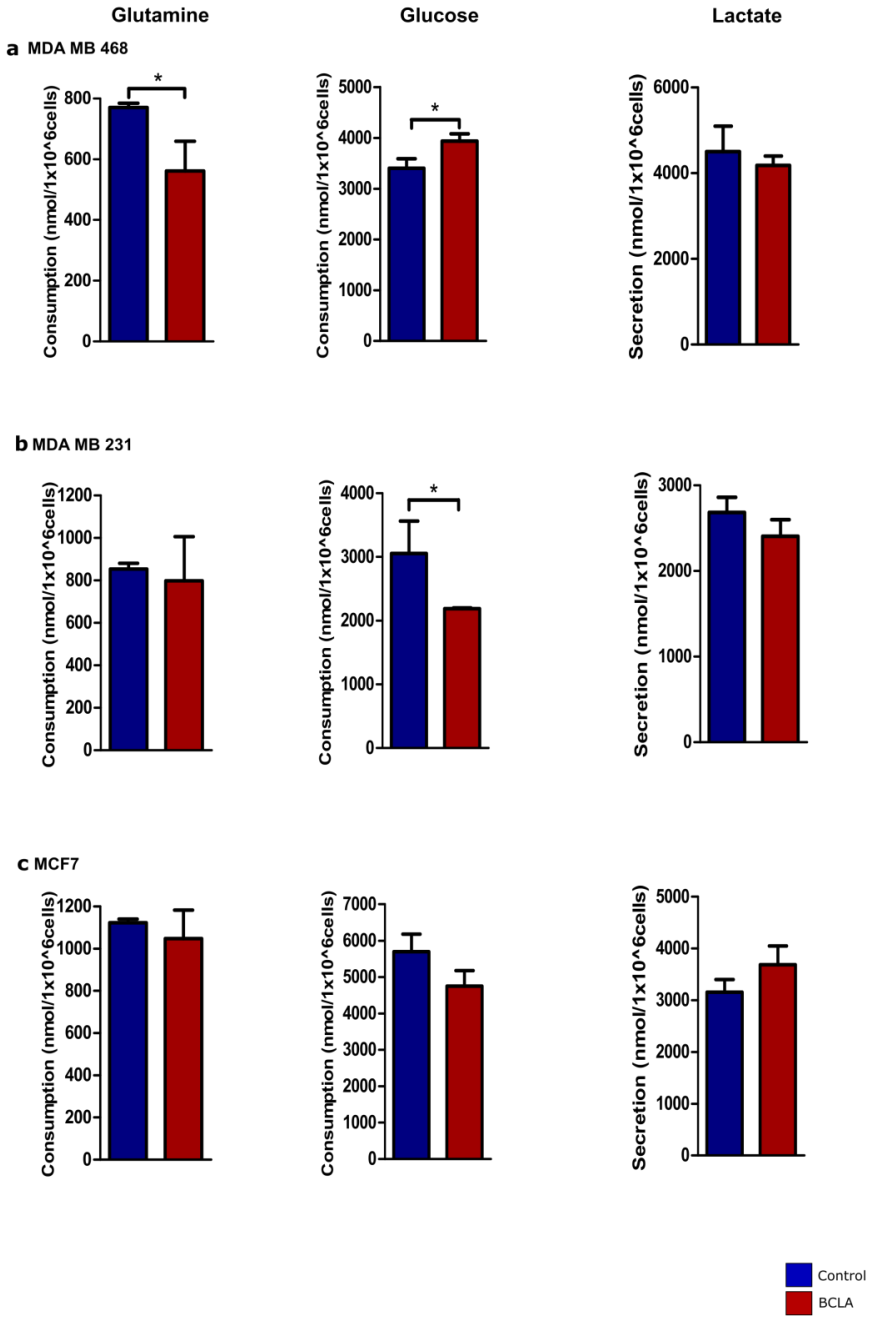

Figure 18: **Effect of GPT2 inhibition on extracellular metabolites.** Cells were treated with GPT2 inhibitor, BCLA (MDA MB 468: 75uM, MDA MB 231: 25uM, MCF7:100uM) for 20h. Spent media was collected and glutamine was measure via HPLC and glucose and lactate were measured with GC-MS. Data are presented as mean ± SD. n=3. *** represents $p < 0.001$, ** represents $p < 0.01$.

To validate the metabolite data obtained from the inhibitor treated cells and to rule out any effects that might arise due to off-target effects, extracellular metabolites were measured of cells with GPT2 knocked down. In this experiment, MDA MB 468 cells were transfected with either GPT2 siRNA or a non- targeting control. After a media change 24h post transfection, the cells were incubated for a further 48h. Spent media was collected and processed according to the procedure described in the methods. Glutamine consumption was found to be significantly decreased in RNAi treated cells (Figure 19a). The decrease in glutaminolysis in the cells were further confirmed by the decrease in ammonia secretion which is one of the main byproducts of this pathway (Figure 19b). GPT2 knockdown did not affect glucose consumption (Figure 19c), while a small yet non-significant decrease in lactate secretion was observed (Figure 19d). The samples were derivatized, measured and initial data was processed by Dr. Gernot Poschet.

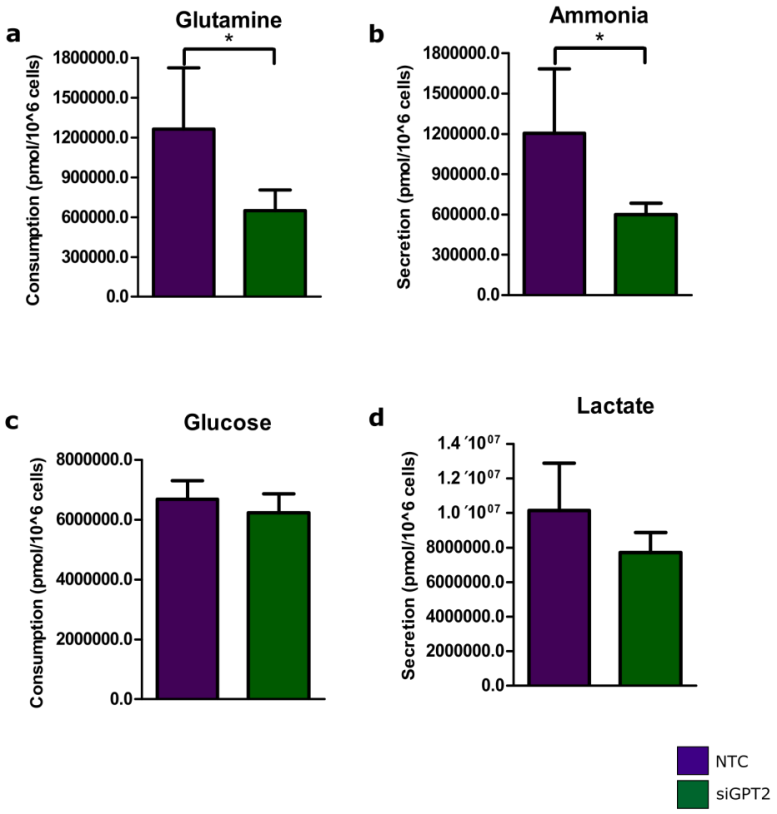

Figure 19: Effect of GPT2 knockdown on extracellular metabolites. Cells were transfected with siGPT2 and control siRNA (NTC). Transfection media was replaced by fresh media 24h after transfection. Spent media was collected after 48h of incubation with fresh media and used to measure (a) glutamine, (b) ammonia (c) glucose, and (d) lactate levels via HPLC. Data are presented as mean ± SD. n=4. * represents $p<0.05$.

4.3.2 Effect of GPT2 on intracellular metabolites

Glutamine is an important source of TCA cycle intermediates in cancer cells. The observed decrease in glutamine consumption upon inhibition or knockdown of GPT2, in MDA MB 468 cells, indicates that the supply of carbon to the TCA cycle may suffer due to the blockage of this pathway. In order to prove this hypothesis, levels of TCA cycle intermediates within the cells were measured 24h after inhibitor treatment. As shown in Figure 20a, MDA MB 468 showed significant decrease in α-ketoglutarate (α-KG) levels, which is the direct product of alanine aminotransferase and other glutaminolytic reactions. Concomitantly, malate and fumarate

levels were also significantly decreased in the cells. Pyruvate and citrate levels, however, did not show any significant change, further validating the fact that the decrease in the TCA cycle intermediates was a result of change in glutamine metabolism. Interestingly, MDA MD 231 (Figure 20b) did not show a similar decrease in the TCA cycle intermediates, instead α-KG even showed a slight increase under inhibitor treatment. Pyruvate and citrate levels remained unchanged in MDA MB 231 cells like in the MDA MB 468 cells. MCF7 cells (Figure 20c), on the other hand did not show any change in α-KG levels, while, succinate, fumarate and malate levels increased slightly which is in line with data showing that MCF7 is least affected by the inhibitor (Figure 15a, 20c). These results indicated that even though the cells show similar phenotypic effects at the cellular level, the adaptation or reaction to inhibitor treatment differs between different cell lines at the molecular level.

a MDA MB 468

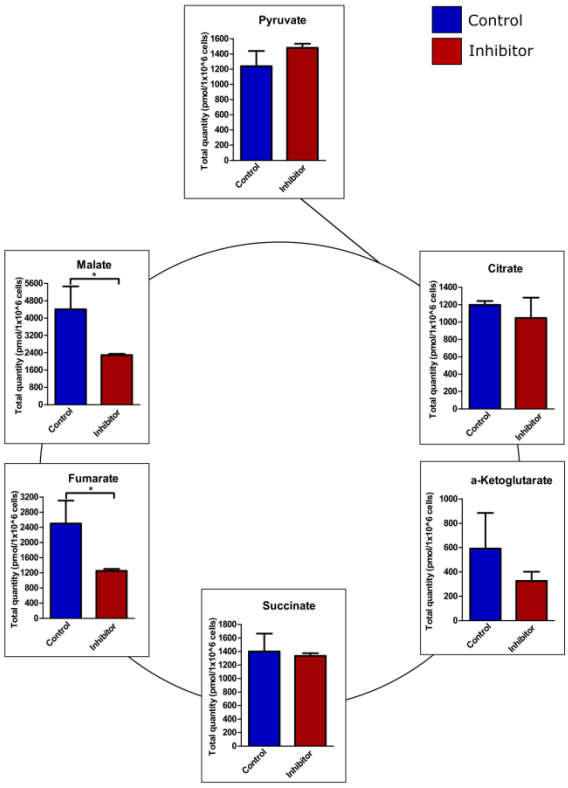

b MDA MB 231

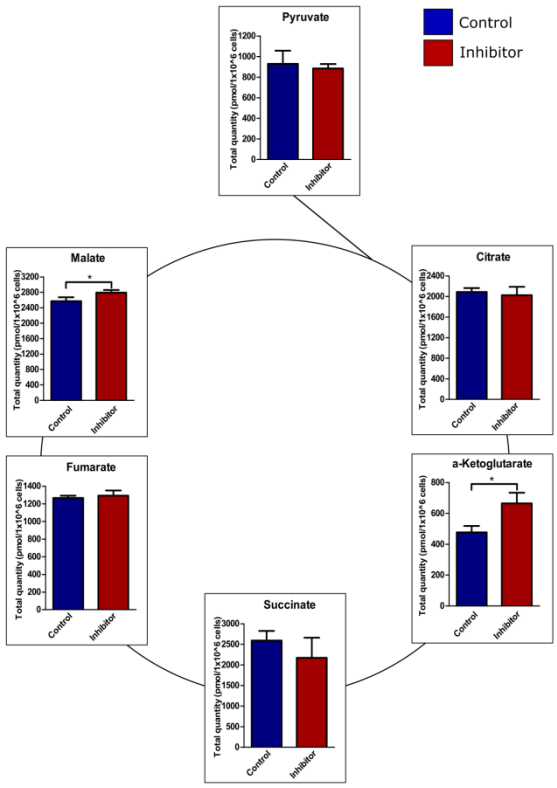

c MCF7

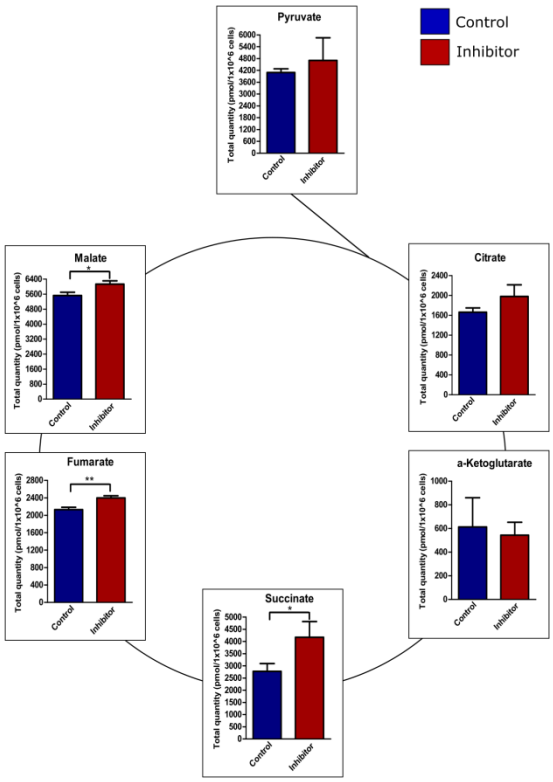

Figure 20: Effect of GPT2 inhibition on TCA cycle intermediates. Cells were treated with inhibitor ((a) MDA MB 468: 75µM, (b) MDA MB 231: 25µM, (c) MCF7: 100µM) for 24h (with a media change after 20h). Cells were harvested, polar metabolites were extracted and TCA cycle intermediates were absolutely quantified via GC-MS. Data are presented as mean ± SD, n=3. ** represents $p<0.01$, * represents $p<0.05$.

4.3.3 Effect of GPT2 inhibiton on metabolic enzymes

The changes in metabolite levels seen after GPT2 inhibition indicated that the cells undergo metabolic rewiring when the alanine aminotranferase reaction is blocked. While these modifications arise as an adaptation to the altered substrate and product levels, there may be additional changes to the enzymes as well. In order to test this, levels of key enzymes in glucose as well as glutamine metabolism and the TCA cycle were analyzed after 24h treatment with the inhibitor (Figure 21). In MDA MB 468 cells, while glutamine metabolism enzymes showed a trend to decrease with inhibitor treatment, the TCA cycle enzymes decreased significantly

which was in concomitance with the changes observed at the metabolic level(Figure 21a). Glucose transporter also displayed a small but significant decrease even though consumption of glucose did not show any significant change. In MDA MB 231, the results again corroborated with the metabolite data as most enzymes tended to increase after inhibitor treatment although the changes were not significant(Figure 21b). MCF7 did not show any sgnificant change and there was not any clear trend in the enzyme levels seen(Figure 21c). RPPA and initial data analysis was done together with Stephan Bernhardt.

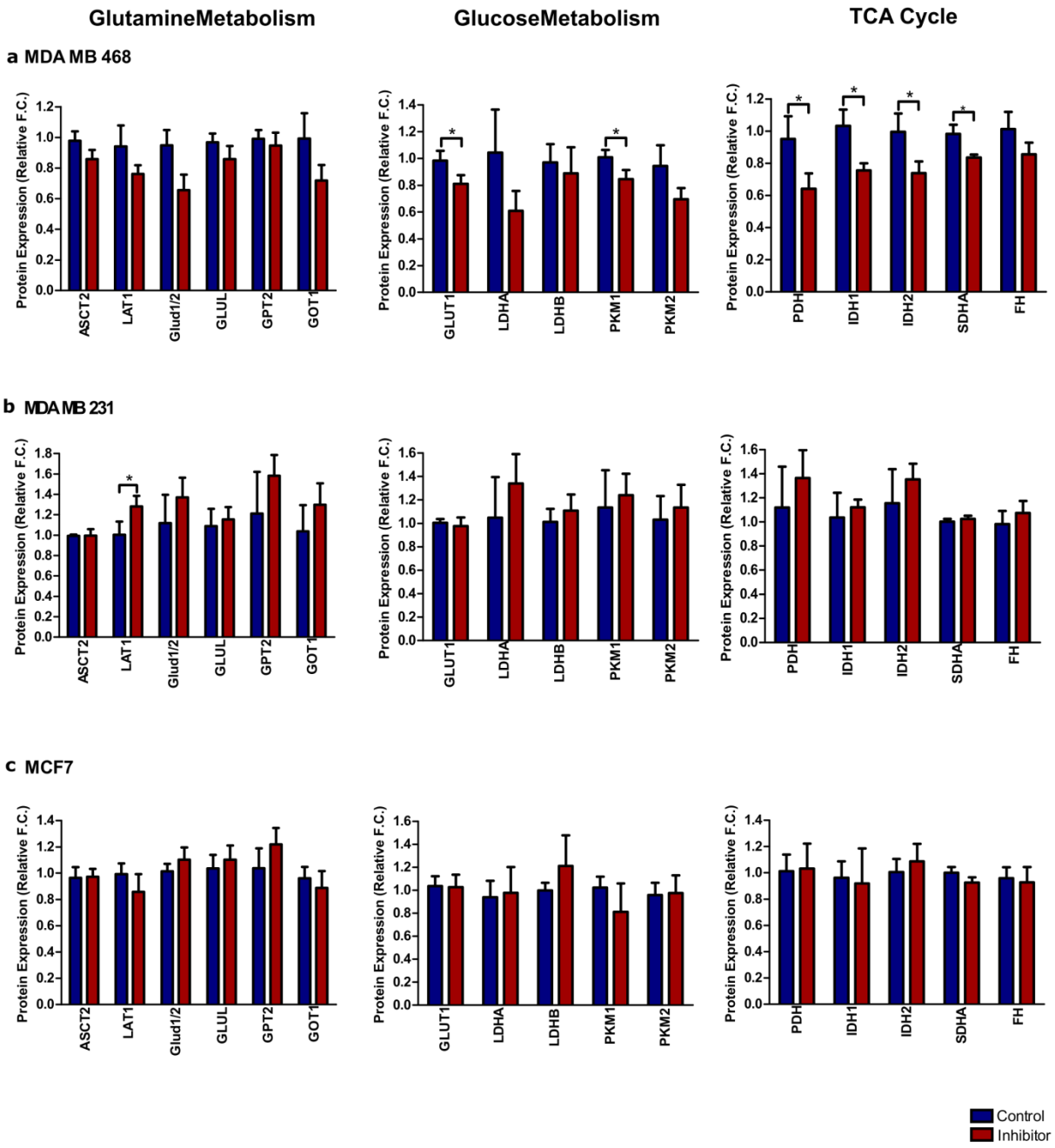

Figure 21: Effect of GPT2 inhibition on key metabolic enzymes. Cells were treated with inhibitor BCLA (MDA MB 468: 75µM, MDA MB 231: 25µM, MCF7: 100µM). Protein was harvested after 24h and expression levels of the different metabolic enzymes were determined via RPPA. Protein levels were first normalized to total protein levels and then to control samples. Data are presented as mean ± SD, n=3. * represents $p<0.05$.

4.3.4 Effect of GPT2 inhibiton on metabolic phenotypes

The significant changes seen in the TCA cycle both at the metabolic and protemic levels in MDA MB 468 cells suggest that upon inhibitor treatment the cells suffer from the lack of crucial TCA cycle intermediates (Figure 20, 21). One of the main functions of the TCA cycle is to provide electron carriers for oxidative phosphorylation, absence of which causes an energy deficit in the cells. In Figure 8, the decrease in luminescence post GPT2 knockdown indicated that there was an energy deficit in the cells due to the fact that the cell titer glo assay measures ATP content in the cells.Therefore, it was intriguing to see what effect the inhibitor has on the oxygen consumption rate (OCR), which is often used as a proxy for oxidative phosphorylation. The seahorse bianalyzer was used to detect OCR (details in section 3.2.9) MDA MB 468 cells treated with BCLA indeed showed decreased oxygen consumption (Figure 22a). Interestingly, despite not showing any significant changes at the metabolite or protein levels, OCR also of MCF7 cells was found to be decreased post inhibitor treatment (Figure 22b). When the cells were pushed to utilize their maximum respirative capacity (via addition of mitochondrial uncoupler FCCP) the difference between control and inhibitor treated cells became even stronger, suggesting that indeed the fitness and flexibility of the cells are affected by the inhibition of GPT2.

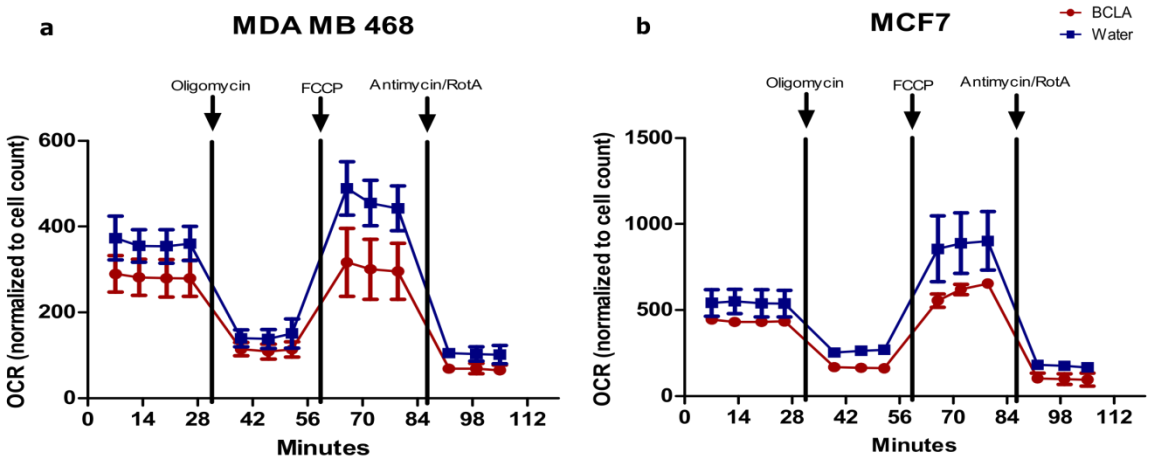

Figure 22: Effect of GPT2 inhibition on oxygen consumption rate. Cells were treated with inhibitor (MDA MB 468: 75µM, MCF7: 100µM) for 24h. Oxygen consumption rate in the cells were analyzed by the seahorse bioanalyzer. Graphs are representative of n=3 (each with 7 technical replicates).

4.3.5 Effect of GPT2 on carbon labeling of intracellular metabolites

The data above indicates that GPT2 inhibition results in a decrease in glutamine uptake in MDA MB 468 cells. This results in a reduction of carbon flow from glutamine into the TCA cycle. However, uptake of glucose which provides the carbon backbone of alanine remains unchanged. Lactate secretion is also unaltered under these conditions. This led to the question of what happens to the carbon from glucose that would enter the alanine aminotransferase pathway in non-perturbed conditions. In the absence of GPT2 activity and change in lactate secretion the excess carbons should lead to a buildup of pyruvate which might then enter into the TCA cycle. This way the decrease in carbon atoms entering the TCA cycle from glutamine could also be compensated for. In order to test this, cells were treated with inhibitor for 24h and then incubated with media supplemented with ^{13}C-glucose instead of ^{12}C-glucose for 30 min. Thereafter, the cells were harvested and the incorporation of carbon-13 in TCA cycle metabolites was determined. In all cell lines, the glucose pools were replaced by 90% or more and lactate labeling remained unchanged by BCLA. The results are represented as % label incorporation into the intermediates which will be referred to as labeling, and total labeled quantities. The results corroborated the initial hypothesis as it was observed that all measured TCA cycle intermediates showed an increase in glucose carbon labeling in MDA MB 468 cells (Figure 23a). However, most interestingly, it was seen that as a result of GPT2 inhibition, MDA MB 468 showed a high increase in pyruvate carboxylase (PC) activity which results in the formation of labeled malate and fumarate m+3 fractions. Citrate m+3 fraction which can originate from both pyruvate dehydrogenase (PDH) and PC catalyzed reactions, also increased significantly. Further analysis of the total labeled products showed that indeed, the 13C labeled malate and fumarate m+3 fractions as well as citrate m+3 fractions were higher when GPT2 activity was inhibited, whereas the m+2 fractions which exclusively originate from the PDH reaction remained unchanged.

MDA MB 231 (Figure 23b) showed a trend of increased ^{13}C-glucose derived incorporation in TCA cycle intermediates although this was not significant, which is in accordance with the fact that carbon flow into the alanine aminotransferase pathway is low in MDA MB 231 already in non-pertubed conditions. Hence, blockage of this pathway was not expected to lead to much

buildup of carbon atoms that could be shuttled elsewhere. Interestingly, MDA MB 231, did not show an increase in PC activity, however, it was observed that the PC reaction was already elevated in these cells compared to the other two cell lines (Figure 23, 24). Subsequently, the labeled quantities coming from the PC reaction did not increase further, however, labeled quantities of products coming from the PDH reaction showed an increasing trend.

MCF7 (Figure 23c) showed a significant increase in fumarate and malate carbon labeling, while citrate, α-KG and succinate, remained unchanged, decreased or showed an increasing trend respectively. Although, MCF7 had a lower PC pathway activity compared to MDA MB 231 and was similar to MDA MB 468, it did not show an increase in PC reaction. Total labeled quantities of malate and fumarate m+2 fractions were higher in inhibitor treated cells, confirming that blockage of the GPT2 pathway shunts glucose carbon atoms into the TCA cycle pathway. Labelling expreiments were performed in collaboration with Nadine Royla, who also did the initial data processing

a MDA MB 468

% Label Incorporation

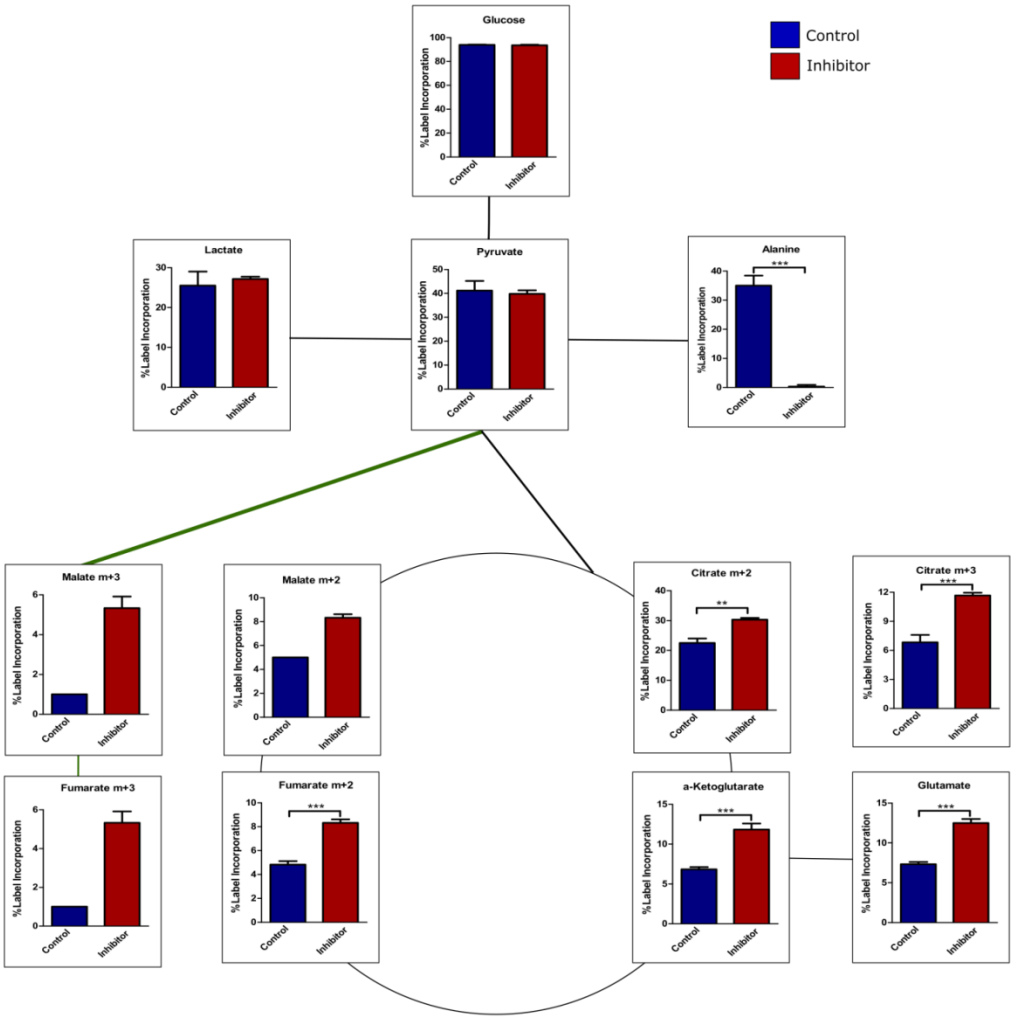

Labeled Quantities

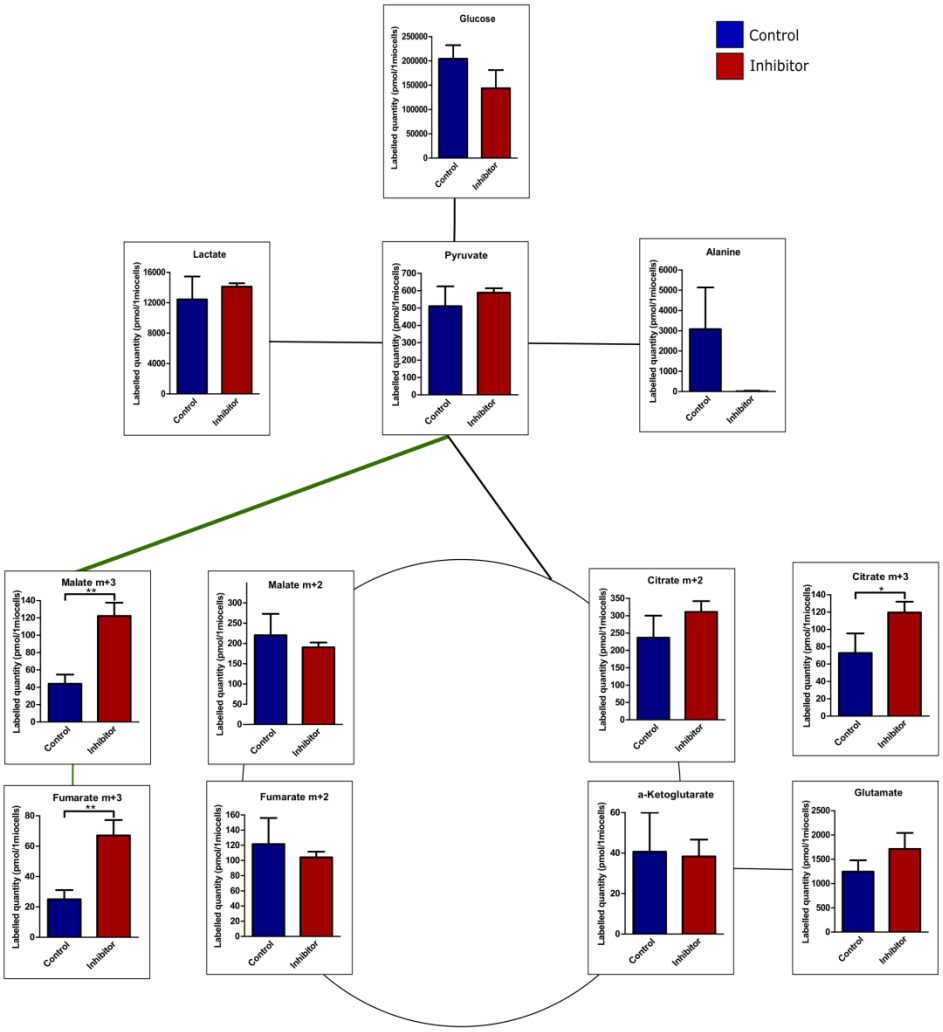

b MDA MB 231

% Label Incorporation

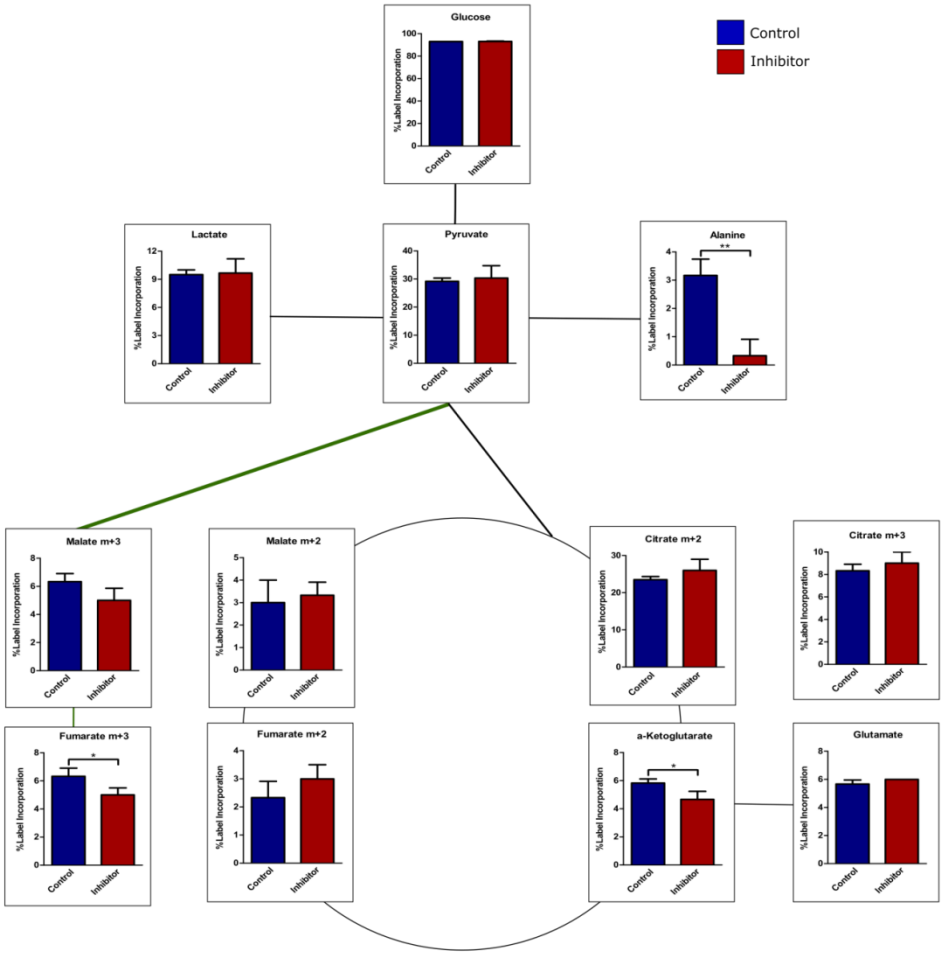

Labeled Quantities

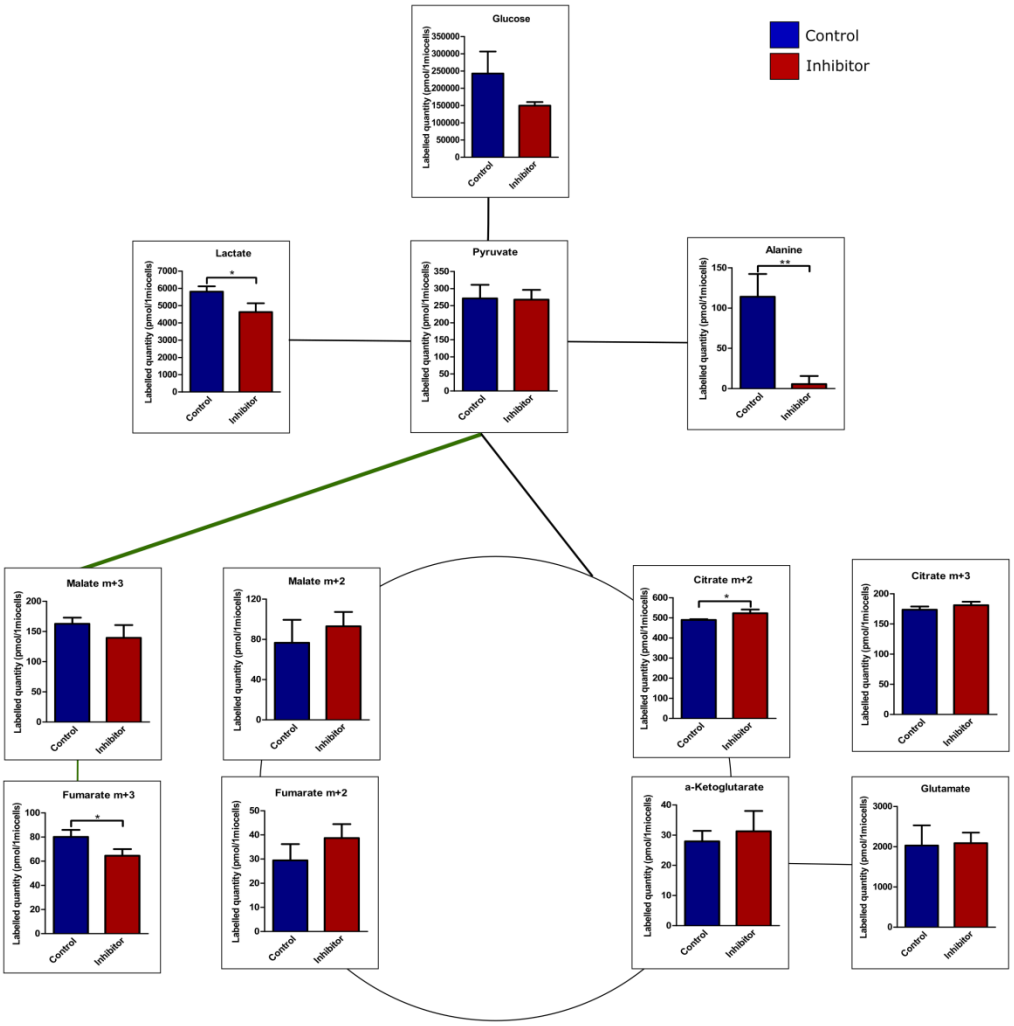

c MCF7

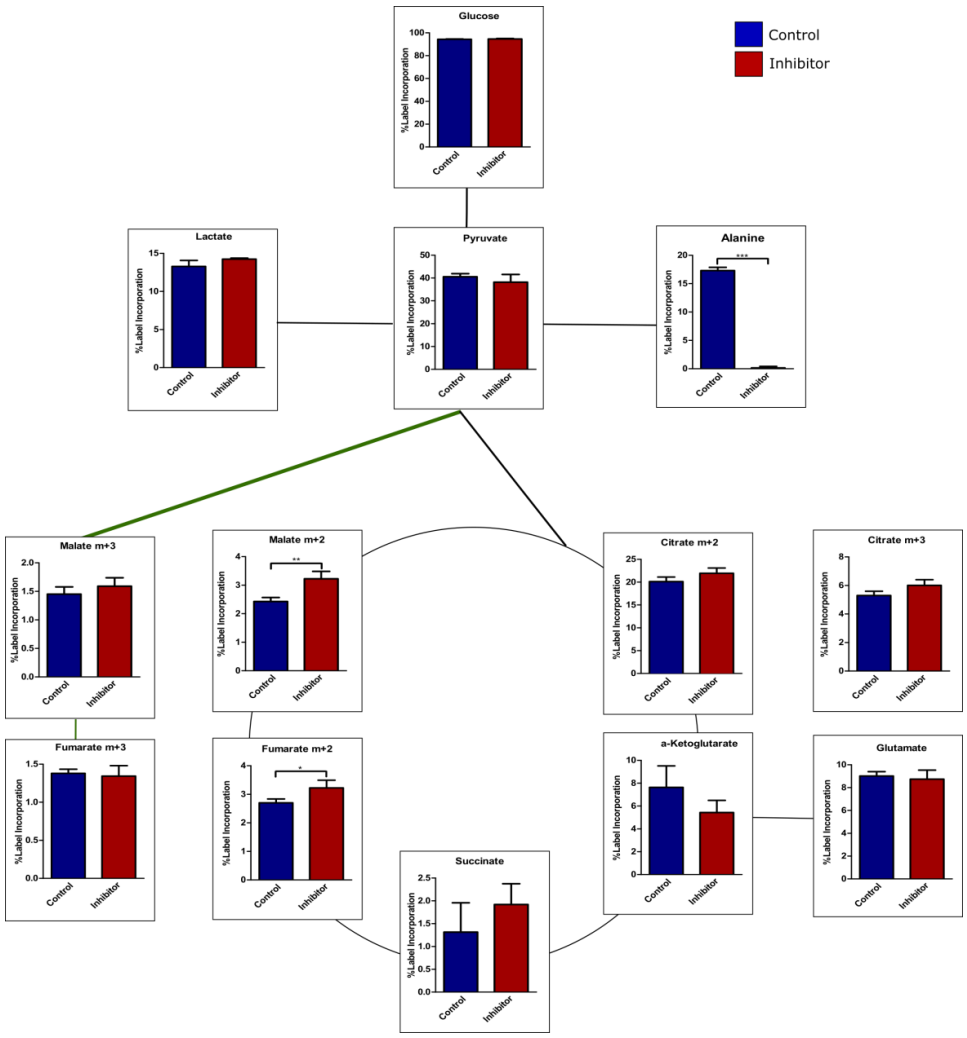
% Label Incorporation
Control
Inhibitor
Glucose
Lactate
Pyruvate
Alanine
Malate m+3
Malate m+2
Citrate m+2
Citrate m+3
Fumarate m+3
Fumarate m+2
Succinate
a-Ketoglutarate
Glutamate
%Label Incorporation

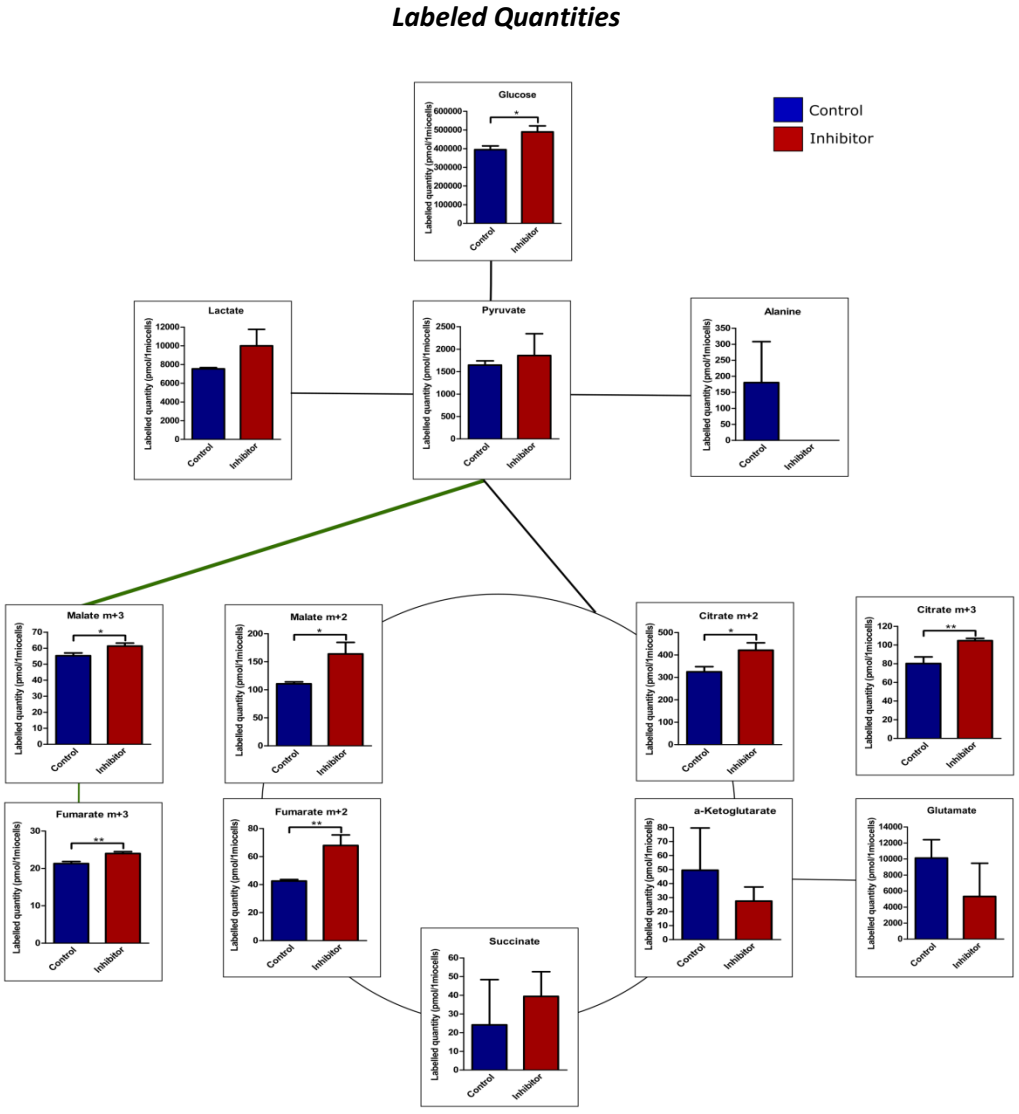

Figure 23: Effect of GPT2 inhibition on Glucose Labeling of TCA cycle intermediates. Cells were treated with inhibitor ((a) MDA MB 468: 75µM, (b) MDA MB 231: 25µM, (c) MCF7:100µM) for 24h (with a media change after 20h). Cells were incubated with media supplemented with ^{13}C-glucose for 30min and subsequently polar metabolites were extracted and incorporation of glucose derived carbon-13 in intracellular metabolites was measured via GC-MS. Data are presented as mean ± SD, n=3. *** represents $p<0.001$, ** represents $p<0.01$, * represents $p<0.05$.

4.4 Effect of Combinatorial targeting of GPT2 and PC

The aforementioned results indicate that inhibition of the GPT2 catalyzed reaction rewires carbon flow in cancer cells. The reduction of TCA cycle intermediate α-KG, which is produced by the GPT2 catalyzed reaction, and the buildup of pyruvate leads to an increased flow of glucose into the TCA cycle. However, glucose can enter the TCA cycle via two routes, PDH catalyzes the forward TCA cycle and PC catalyzes the reverse cycle. PDH irreversibly catalyzes the reaction that results in oxidative decarboxylation of pyruvate to form acetyl CoA and NADH, while PC catalyzes the carboxylation of pyruvate to form oxaloacetate, products from both reactions can then be used to fuel the TCA cycle. Different cell lines behave diversely, depending on their metabolic landscape. MDA MB 468 cells switched to a PC-driven TCA cycle under GPT2 inhibition, while the other two cell lines did not and instead upregulated the PDH catalyzed reaction (Figure 23). While PDH activity was observed to be similar at basal conditions for these cell lines (Figure 24 a-c). In contrast, PC activity was diverse in the cell lines also at basal conditions which could be the rationale for differential usage of this pathway under metabolic stress (Figure 24 d-f). RPPA was done by Stephan Bernhardt, labelling was done together with Nadine Royla who did the initial data processing.

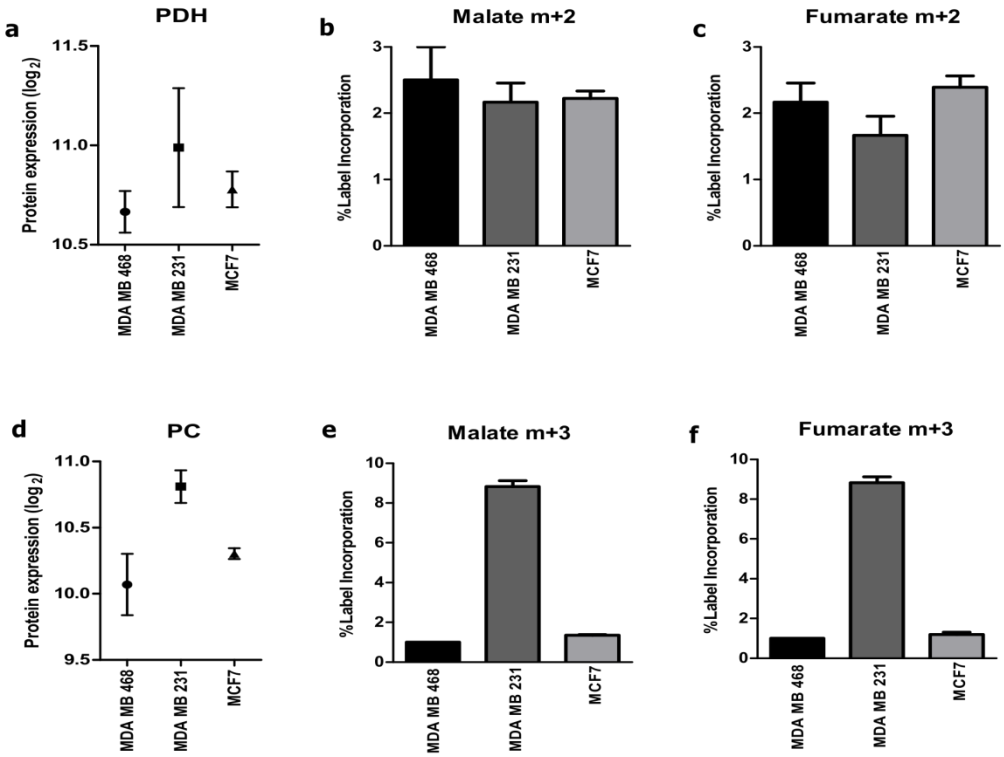

Figure 24: PDH and PC expression and activity in different breast cancer cell lines. (a,d) Basal levels of PDH and PC were measured by RPPA. (b-c, e-f). Protein expression was normalized to total protein levels Cells were labeled for 30min with glucose labeled media and subsequently harvested and labeling in intracellular metabolites was measured via GC-MS. Data are presented as mean ± SD, n=3.

In order to see how much the cells depend on PC for their growth, first PC was knocked down using 4 siRNAs and knockdown efficiency was assessed 72h post transfection. All 4 siRNAs showed greater than 70% decrease in mRNA and protein levels in MDA MB 468 and MDA MB 231 cells (Figure 25). siPC#3 and siPC#4 were used for further experiments.

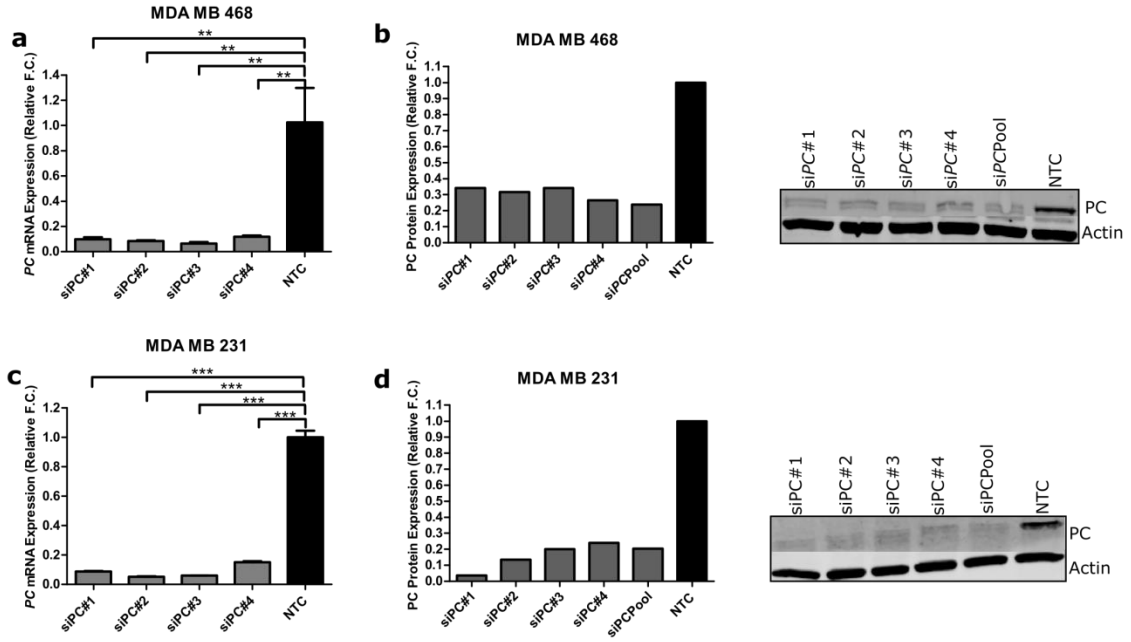

Figure 25: Knockdown efficiency of siPC in MDA MB 468 and MDA MB 231 cells Cells were transfected with siPC (pool and individual). RNA and protein were harvested 72h after transfection and knockdown efficiency was determined by qPCR (a,c) and western blot (b,d) respectively. All values were normalized to NTC. Values for mRNA expression were first normalized to *PUM1* levels and are presented as mean ± SD of 3 technical replicates. Protein expression values were first normalized to actin levels. n=1 *** represents $p < 0.001$, ** represents $p < 0.01$

In the next experiments the effect of PC knockdown on cell proliferation was tested. While MDA MB 468 was affected the most, MDA MB 231 was least affected despite having a higher activity of PC. (Figure 26 a-c) This was contrary to expectations as MDA MB 231 had the highest PC protein expression as well as activity (Figure 24).To investigate the effect of GPT2 inhibition on cells lacking PC, cells were treated with BCLA 8h after transfection with PC siRNA (Figure 26a and b). MDA MB 468 cells showed a moderate but significant decrease in cell proliferation following the combinatorial treatment with a PC siRNA and BCLA compared to the individual treatment (Figure 26a). MDA MB 231 showed no significant additional change in proliferation when treated with inhibitor in combination with siPC#3, while the minor difference seen with siPC#4 indeed reached significance (Figure 26b). MCF7 also seemed to be affected by combinatorial treatment since this showed a slight albeit significant change in cell proliferation

(Figure 26c). Knockdown of *PC* mRNA after 8h of transfection was confirmed in MDA MB 468 cells (Figure 26d).

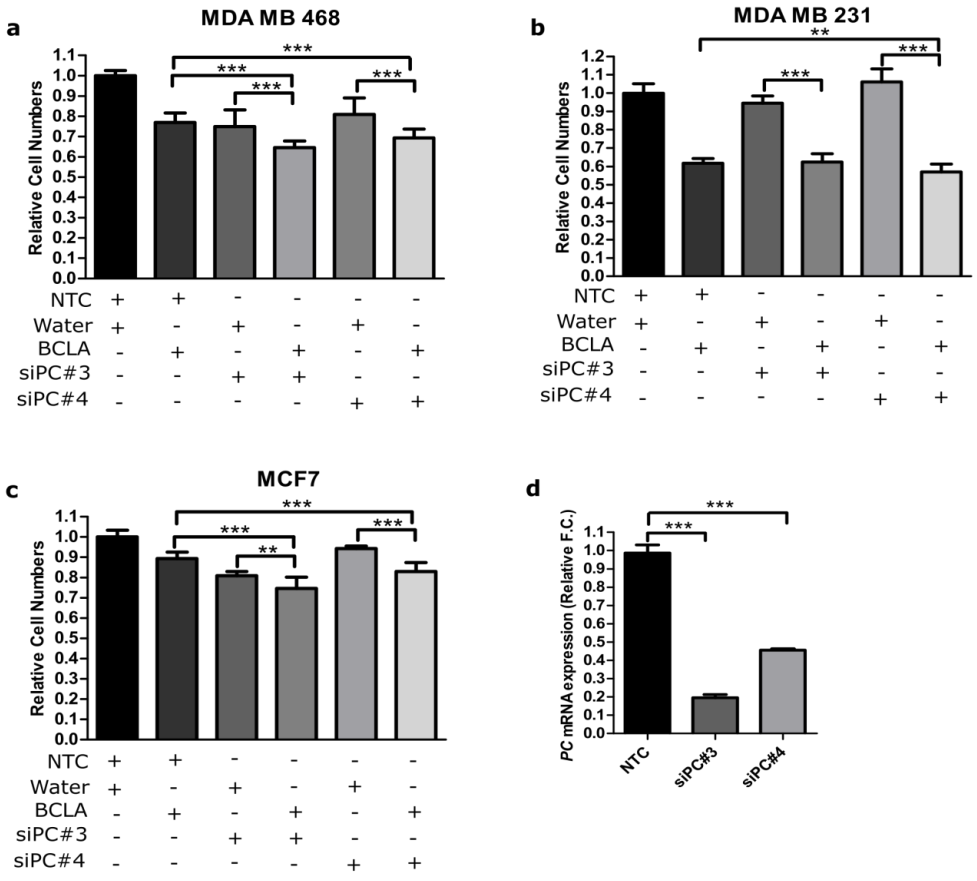

Figure 26: Combinatorial Effect of GPT2 inhibition and PC knockdown on cell growth. (a-c) Cells were transfected with PC siRNA. 8h post transfection cells were treated with inhibitor (MDA MB 468: 75µM, MDA MB 231: 25µM, MCF7:100µM) for 72h. Microscopy based nuclei counting was performed to determine cell numbers. (d) RNA was harvested from MDA MB 468 8h after transfection and knockdown efficiency was determined by qPCR. All values were normalized to control (NTC + water). For cell numbers data are presented as mean ± SD, n=2(each with 6 technical replicates). Values for mRNA expression were first normalized to *PUM1* levels and are presented as mean ± SD of 3 technical replicates. *** represents $p < 0.001$, ** represents $p<0.01$.

Knockdown efficiency of the siRNAs in MCF7 was tested at both RNA and protein levels and was found to be >70% (Figure 27).

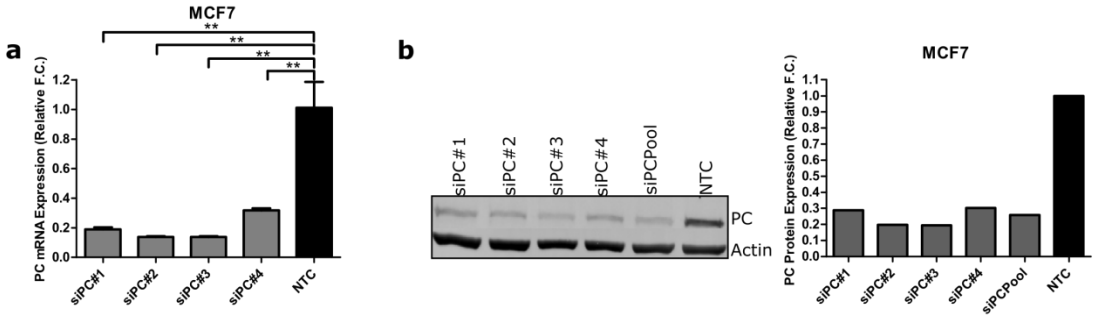

Figure 27: Transfection efficiency of siPC in MCF7 cells. Cells were transfected with siPC (pool and individual). RNA (a) and protein (b) were harvested 72h after transfection and knockdown efficiency was determined by qPCR and western blot respectively. All values were normalized to non-targeting control siRNA (NTC). Values for mRNA expression were first normalized to *PUM1* levels and are presented as mean ± SD of 3 technical replicates. Protein expression values were first normalized to actin levels. n=1. ** represents $p < 0.01$

As MDA MB 468 cells showed an increase in the flow of carbon atoms through the PC catalyzed pathway after inhibitor treatment, further investigation was required to answer the question of what effects PC and GPT2 proteins have on each other. Preliminary experiments showed that while GPT2 knockdown or inhibition did not have an effect on PC protein expression (Figure 28a, inhibitor data not shown), PC knockdown did increase the levels of GPT2 protein (Figure 28b). Further experiments need to be done to confirm these observations.

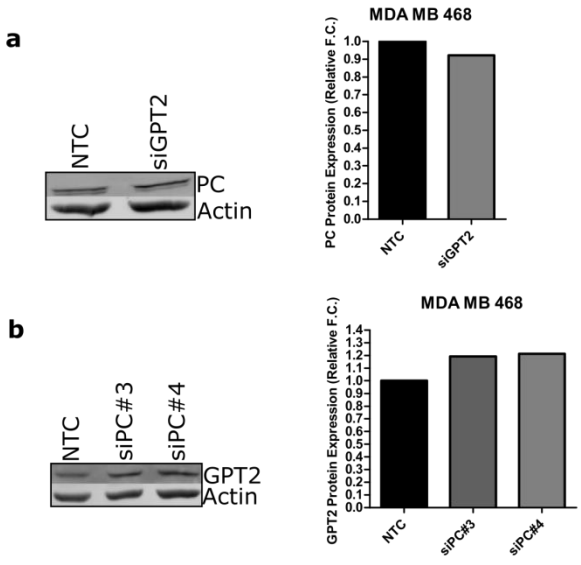

Figure 28 : Effect of GPT2 and PC on the expression of one another. Cells were transfected with siGPT2 (a) or siPC (b). Protein was harvested 72h after transfection and expression levels were determined by western blot. All values were first normalized to actin levels and then to NTC, n=1.

4.5 Combinatorial Treatment of GPT2 and Oxidative Phosphorylation Inhibition

4.5.1 Combinatorial Treatment of GPT2 Inhibitor and Rotenone

Glycolysis and TCA cycle are important sources of electron carriers which are used in oxidative phosphorylation to generate ATP. The rewiring of the TCA cycle as a result of GPT2 inhibition, therefore not only affects the macromolecular biosynthetic pathways it supports but also energy generation which the cells strive to keep operative by pushing carbon flow into the TCA cycle. Therefore, it was hypothesized that a combinatorial treatment inhibiting GPT2 and oxidative phosphorylation be more effective in retarding cancer cell growth. Rotenone is a highly potent mitochondrial complex I inhibitor used in several studies to induce mitochondrial dysfunction(W. Hu et al., 2016). It inhibits the oxidation of NADH to NAD leading to oxidative stress. In breast cancer it has been shown to cause DNA damage and apoptosis(Deng, Huang, & Lin, 2009).

Using various concentrations of rotenone reported in previous studies conducted with the cancer cell lines, the effects of rotenone on the 3 cell lines used in this project were studied. All cell lines showed significant decreases in cell numbers 72h after treatment in a dose dependent manner (Figure 29a). However, MDA MB 231 cells were affected most severely, with an 80% decrease in cell numbers at the higher concentrations. Notably, in all three cell lines there was a sharp drop in cell numbers at 1µM concentration of rotenone. To confirm the effects of rotenone on the cell lines, reported markers, cleaved PARP (marker for DNA damage) and Bcl2-L-4 (apoptosis marker), were tested (Figure 29 b-d). Cleaved PARP indeed increased in MDA MB 468 and MCF7 even at the lowest concentration of rotenone tested, MCF7 showed a greater increase in cleaved PARP levels in line with the effect on cell numbers. Cleaved PARP could not be detected in MDA MB 231. Interestingly, even though MDA MB 231 showed a greater effect in cell proliferation, increase in Bcl2-L-4 was similar to that in MDA MB 468, while MCF7 had the highest increase in Bcl2-L-4 levels. Bcl2-L-4, however, increased in all three cell lines confirming the toxic effect of rotenone on all three cell lines

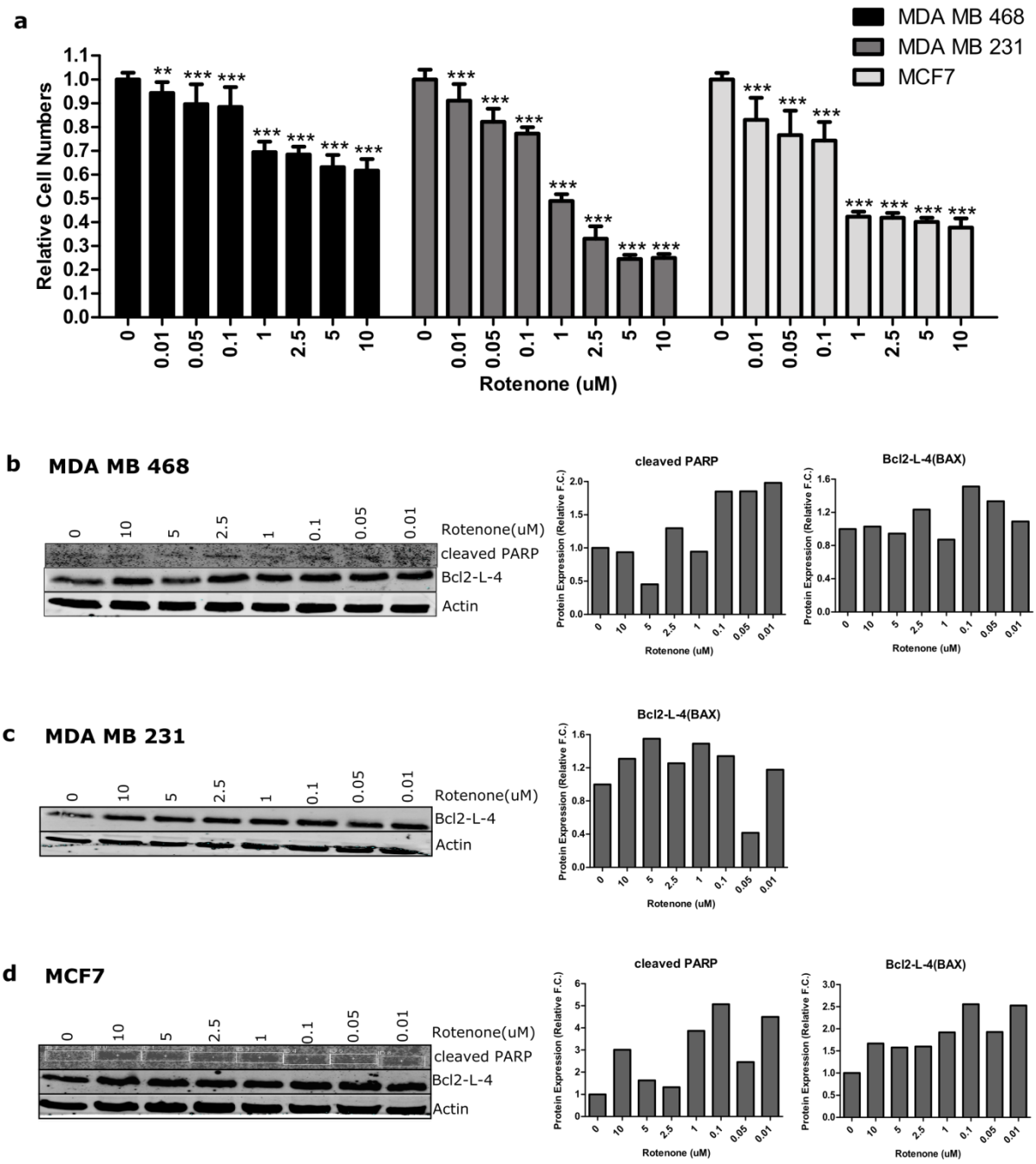

Figure 29: Effect of rotenone on breast cancer cells. (a) Cells were treated with different concentrations of rotenone for 72h. Microscopy based nuclei counting was performed to determine cell numbers. (b-d). Protein was harvested after treatment with different concentrations of rotenone for 24h and expression levels of target proteins were determined via Western blotting. All values were normalized to the untreated control (0). For cell numbers, data are presented as mean ± SD, n=1(with 6 technical replicates). Values for protein expression were first normalized to actin levels, n=1. *** represents $p < 0.001$, ** represents $p<0.01$.

Next, cells were treated with a combination of rotenone (rot) and the GPT2 inhibitor. For this experiment 3 concentrations of rotenone were chosen. Firstly, 1µM was chosen as it was the least tested concentration showing the most pronounced effect in all 3 cell lines, thereafter, 0.1 and 10µM were chosen to cover a large spectrum. BCLA concentrations were kept the same as before. As predicted, the combination of 0.1µM rotenone with the BCLA had an additive effect on the decrease in cell proliferation of MDA MB 468 cells (Figure 30a). In MDA MB 231, BCLA showed high toxicity and possibly therefore, the combination did not show any further effect (Figure 30b). In order to circumvent this, a lower concentration of the BCLA (10µM) was used in combination with rotenone, and similar to MDA MB 468, the combination of BCLA and 0.1 µM rotenone in MDA MB 231 cells showed an additive effect on growth (Figure 30c). MCF7 did not show a strong effect as a result of the combinatorial treatment (Figure 30d). While the effect of rotenone alone was high, the effect of BCLA was minor. Therefore, a higher concentration of BCLA (100µM) was used in combination with rotenone, the combinatorial effect was negligibly more than the effect of rotenone (Figure 30e), further proving that the effect of GPT2 inhibition strongly affects MDA MB 468 and MDA MB 231 but is not significant in MCF7.

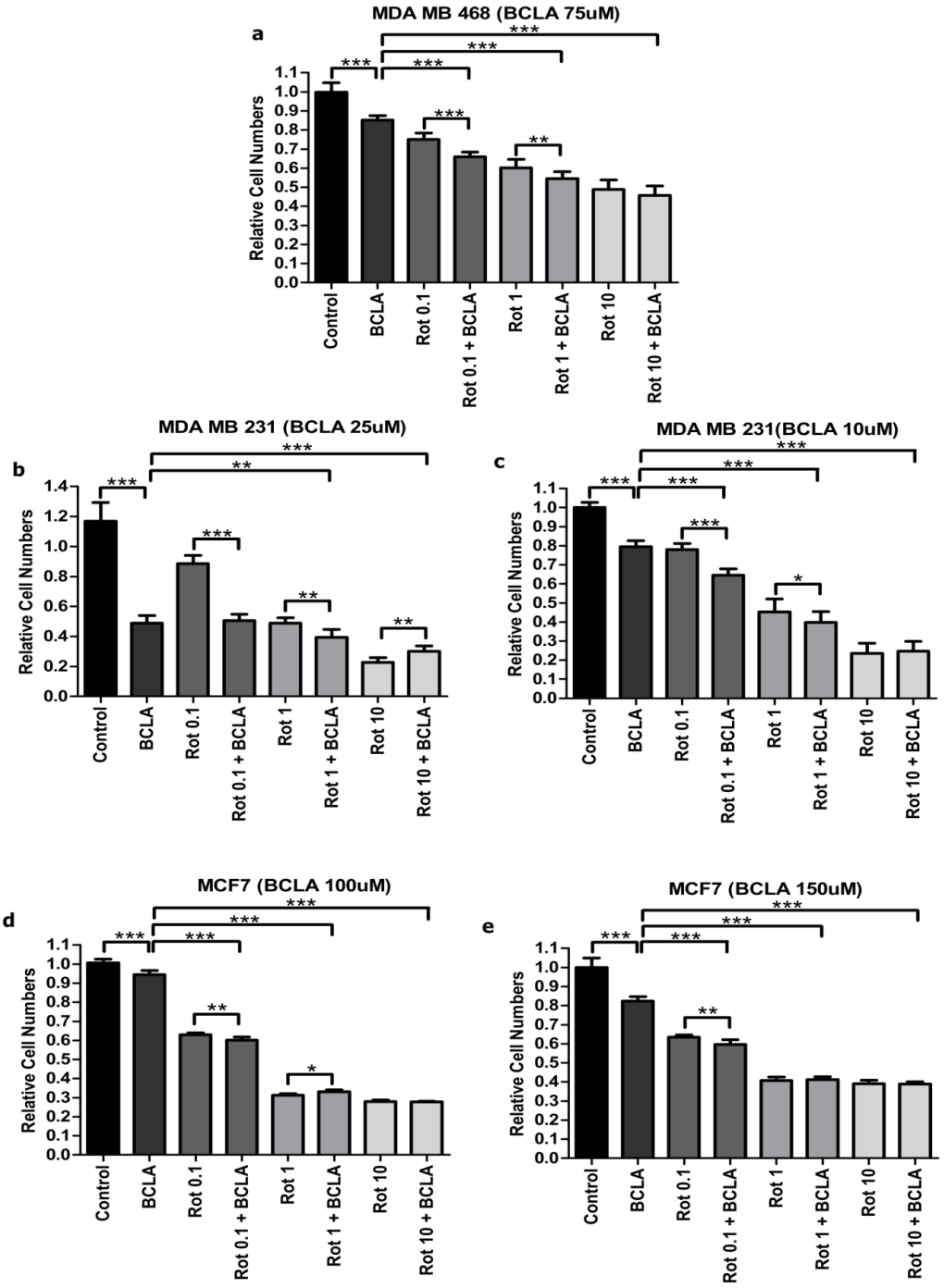

Figure 30: Combinatorial effect of rotenone and BCLA on breast cancer cells. (a) Cells were treated with different concentrations (μM) of rotenone (rot) and BCLA for 72h. Microscopy based nuclei counting was performed to determine cell numbers. All values were normalized to untreated control. Data are presented as mean ± SD, n=2(each with 6 technical replicates). *** represents $p < 0.001$, ** represents $p<0.01$, * represents $p<0.05$.

4.5.2 Combinatorial Treatment of GPT2 Inhibitor and Metformin

To further validate the findings made with rotenone, a different complex I inhibitor, namely, metformin was used. While rotenone is a specific inhibitor of complex I, metformin is not specific and has a milder effect on complex I(Madiraju et al., 2014). Similar to rotenone, a range of concentrations were used for metformin treatment as obtained from studies with breast cancer cell lines(Liu et al., 2009). For metformin, MDA MB 468 and MCF7 showed maximum and similar effects. Contrary to rotenone, metformin had the least effect on MDA MB 231 which could be due to difference in efficiency or due to the fact that the two drugs act via different routes (Figure 31a). As metformin acts via phosphorylation of AMPKa, the levels of phosphoAMPKa were determined(Galdieri, Gatla, Vancurova, & Vancura, 2016). All cell lines showed an increase in phospho AMPKa levels (Figure 31 b-d). Furthermore metformin causes dephosphorylation of RPS6 which leads to growth arrest(Sacco et al., 2016). All the 3 cell lines showed significant decrease in PRPS6 (Figure 31 b-d).

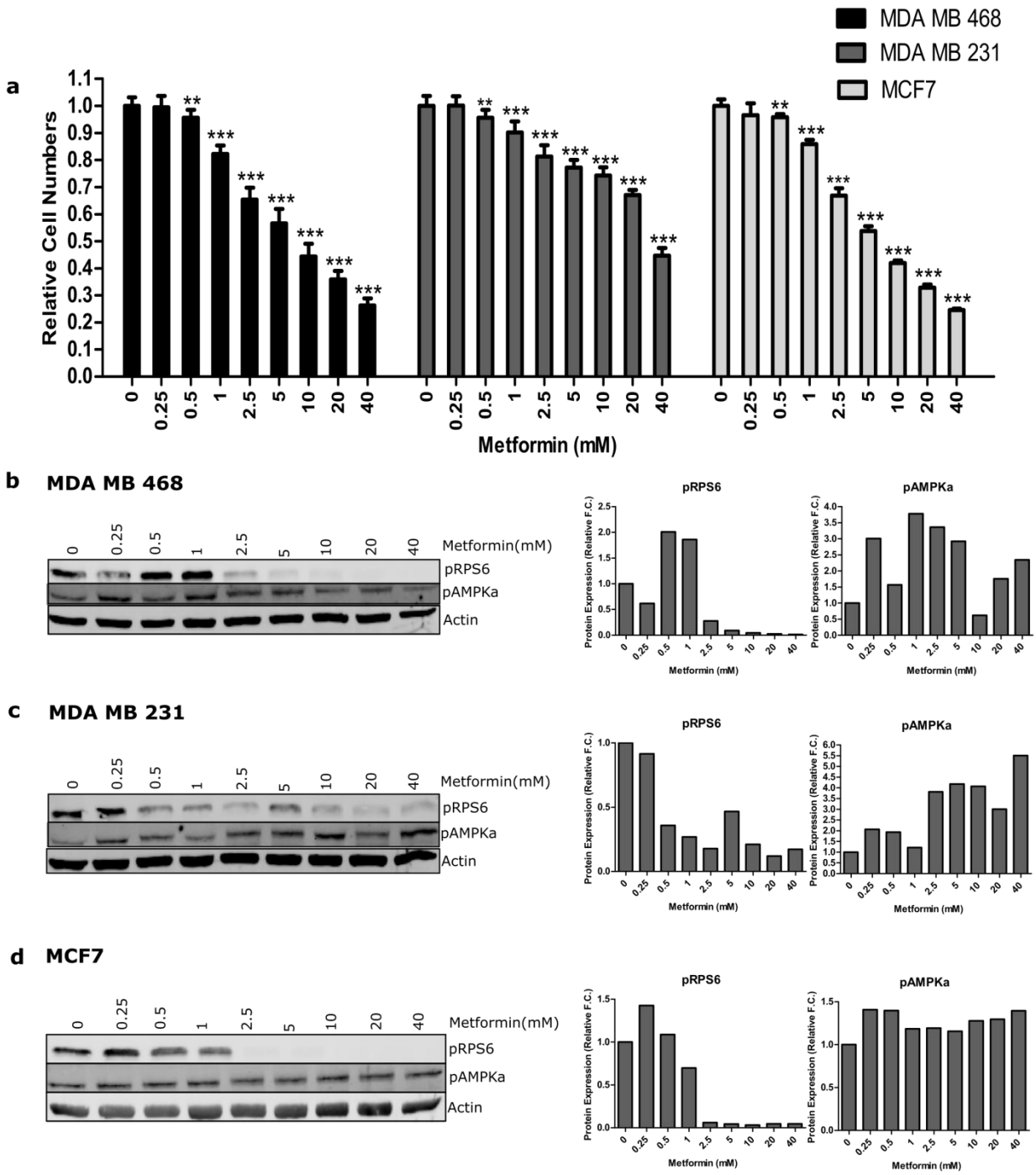

Figure 31 : Effect of metformin on breast cancer cells. (a) Cells were treated with different concentrations of metformin for 72h. Microscopy based nuclei counting was performed to determine cell numbers. (b-d). Protein was harvested after treatment with different concentrations of metformin for 24h and expression levels of target proteins were determined via western blotting. All values were normalized to untreated control. For cell numbers data are presented as mean ± SD, n=2(each with 6 technical replicates). Values for

protein expression were first normalized to actin levels, data is representative of two experiments. *** represents $p < 0.001$, ** represents $p<0.01$.

As MDA MB 468 and MCF7 showed a sharp decrease in cell numbers at 2.5mM Metformin concentration and MDA MB 231 at 5mM these were chosen as the effective concentrations. In order to test a range of combinations, 0.25mM and 20mM were also tested. MDA MB 468 showed a slight additional decrease in cell numbers when a combination of metformin 2.5 mM and BCLA was applied (Figure 32a) compared to individual BCLA or metformin treatment. The combinatorial treatment did not result in any additional effects when higher or lower concentrations of metformin were applied. Effects seen in MDA MB 231 were similar to those observed with the combination of rotenone and BCLA (Figure 32b). However, in this case reducing the BCLA concentration did not change the effect of the combination (data not shown). MCF7 on the other hand showed an additional effect with combination of highest concentration of metformin and BCLA (Figure 32c), while increasing BCLA concentration did not have any additional effect in combination with lower concentrations of metformin (data not shown).

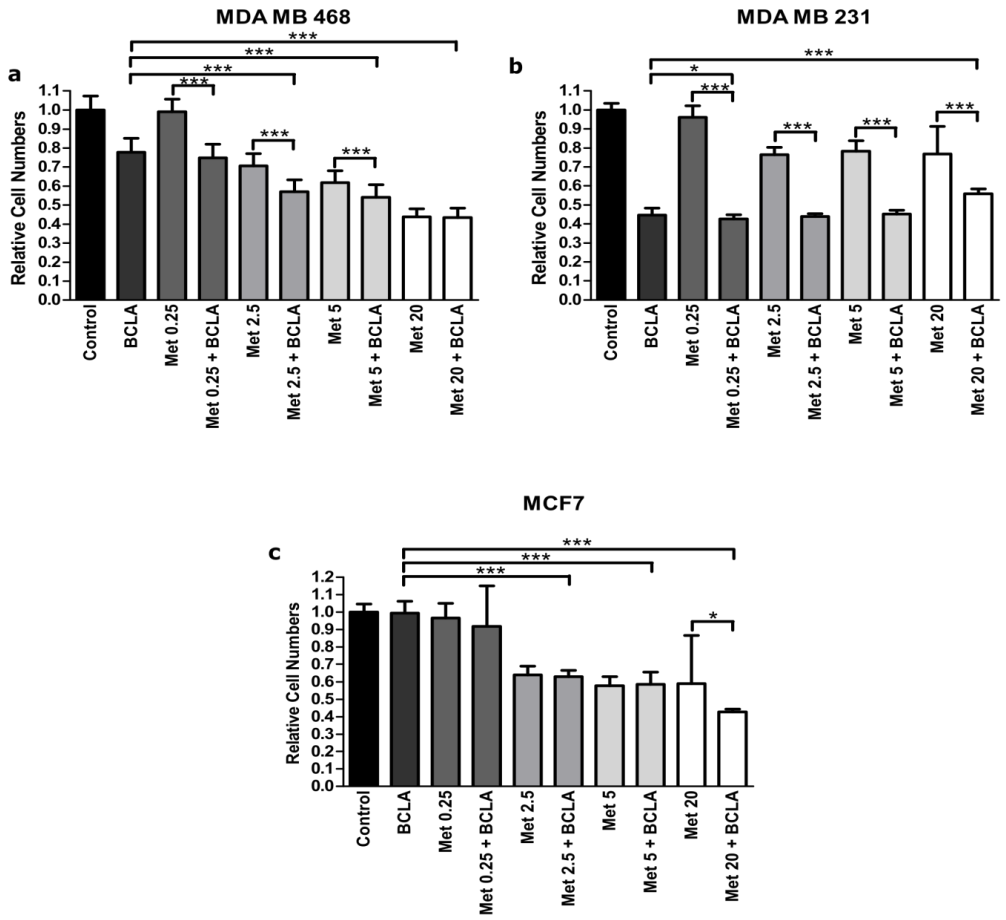

Figure 32 : Combinatorial effect of GPT2 inhibition and metformin on cell growth. (a-c) Cells were treated with different concentration of metformin (Met) and BCLA (MDA MB 468: 75µM, MDA MB 231: 25µM, MCF7:100µM) for 72h. Microscopy based nuclei counting was performed to determine cell numbers. All values were normalized to untreated control. Data are presented as mean ± SD, n=2(each with 6 technical replicates). *** represents $p < 0.001$, ** represents $p<0.01$, * represents $p<0.05$.

Therefore, the combination of BCLA, which has an impact on the TCA cycle and, likely, also on oxidative phosphorylation, and complex I inhibition further stresses the cells. However, this additional effect is dependent on the effect of the GPT2 inhibitor on the cells.

4.6 Clinical significance of *GPT2*

The above experiments prove that in an *in vitro* setup, GPT2 plays a crucial role in maintaining cancer cell growth. However further investigation was required to establish a clinical role of GPT2 in breast cancer patients. Using two publicly available datasets METABRIC (2000 patients) and TCGA (1200 patients), the expression of *GPT2* was analyzed. It was observed that in both datasets *GPT2* expression is the highest in the basal subtype of breast cancer, which has the worst prognosis (Figure 33 a, b). A more in depth analysis of the METABRIC dataset showed that *GPT2* expression significantly increases with increasing grade of tumor, which substantiates its role in aggressive cancers (Figure 33 c). As the METABRIC dataset has long follow-up data of patients (20 years), impact of *GPT2* on overall patient survival was analyzed. The dataset showed that high *GPT2* expression was associated with poor patient prognosis thus further consolidating the role of *GPT2* in tumor progression (Figure 33c).

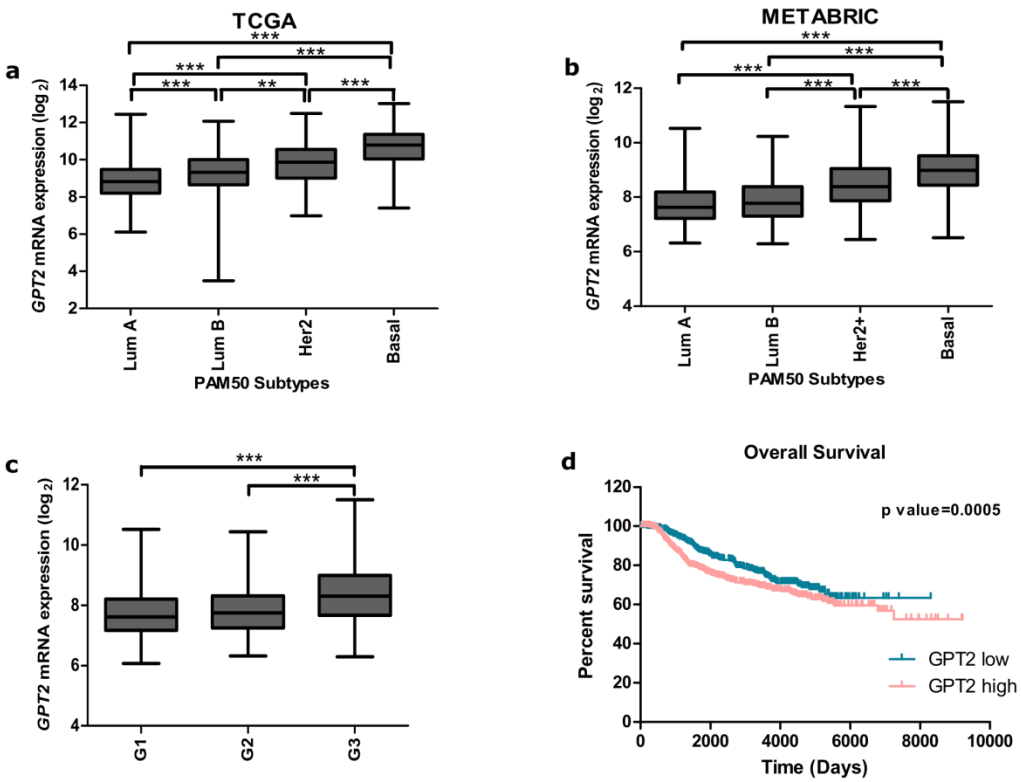

Figure 33: *GPT2* expression in breast cancer patients and correlation with overall survival. (a) *GPT2* mRNA expression analysis [$\log_2$ (x+1) rsem] of the TCGA dataset comparing the PAM50 subtypes Lum A

(n=421), Lum B (n=192), Her2 (n=67) and Basal (n=141). (b) *GPT2* mRNA expression analysis (log_2 a.u.) of the METABRIC dataset comparing the PAM50 subtypes Lum A (n=721), Lum B (n=492), Her2 (n=240) and Basal (n=331). (c) *GPT2* mRNA expression analysis of the METABRIC dataset comparing different grades, G1(n=170), G2(n=775) and G3(n=957). Quartile based survival analysis of the METABRIC dataset (Curtis et al., 2012) of *GPT2* high vs. low gene expression (for each quartile n=492). *** represents $p < 0.001$, ** represents $p<0.01$, * represents $p<0.05$.

The two analyzed datasets comprised of mRNA expression of genes. It was, therefore, important to find out whether or not these associations were correlating also at the protein level. Using an independent dataset from our group, containing clinical information of 800 breast cancer patients, the expression of GPT2 was explored. In corroboration with the mRNA data, GPT2 protein levels were the highest in triple negative breast cancers most of which are basal (Figure 34a). GPT2 protein also positively correlated with increasing grade of tumors in this dataset (Figure 34b). RPPA and raw data processing was done by Stephan Bernhardt. Statistical analysis was done by collaboration partners at Freiburg Institute for Advanced Studies

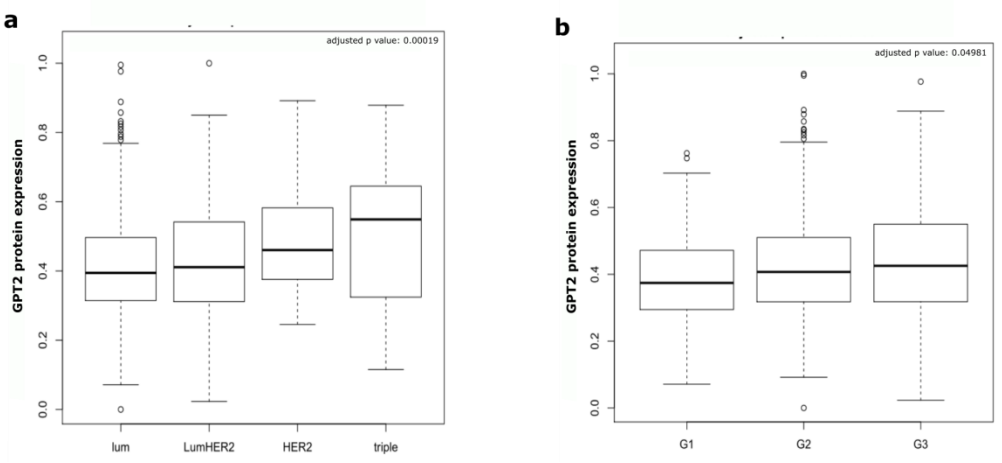

Figure 34: GPT2 protein expression in breast cancer patients. Box plots show GPT2 protein expression analysis of the 800 patient cohort comparing (a) molecular subtypes Lum (n=614), Lum HER2 (n=76), HER2 (n=35) and triple negative (n=75) and (b) different grades, G1 (n=91), G2 (n=501) and G3 (n=207). Kruskal-

Wallis Rank Sum test was applied to compare the groups and p-values were adjusted using the Benjamini-Hochberg procedure (Section 3.2.5.2).

4.7 Regulation of GPT2 expression

4.7.1 Regulation of GPT2 expression by c-Myc

The high expression of GPT2 seen in patients having a poor prognosis indicates that cancer cells rewire their metabolic pathways to increase alanine production. This reveals a higher level of regulation that may take place. c-Myc has been shown to regulate glutamine metabolism in several tumor entites including breast cancer (Korangath et al., 2015). To test if GPT2 levels might also be regulated by c-Myc, the MDA MB 468 cell line was used as a biological test system. Indeed, GPT2 both mRNA and protein levels decreased upon knockdown of c-Myc (Figure 35 a, c). c-Myc knockdown was confirmed at both mRNA and protein levels (Figure 35 b,d). Furthermore, GLS levels (Figure 35e) were also tested as a positive control for c-Myc knockdown(Gao et al., 2009) and showed a significant decrease.

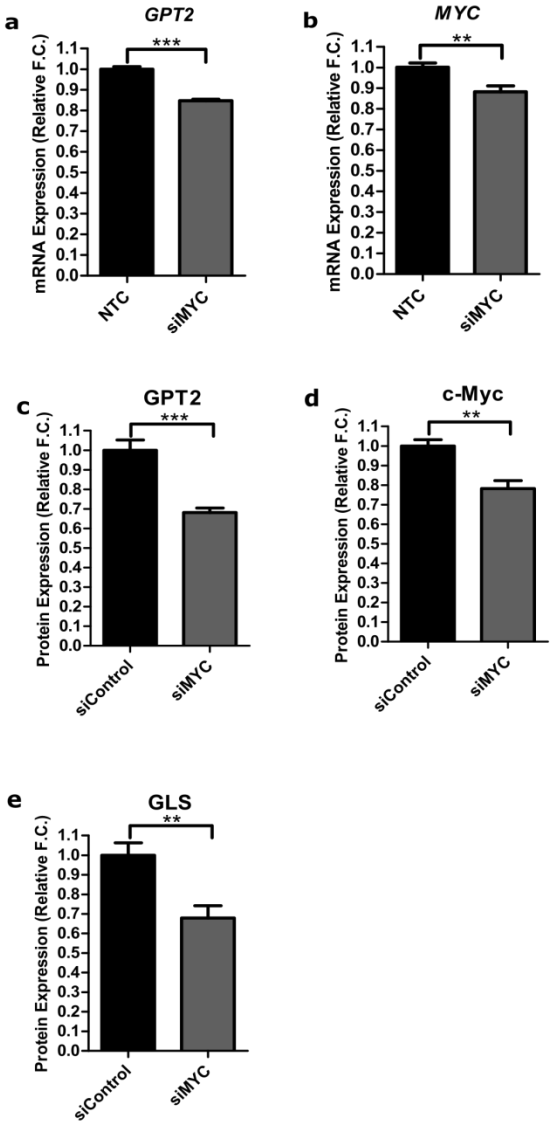

Figure 35: Regulation of GPT2 expression by c-Myc. (a-f) Cells were transfected with siMYC (30nM). RNA and protein were harvested 72h after transfection and knockdown efficiency was determined by qPCR (a-b) and RPPA (c-f) respectively. All values were normalized to non-targeting control. For mRNA the values were first normalized to *PUM1* levels and are presented as mean ± SD of 3 technical replicates. For protein levels the values were first normalized to total protein levels and are presented as mean ± SD, n=3. *** represents $p < 0.001$, ** represents $p<0.01$. (g)

To understand whether c-Myc regulation plays a role in breast cancer patients, c-Myc levels were next correlated with GPT2 levels in the the METABRIC dataset as well as in the in-house 800 patient dataset (RPPA done by Stephan Bernhardt, analysis done by Khalid Abnaof)(Figure

36 a,b). Myc levels correlated positively with GPT2 levels at both mRNA and protein levels. In fact the correlation was better at the protein levels.

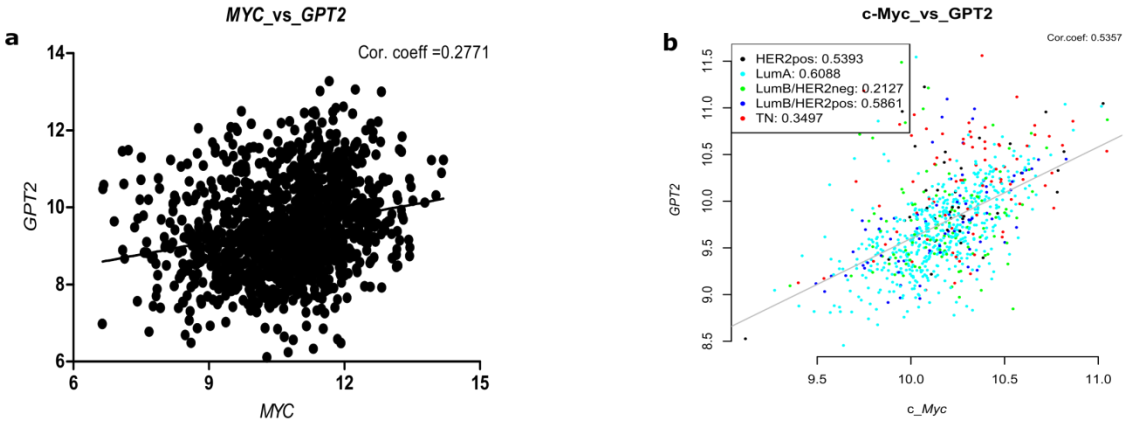

Figure 36: Correlation between MYC and GPT2 expression in patients. (a)Correlation analysis of *MYC* with *GPT2* gene expression of the TCGA dataset (n= 1215). (b) Correlation analysis of c-Myc with GPT2 protein expression of the 800 patient cohort (n=800). Correlation coefficient was calculated using Pearson correlation.

4.7.2 Regulation of GPT2 expression by ATF4

The previous experiments revealed that while c-Myc does play a role in GPT2 regulation, it does not regulate the entire expression, and *GPT2* could thus be regulated also by other transcription factors. ATF4 has been reported to regulate *GPT2* expression in other cell types(Salgado et al., 2014a). Therefore, it was interesting to see whether it also plays a role in breast cancer. Indeed *GPT2* mRNA levels decreased significantly upon ATF4 knockdown (Figure 37 a,b). Additionally, tunicamycin treatment, which is a commonly used ER stress inducer(Salgado et al., 2014a), led to ATF4 up regulation(Figure 37d), and it also increased *GPT2* expression significantly (Figure 37c).

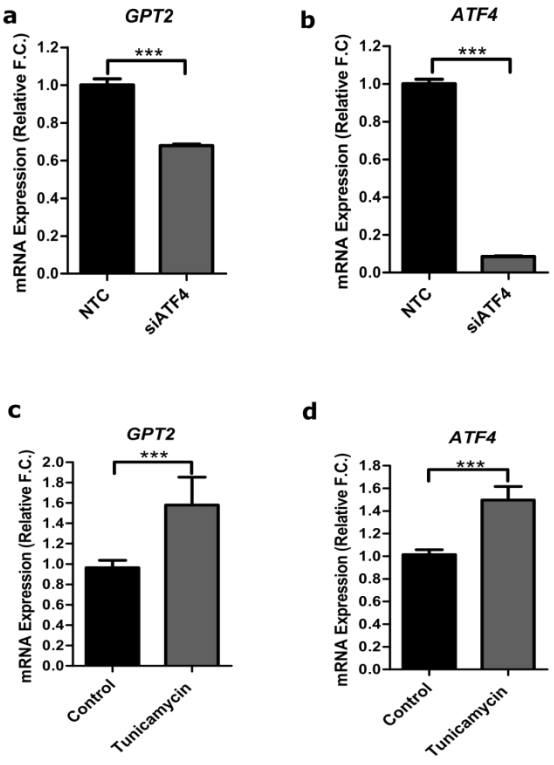

Figure 37: Regulation of GPT2 expression by ATF4. (a-d) Cells were transfected with siATF4. RNA and was harvested 72h after transfection and mRNA levels were determined by qPCR. All values were normalized to *PUM1* levels and non-targeting control. Data are presented as mean ± SD of 3 technical replicates. *** represents $p < 0.001$.

This observed regulation in the previous figure was further consolidated by a positive correlation between the expression of *ATF4* and *GPT2* at the patient level in the TCGA dataset (Figure 38).

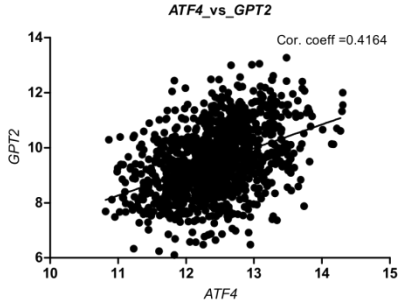

Figure 38: Correlation between *ATF4* and *GPT2* expression in patients. Correlation of *ATF4* with *GPT2* expression of the TCGA dataset (n= 1215). Correlation coefficient was calculated using Pearson correlation

.

5. Discussion

Breast cancers, like several other cancers undergo global metabolic shifts in order to sustain their growth and survival. Considerable evidence suggests that unraveling these metabolic transformations holds the promise for discovery of new therapeutic susceptibilities(Chakrabarti et al., 2015; Morin, Letouzé, Gimenez-Roqueplo, & Favier, 2014; Sotgia, Martinez-Outschoorn, & Lisanti, 2013; Tennant, Durán, & Gottlieb, 2010; X. Zhang et al., 2016). In this project I aimed to dissect the metabolic landscape of breast cancer with the aim of finding important players in the bioenergetics and biosynthetic pathways of tumor cells. This led to the identification of alanine aminotransferase (GPT2) which I found to have a strategic role in maintaining the glycolytic and glutaminolytic equilibrium of breast cancer cells and may thus qualify as a potential target for therapeutic intervention. This study also underlines metabolic heterogeneity within and between different subtypes of breast cancer, highlighting the fact that when it comes to metabolism, the conventional classifications may not apply.

5.1 Metabolic characterization of cancer cells reveals heterogeneity within breast cancer cell lines

While it is widely accepted that the aggressive subtypes of breast cancer, like triple negative breast cancers, display pronounced dependence on metabolic rewiring (Lim et al., 2016; Maiti, Kundranda, Spiro, & Daw, 2010; J. H. Park et al., 2016; Pelicano et al., 2014; Peterson, Walker, Sloan, & Creek, 2016; Shen et al., 2015; van Geldermalsen et al., 2015b), there is a large body of evidence which suggests that less aggressive subtypes of breast cancer such as the ER positive ones, can also undergo large-scale metabolic transformations (Audet-Walsh et al., 2016; A. R. Clark & Toker, 2014; Lloyd, Arnold, & Sreekumar, 2015; Mishra & Ambs; S. Park et al., 2016; Penkert et al., 2015). This could also be recapitulated in this project where all three cell lines, MDA MB 468, MDA MB 231 and MCF7, despite their genetic differences, showed comparable levels of glucose and glutamine consumption, as well as active breakdown of these carbon sources as marked by high levels of lactate and ammonia secretion (Figure 5). However, amino

acid metabolism activity was found to be higher in the triple negative breast cancer cell lines as seen by the protein levels of the enzymes involved in these pathways (Figure 6c). Previous studies have also reported aberrant amino acid metabolism in triple negative breast cancer cells (M. I. Gross et al., 2014; Possemato et al., 2011a; Timmerman et al., 2013; van Geldermalsen et al., 2015a). It is to be noted however, that MDA MB 468 showed a higher consumption of both carbon sources as well as higher secretion of their end products when compared to MDA MB 231 (Figure 5). Additionally, MDA MB 468 had a higher expression of oxidative phosphorylation (OXPHOS) related proteins compared to MDA MB 231 (Figure 6d), validating functional experiments which showed higher oxygen consumption rates of MDA MB 468 (Lanning et al., 2017). This is not surprising as TNBC patients have high levels of genetic heterogeneity (Lehmann et al., 2011; Lehmann, Jovanović, et al., 2016). While both the MDA cell lines belong to the triple negative subtype of breast cancer, they are assigned to different subclasses. MDA MB 468 belongs to the basal A subclass while MDA MB 231 is basal B (Lehmann, Jovanovi, et al., 2016) (it was previously assigned to mesenchymal like (Lehmann et al., 2011)). MCF7, which is a luminal cell line, had the highest expression of enzymes involved in oxidative phosphorylation, in concordance with previous studies (Pelicano et al., 2014) (Figure 6d). Expression of enzymes of the citric acid (TCA) cycle, which directly feeds OXPHOS, was also higher in MCF7 compared to the triple negative breast cancer cell lines (Figure 6b), further underlining the difference between the luminal and triple negative subtypes.

While basal metabolic rates and enzyme levels are important to understand the metabolic tendencies of the cells, tumor cells can easily switch between pathways and sources to quickly adapt to changing metabolic environments, thereby increasing fitness of the cells resulting in sustained growth and proliferation. It is important to introduce perturbations to these cells and find out how they behave under different stress conditions and what alternative pathways can get activated in order to target them efficiently. All 3 cell lines were grown under different nutrient starvation conditions, namely, glucose and glutamine deprivation. It was clear that all cell lines were affected by the lack of either nutrient, however, the extent of the effect varied between the different cell lines (Figure 4 a-f). In line with previous studies (Dilshara et al., 2017; Korangath et al., 2015; Timmerman et al., 2013; van Geldermalsen et al., 2015b) MDA MB 231

cells were most sensitive to glutamine deprivation. In contrast, MCF7 cells were most affected under glucose deprived conditions. Other studies have shown that ER+ cells are more dependent on glucose than on glutamine (Timmerman et al., 2013). However, the subtypes are not clearly separated into glucose and glutamine dependent groups, for example, glucose is a critical source for ER- cells as well and they tend to have higher glycolytic rates, as I have shown in this project and has also been reported(Rizwan et al., 2013; Shen et al., 2015). MDA MB 468 cells showed moderate dependence on both carbon sources which was also in line with other studies (Lampa et al., 2017; Lukey, Greene, Erickson, Wilson, & Cerione, 2016), suggesting that they may be metabolically more flexible and can switch on/off certain pathways rapidly to adapt to changes in the environment. In fact, another study has shown that even though MDA MB 468 cells have higher OXPHOS versus glycolytic levels compared to MDA MB 231 cells, under conditions of glycolytic stress they survive better as they have a higher glycolytic reserve (Lanning et al., 2017). MDA MB 468 cells depend on arginine as an important source for nitrogen to sustain polyamine biosynthesis and blocking the breakdown of this amino acid can lead to cell apoptosis (Singh, Pervin, Karimi, Cederbaum, & Chaudhuri, 2000). In this project, as well, it was clear that this pathway was active from the high levels of arginase 2 (ARG2) particularly in MDA MB 468 cells (data not shown).This data suggests that MDA MB 468 cells can use multiple nutrient sources for their sustenance and can thus compensate for the lack of one source by switching to other sources they are already ready to utilize. However, further experiments need to be done to confirm this hypothesis.

Metabolic intermediates derived from both glycolysis and glutaminolysis, provide the biosynthetic molecules required for the cancer cells. In cancer cells, glycolysis provides carbon atoms for different biosynthetic intermediates that lead to the production of building blocks required for the cell growth(Lunt & Vander Heiden, 2011). Conventionally, glutamine is the primary nitrogen donor of the cells which supports nucleotide and protein synthesis, however, in cancer cells the role of glutamine is extended to become the second major carbon source as it also supplies intermediates that keep the TCA cycle functional(R. J. DeBerardinis et al., 2007; L. Yang et al., 2017). As a result, cancer cells have highly deregulated amino acid metabolism. These deregulated pathways facilitate the transport of carbon from glutamine into the

biosynthetic pathways. An important example of this, particularly in breast cancer, is the serine synthesis pathway which is upregulated in cancers with poor outcome, especially the ER^- subtype(Pacold et al., 2016; Possemato et al., 2011b). Serine synthesis pathway has a dual role in these cells. On the one hand, it leads to the production of glycine which contributes to the one carbon metabolism which has an impact on diverse pathways including nucleotide, protein and lipid metabolism, as well as epigenetic regulation and redox balance. On the other hand, breast cancer cells have been shown to suffer under blockage of serine synthesis as a result of depletion of the α-Ketoglutarate (α-KG) pool. Indeed, glutamine contributes to the TCA cycle mainly via maintaining α-KG levels in the cells (Lampa et al., 2017; C. Yang et al., 2014b). While α-KG is important for TCA cycling, it can also undergo reverse carboxylation to produce citrate which feeds the fatty acid biosynthesis (Zaidi, Swinnen, & Smans, 2012). Additionally, it can provide the substrate for the oncometabolite 2-HG production, which can promote tumorigenesis(L. Dang et al., 2009). α-KG is therefore, the crucial metabolite that cancer cells depend on glutamine for. As a consequence, high glutamine uptake in the cells results in the upregulation of aminotransferase reactions, in addition to the serine biosynthesis pathway. Indeed alanine and aspartate aminotransferases play critical roles in cancer cells(Korangath et al., 2015; Thornburg et al., 2008).

5.2 Alanine aminotransferase (GPT2) is deregulated in breast cancers and is crucial for their growth

I have shown (Figure 7b, c) that several breast cancer cell lines have high expression of GPT2 both at the mRNA and protein levels. This is consistent with other studies which have shown that glutamine addicted cells upregulate their aminotransferase expressions including GPT2(Korangath et al., 2015; Son et al., 2013b). In liver tumors, GPT1 activity is elevated already in the pre-tumor state and increased secretion of alanine has been found to be among the earliest metabolic changes that occur (S. Hu, Balakrishnan, Bok, Anderton, Larson, Nelson, Kurhanewicz, Vigneron, Goga, et al., 2011). The expression of GPT2 correlated with alanine levels, MDA MB 468 cells (which have the highest expression of GPT2) showed the highest

production and secretion of alanine (Figure 7a, d). Furthermore, high GPT2 activity in these cells was confirmed by the high rates of glucose label incorporation into alanine (Figure 7e).

Interestingly, *GPT1* is expressed at much lower levels than *GPT2* at the mRNA level and does not show any difference between the three tested cell lines (MDA MB 468, MDA MB 231 and MCF7) and (Figure 7b). It must be noted that *GPT1* and *GPT2* genes map to two different chromosomes suggesting that the genes are regulated independently(Yang, Roong-Ze; Blaileanu, Greorche; Hansen, Barbara C;Shuldiner, Alan R; Gong, 2002). Furthermore, the GPT1 protein is cytosolic, whereas GPT2 is mitochondrial. GPT1 is expressed in the kidneys, liver, skeletal muscle, and in low amounts in the heart, whereas GPT2 is expressed in the heart, skeletal muscle and pancreas. While GPT1 is mostly abundant in liver and is a biomarker for liver toxicity, GPT2 has higher expression in other specific organs(Salgado et al., 2014a). Therefore, the upregulation of GPT2 in cancer and the lack thereof of GPT1 suggest that when the need to upregulate alanine aminotransferase activity arises in cancer cells, they tend to rely on GPT2. Indeed, in cancer cells it has been shown that alanine is produced mainly by the mitochondrial pyruvate (Vacanti et al., 2014; C. Yang et al., 2014a).

The dependence of breast cancer cells on GPT2 was confirmed with two independent approaches. In one, RNAi approach was used to specifically knockdown GPT2. This led to decreases in viability and cell growth in all cell lines tested except T47D (luminal subtype) which had the lowest expression of GPT2 (Figure 8, 9 and 10). Notably, MDA MB 231 which had low GPT2 expression and activity, as seen by the low labeled glucose carbon incorporation into alanine, showed significant dependence on alanine biosynthesis pathway, in accordance with a previous report (Korangath et al., 2015). Although this result was surprising in the light of GPT2 activity levels (which had not been tested in the previous report (Korangath et al., 2015)) in the cells, it highlighted the fact that this enzymatic reaction is crucial to the cells even when protein levels are low.

The second approach was to use a commercially available alanine aminotransferase inhibitor, β-chloro-L-alanine (BCLA), a substrate analog of the enzyme. Previously used in a study in lung cancer cell lines(Beuster et al., 2011), this inhibitor is not specific to either isoform of GPT but

since breast cancer cell lines did not have high or changing expression of GPT1 (Figure 7b)and the aim was to inhibit the production of alanine, this inhibitor was chosen. In this approach, MDA MB 468 showed a significant decrease in cell proliferation while MCF7 was the least affected (Figure 15a and 16a). MDA MB 231 turned out to be the most affected cell line, in line with the data obtained with the siRNA approach (Figure 9d, 10b, 15a and 16b). This indicates that the GPT2 catalyzed reaction is still important for MDA MB 231 cell survival and the cells cannot quickly compensate for the perturbation in this pathway. In the study on lung cancer cells previously stated, inhibition of alanine transaminase impaired cell growth by reducing ATP production and growth inhibitory signals leading to an increase in AMPK and reactive oxygen species (ROS) and a decrease in cell cycle proteins (Beuster et al., 2011). Aminooxyacetate, a broad spectrum inhibitor of aminotransferase, has been shown in several studies to suppress cell growth. In breast cancer cell lines, aminooxyacetate treatment increases the sub-G1 population and S-phase arrest (Korangath et al., 2015). Furthermore, inhibition of aminotransferase causes a decrease in amino acids thus activating the ER stress pathway and leading to cytotoxicity (Hao et al., 2016; Korangath et al., 2015). The disadvantage of this approach is that aminooxyactate is a broad spectrum aminotransferase inhibitor and its effects cannot be solely attributed to GPT2 inhibition. BCLA, on the other hand, has been shown in previous studies to specifically target alanine aminotransferase. This is the first time that the effect of specific inhibition of GPT2 has been studied in breast cancer.

5.3 Perturbation of alanine metabolism affects nutrient utilization capacity of cancer cells

Alanine, produced via the transfer of α-nitrogen from glutamate to pyruvate, supports protein synthesis, but is also secreted from the cells in large amounts to get rid of excess carbon from glycolysis and nitrogen from glutaminolysis (R. Deberardinis & Cheng, 2009). One report even revealed that alanine may function as an important carbon fuel in pancreatic cancer cells which take it up from the tumor microenvironment where it is secreted by the pancreatic stellate cells (Sousa et al., 2016). The alanine amintransferase reaction is one of the pivots joining the

glycolysis and glutaminolytic pathways. Therefore, it was interesting to find out whether GPT2 inhibition affects either pathway. In colorectal cancer cells upregulation of GPT2 leads to increased glutamine consumption (Hao et al., 2016). A study in mammary epithelial cells demonstrated that the transition from quiescence to proliferation is accompanied by an increase in glutamine consumption and subsequent GPT2 expression (Coloff et al., 2016). Indeed, it was observed that a decrease in alanine production in MDA MB 468 cells results in reduced uptake of glutamine (Figure 18a and 19a). This was further validated by a decrease in ammonia production, an important outlet for excess nitrogen (Figure 19b). In MDA MB 231 and MCF7 cells, glutamine uptake showed a tendency to decrease, indicating that this aminotransferase pathway might be one of several routes for glutamine cycling and that MDA MB 231 as well as MCF7 cells do not depend on it for nitrogen cycling to the same extent as MDA MB 468 (Figure 18b,c). This is also seen in other cancer entities, which demonstrates that alanine production is an important glutaminolytic route (Hao et al., 2016; Smith et al., 2016a)**.** Glucose uptake and lactate secretion on the other hand did not show considerable change in MDA MB 468 cells (Figure 18a and 19c, d) whereas MDA MB 231 cells displayed a slight but significant decrease in glucose uptake, underlining the fact that the two cell lines are metabolically quite diverse (Figure 18b). The lack of any significant change in nutrient uptake in MCF7 cells further supports the fact that it is least affected by GPT2 inhibition (Figure 18c).

5.4 GPT2 Inhibition reduces the pool of TCA cycle intermediates in cancer cells

Alanine is an important nitrogen source in cells which can provide building blocks for protein and nucleotides that are essential for cell growth. However, it has been shown in other cancers that the GPT2 catalyzed reaction is also an important source of α-KG for the cells. In colorectal cancer, PI3KCA mutations have been shown to render the cells addicted to glutamine and thereby dependent on aminotransferases, in order to replenish the α-KG pools driving the TCA cycle (Hao et al., 2016). In another study, young adult murine colon (YAMC) cells which were transformed to malignant cells via activation of RAS and p53 mutation showed upregulation of

GPT2 expression(Smith et al., 2016). These cells became GPT2 dependent. GPT2 is, therefore, a critical factor that utilizes products of glycolysis (i.e., pyruvate) to shunt glutamine-derived carbon atoms into the TCA cycle. Similarly, studies in mammary epithelial cells have shown that as the cells transition from quiescent to proliferative states, similar to cancer cells, they become more dependent on transaminase reactions to support glutamine catabolism which, in turn, promotes cell proliferation (Coloff et al., 2016). In corroboration with other reports, I have shown that inhibitor treatment in breast cancer cells led to a decrease in α-KG pools (Figure 20a). It is however, interesting to note that even though MDA MB 231 cells were severely affected by GPT2 inhibition, they showed an increase in α-KG levels (Figure 20b). This indicates that even though both MDA MB 468 and MDA MB 231 have similar phenotypic reactions in response to GPT2 inhibition they respond differently at the molecular level. It has been shown in other studies that increases in α-KG can stabilize hypoxia inducible factor 1 α (HIF1α) resulting in a stressful environment in the cells. Hence, this could be the mechanism activated in MDA MB 231 cells which leads to slowing cell growth (Hou et al., 2014). However, the exact source of this α-KG needs further investigation.

The decrease in α-KG is concurrent with a decrease in the pool of TCA cycle intermediates downstream of α-KG, further supporting the data that cells are affected by a decrease in glutamine uptake and alanine production both of which contribute to the TCA cycle via α-KG production (Figure 20a). An earlier study in colorectal cancer (Hao et al., 2016) showed that upregulation of GPT2 expression and glutamine increased the flux of glutamine derived TCA cycle intermediates, the entry point for which is α-KG. Decrease in TCA cycle activity extended to reduced oxygen consumption rates, which indicated reduced cellular respiration (Figure 22).

5.5 GPT2 activity influences expression of enzymes involved in anaplerosis

Here, I have also demonstrated that the effect of GPT2 inhibition on nutrient cycling extends to the enzymatic level (Figure 21). MDA MB 468 cells showed a decrease in glutamine transporters as well as glutaminolytic proteins, while glycolytic proteins remained unchanged in line with the

metabolite data (Figure 18, 19 and 21a). In concurrence with metabolite data TCA cycle enzymes showed significantly decreased levels upon GPT2 inhibition. Interestingly, most tested enzymes tended to increase in MDA MB 231, indicating that the cells might be responding to the perturbation by upregulating these enzymes in order to maintain/regain the rapid proliferation rates seen in MDA MB 231, though most changes were not significant (Figure 21b). MCF7 did not show any clear tendencies (Figure 21c). However, understanding the mechanism by which enzyme levels are adjusted entails further study.

5.6 GPT2 inhibition redistributes glucose carbon utilization in cancer cells

The data discussed above demonstrate that GPT2 is indeed used by breast cancer cells to propel glutamine derived α-KG into the TCA cycle. However, this reaction is also fed by glucose. The fate of glucose carbon atoms under GPT2 inhibition has not been explored so far. In this study two of the cell lines did not show any significant decrease in glucose consumption levels, MDA MB 468 rather increased slightly, MDA MB 231 showed a small decrease in uptake in glucose (Figure 18, 19 c). Pyruvate which is the final glycolytic product has three main fates, it can feed into the TCA cycle to produce ATP via OXPHOS and other biosynthetic intermediates or produce lactate which builds up the NADH reserves in the cells or produce alanine. In the absence of alanine production the pyruvate buildup can lead to an increase in lactate production or TCA cycle intermediates.

As the total levels of lactate did not change (Figure 18 and 19d) it is clear that the excess carbon atoms from glucose do not feed into this pathway and could thus flow into the TCA cycle to compensate for the reduced input from glutamine. Indeed glucose labeling showed significant increase in carbon atoms flowing from glucose into the TCA cycle (Figure 23). In the PDH-catalyzed forward TCA cycle the percentage of glucose carbon increased, likely due to decrease in carbon flow from glutamine, but this could not be observed in the total labeled quantities(citrate showed a small but insignificant increase in total labeled levels) (Figure 23a). Intermediates of the reverse reaction catalyzed by pyruvate carboxylase showed an increased

input of carbon atoms from glucose both in percentage and quantity. The oxaloacetate derived from pyruvate by PC can feed the reverse TCA cycle via malate or can be converted to citrate. In MDA MB 468 cells there was a significant increase in carbon labeling of malate and fumarate coming from this reverse reaction. Citrate, whose sources are a little more difficult to detect, also showed an increase of ^{13}C-incorporation if the fragment indicating the forward and reverse reaction but not the fragment reflecting the forward reaction.. This indicates that the oxaloacetate coming from pyruvate cycles into the TCA cycle via malate but some of it might also be used to produce citrate. The absence of a change in the labeled quantities of α-KG may indicate that either the labeling time was too short for the reverse reaction to reach it and/or produced citrate was utilized to be transported outside mitochondria in order to feed other biosynthetic pathways. Further experiments are required to confirm this.

While the labeling data clearly showed that in MDA MB 468 cells the inhibition of GPT2 shunts more carbon atoms from glucose into the TCA cycle via the PC catalyzed pathway, the results from the other two cell lines were more complicated to interpret. MDA MB 231 cells did not show any change in the proportion of glucose labeling, but the total labeled quantities of the intermediates in the PDH catalyzed forward reaction showed a tendency to increase (Figure 23b). This could be due to the fact that MDA MB 231 cells already have a high PC activity and probably this pathway is functioning to its maximum capacity and therefore, under conditions of stress, they cannot switch to this pathway and have to rather push the forward reaction.

MCF7 cells, similar to MDA MB 468 cells, showed significant increase in malate and fumarate labeled proportions and quantities of the forward reaction (Figure 23c). However, despite their basal PC activity being similar to MDA MB 468 cells, MCF7 cells did not increase PC activity under stress.

Thus, even though the increase in PC activity under inhibition is unique to MDA MB 468 cells, it is clear from the labeling data that when the GPT2 pathway is not available to the cells, the carbon from the glucose flows into the TCA cycle. As MDA MB 231 cells already have a higher PC activity, they tend to push more carbon through the PDH catalyzed pathway, and it is clear that both routes are active under stress. MCF7 does not increase PC activity despite having a

low basal activity, this could be due to the metabolic landscape of the cell line in general or that the GPT2 inhibitor has the least effect on the cells and the cells probably have other compensatory pathways to overcome the blockage. Higher concentrations of the inhibitor and the identification of possible compensatory pathways need to be tested.

5.7 Combinatorial perturbation of GPT2 and PC retards cell growth

Pyruvate carboxylase (PC) is a mitochondrial enzyme which is highly active in liver and kidneys where it promotes gluconeogenesis. It is also expressed in other organs where it has a role in replenishing the TCA cycle by converting pyruvate to oxaloacetate. The alternative to PC catalyzed replenishment of TCA-cycle intermediates is glutamine dependent anaplerosis. Cancers use different anaplerotic sources. Lung cancers chose PC-dependent anaplerosis over GLS1 activity (Sellers et al., 2015), however, major changes in the tumor microenvironment have been shown to shift lung cancer cells to being more dependent on glutamine (Davidson et al., 2016). Breast cancers mostly use the glutamine anaplerotic route and thus, have low PC activity (Christen et al., 2016), as is also evident in some of the cell lines tested in this project (Figure 24 a-c). MDA MB 231, despite having the highest basal activity of PC, was not affected by PC knockdown, while MDA MB 468, which has very low basal activity of PC, is significantly more affected (Figure 26 a, b). This could be traced back to differential glutamine metabolism between the cell lines (Figure 4 a-f). While MDA MB 231 is more dependent on glutamine for survival, MDA MB 468 is just moderately affected by changing levels of glutamine indicating that this cell line might use other anaplerotic sources to maintain a functional TCA cycle. PC has been associated with glutamine independent growth (Biancur et al., 2017; T. Cheng et al., 2011). Thus, it makes sense that when cells reduce their uptake of glutamine under GPT2 inhibition, PC driven anaplerosis is induced to feed the TCA cycle. PC activity therefore, may be a compensatory route that is activated by cells to offset the effect of decreased or abolished GPT2 activity (Figure 23a). The combination of PC knockdown and GPT2 inhibition consequently, had a stronger effect compared to the individual treatments, in both MDA MB

468 and MCF7 (even though MCF7 cells did not show an activation of PC pathway) (Figure 26 a,c). However, the lack of a synergistic effect signals that there are other compensatory pathways that can get activated in the cells. In MDA MB 231 cells, the combined knockdown of PC did not have any additional effect probably because the effect of the inhibitor was severe (Figure 26b).

5.8 Dual targeting of alanine and energy metabolism has a combinatorial effect on cell growth

The TCA cycle provides energy precursors to be fed into the electron transport chain via oxidative phosphorylation. Depletion in TCA cycle intermediates will therefore, directly impact OXPHOS. Following GPT2 inhibition the cells displayed a decrease in oxygen consumption rate, a measure of OXPHOS (Figure 22). As discussed earlier, under conditions of stress the cells compensate for the lack of glutamine anaplerosis with PC driven anaplerosis which could be used to feed the ETC as well. Additionally, targeting the respiratory chain directly upregulates reductive glutamine metabolism (Fendt, Bell, Keibler, Olenchock, et al., 2013), which in turn could render the cells more susceptible to inhibition of glutamine metabolism. As GPT2 inhibition showed a change in glutamine metabolism, combinatorial targeting of GPT2 and OXPHOS could provide a more effective treatment strategy for cancer cells. In order to test this hypothesis, the cell lines were treated with the two drugs, rotenone and metformin.

Rotenone, an irreversible complex I inhibitor, blocks the NADH oxidation in the respiratory chain and has been show to induce apoptosis in breast and lung cancer cells (Deng et al., 2009; W. Hu et al., 2016) mainly via ROS generation. Figure 29 shows that all three cell lines were sensitive to rotenone treatment. MDA MB 231 was found to be the most susceptible even though it is the least OXPHOS dependent cell line (Lanning et al., 2017; Pelicano et al., 2014). As mentioned earlier, respiratory chain targeting has been shown to make cancer cells more dependent on glutamine metabolism. Combinatorial treatment of rotenone and BCLA (Figure 30a-c) in MDA MB 468 and MDA MB 231 cells showed some additional effect than the individual inhibitors, while MCF7 showed effects similar to rotenone treatment alone. This is in

line with data that shows that ER^+ cell lines are more OXPHOS dependent (Pelicano et al., 2014) and less dependent of glutamine.

Metformin is another complex I inhibitor which is widely used to control blood sugar levels in type 2 diabetes patients. Epidemiological data suggests that diabetic patients treated with metformin have a lower risk of developing cancer (Evans, Donnelly, Emslie-Smith, Alessi, & Morris, 2005). Preclinical studies have also provided evidence for metformin being a potential candidate for anticancer treatment (Birsoy et al., 2014). One report showed that in triple negative breast cancers, which occur frequently in women with obesity or type II diabetes, metformin treatment can be used as effective therapy(Liu et al., 2009). The same report showed that treatment results in growth arrest and apoptosis and has been shown to also reduce tumor formation in xenograft models. Another report, however, suggests that metformin can have diverse effects, such as cell cycle arrest and reduction in colony formation and cell growth, in all molecular subtypes of breast cancer(Alimova et al., 2009).

Metformin can act through several routes. In diabetes, it is used for its ability to reduce blood glucose levels by increasing glucose uptake by skeletal muscles, inhibiting gluconeogenesis in the liver, and controlling the blood insulin levels (Teicher, Linehan, & Helman, 2012). Metformin targets gluconeogenesis via glycerophosphate dehydrogenase (Madiraju et al., 2014). This is important also for cancer cells as glycerophosphate dehydrogenase is an important enzyme which supports the glycolytic phenotype of the cells and provides electrons for the respiratory chain (Chowdhury, Gemin, & Singh, 2005). Moreover, the role of metformin in targeting the mitochondrial complex I and inhibiting the energy metabolism of cells makes it an attractive drug. Unlike rotenone, metformin is a reversible inhibitor and less toxic and is also thought to be targeting complex I at a different site(Wheaton et al., 2014). In this study metformin is shown to induce significant retardation of cell growth in all three cancer cell lines, though it should be noted that MDA MB 231 is comparatively least affected (Figure 31). These results corroborate previously reported data (Liu et al., 2009). The difference in the behavior of the cell lines to the two complex I inhibitor treatments could be due to different efficiencies of the drugs or due to the notion that they act on different sites. Additionally, metformin can act on

targets other than complex I for example the targeting of glycerophosphate dehydrogenase, which may contribute to the difference as the cell lines are also metabolically distinct. However, further experiments need to be done to confirm this.

Similar to rotenone, metformin-induced reduction in glucose oxidation induces a switch to glutamine anaplerosis (Fendt, Bell, Keibler, Davidson, et al., 2013; Fendt, Bell, Keibler, Olenchock, et al., 2013). In triple negative breast cancer xenografts, metformin has been shown to reduce cancer cell growth by reducing c-Myc and HIF1α levels(Li, Xue, Xi, & Xie, 2017; J. Zhang et al., 2017). These reports in combination show that metformin can directly target tumor cells and render the cells sensitive to glutamine targeting therapy. In this study as well, I have shown that treatment of metformin and BCLA had a combinatorial effect on MDA MB 468 (Figure 32). These changes could not be recapitulated in the other cells, and can potentially be attributed to the fact that the change in glutamine metabolism after GPT2 inhibition is not as prominent in these other cell lines as in MDA MB 468 cells. Additionally, as MDA MB 231 is least affected by metformin, it clearly can bypass any inhibitory effect coming from this drug, while MCF7 are more dependent on OXPHOS than glutamine anaplerosis, hence they are more affected by the drug than by GPT2 inhibition.

5.9 GPT2 expression correlates with poor prognosis in breast cancer patients

There is substantial evidence that alanine metabolism is important for cancer cell growth in culture(Hao et al., 2016; Korangath et al., 2015; Smith et al., 2016a). However, the potential relevance of these findings depends on the clinical implications they have.

Earlier findings focused on the role of GPT1 rather than GPT2, owing to its association with liver toxicity(Conde et al., 2015; S. Hu, Balakrishnan, Bok, Anderton, Larson, Nelson, Kurhanewicz, Vigneron, & Goga, 2011; Maximos et al., 2015). A review of different population studies showed that GPT1 expression is associated with the risk of cancers in digestive organs(Kunutsor, Apekey, Hemelrijck, Calori, & Perseghin, 2014). Similarly, in liver tumors, GPT1 activity is elevated in the pre tumor state and increased secretion of alanine is one of the

earliest metabolic changes that occur (S. Hu, Balakrishnan, Bok, Anderton, Larson, Nelson, Kurhanewicz, Vigneron, Goga, et al., 2011).

Studies have shown that tissues and blood samples from cancer patients, including breast cancers, have elevated levels of Alanine (Budczies et al., 2012; Poschke et al., 2013)**,** suggesting that it is indeed secreted at a higher rate by neoplastic cells. A study in a small group of patients also showed that compared to healthy samples, serum from breast cancer patients have a higher activity of alanine and aspartate transaminase(Al-Mashhadani, Muk, & Al-Faraji, 2012).

While upregulation of GPT2 expression in cancer cells is evident from *in vitro* studies(Hao et al., 2016; Korangath et al., 2015; Smith et al., 2016a), there is a need for population studies into the association between GPT2 expression and tumorigenesis. Analysis of the TCGA and METABRIC datasets (Cancer Genome Atlas Network, 2012; Curtis et al., 2012) revealed that GPT2 expression is upregulated in the more aggressive subtypes of breast cancer, including basal and HER2+ (Figure 33a, b). It is also associated with a more malignant phenotype owing to a positive correlation with increasing grades of cancer (Figure 33c). GPT2 expression also correlated significantly with poor overall survival (Figure 33 d).

However, most available information is comprised of mRNA data which requires researchers to assume that the same is reflected at the protein level which may be inaccurate in certain cases. There is, therefore, the need for more functional studies in patient tissues to confirm the conclusions drawn from genetic data. Using an in house generated dataset of 800 breast cancer patients, GPT2 was analyzed at the proteomic level for the first time in a large scale breast cancer cohort (Figure 34a) (Bernhardt et al., 2017). This analysis confirmed that the upregulation of GPT2 in the more aggressive subtypes also translates to the protein level. This association also extended to other clinical parameters, including grading of tumors (Figure 34b). This study, thus consolidates the fact that GPT2 is indeed deregulated in tumors, and better detection methods for this enzyme might prove to be an important analytical tool. Despite some smaller cohorts showing higher alanine levels in patients versus normal patients, as discussed earlier, there is a lack of large scale analysis of alanine levels in patients of different

subtypes of breast cancer. Furthermore, it would be worth investigating the correlation between the levels of GPT2 expression with alanine secretion levels in the patients.

5.10 GPT2 expression is controlled by metabolism regulators c-Myc and ATF4

Progress in the field of cancer metabolism has established this as a hallmark of cancer (Hanahan & Weinberg, 2011). To better comprehend tumorigenesis it becomes vital to understand how the cancer cells efficiently rewire their metabolic pathways to ensure a 'favourable' outcome for their growth. While some metabolic genes, like *IDH*, are mutated in certain cancer entities like brain cancer(Yan et al., 2009), most metabolic genes especially those belonging to glutamine metabolism do not have any reported mutations or amplifications in cancers. Therefore, understanding the rewiring of metabolic pathways in cancers necessitates a deeper look into the genetic background of the tumor and its microenvironment. Indeed, several oncogenic signaling pathways have been implicated in orchestrating metabolic rewiring to fuel the tumorigenic properties that they propagate(Cairns et al., 2011; Iurlaro et al., 2014). In a recent study it was also shown that several cancer associated metabolic genes, due to their proximity to oncogenic genes get co-altered (Sharma, Eils, & König, 2016). Therefore, large scale metabolic changes in cancers may be driven by the virtue of proximity of metabolic genes to other mutated genes or as a result of regulation by oncogenic proteins. Prominent among them, is c-Myc which is frequently deregulated in cancers. In breast cancer, it is overexpressed in 30-50% high grade tumors and which are mostly basal (Blancato, Singh, Liu, Liao, & Dickson, 2004; Deming et al., 2000). c-Myc has been linked to several of the metabolic changes that cancer cells undergo (Anso et al., 2013; Chi V Dang, n.d.; Chi V Dang et al., 2009; Hsieh, Walton, Altman, Stine, & Dang, 2015; Shen et al., 2015). While its role in glycolysis has been well established(Le et al., 2012; Shim et al., 1997), recent studies have focused on the role of c-Myc in glutamine metabolism. c-Myc is considered to be the master regulator of glutamine metabolism in cancer cells(C. V. Dang, 2013; Chi V Dang, n.d.; R. Deberardinis & Cheng, 2009; Le et al., 2012; McCarthy, 2015). By upregulating glutamine transporters, c-Myc triggers glutamine

addiction in tumors(David R Wise et al., 2008). Subsequently, efficient utilization of glutamine is ensured by c-Myc which also regulates the expression of glutaminolytic genes(Gao et al., 2009). In a study in breast cancer cell lines, glutamine dependence and expression of glutaminolytic genes increased in a c-Myc dependent manner (Korangath et al., 2015). c-Myc either directly targets metabolic genes, or indirectly for example via microRNAs(Gao et al., 2009).

In this study, c-Myc knockdown resulted in significant knockdown of GPT2 levels (Figure 35 a, c). In addition to the positive correlation between the *MYC* and *GPT2* at the mRNA level (Figure 36a), there was a positive correlation observed even at the protein levels in patients (Figure 36b). The correlation was positive for each individual subtype of breast cancer. In fact the correlation was higher at the protein level compared to the mRNA level emphasizing the need for proteomic and functional analyses to complement genetic studies.

c-Myc, however, does not account for the all the metabolic changes that occur in cancer cells. In this study it was observed that knockdown of c-Myc did not completely obliterate GPT2 levels. This finding led me to explore other transcription factors that might be relevant for regulating GPT2 expression. ATF4 has a well-recognized role in amino acid management: under conditions of ER stress, redox imbalance, hypoxia and nutrient deprivation, it regulates the amino acid synthesis genes to ensure cell survival (Harding et al., 2003; Quirós et al., 2017; Ye et al., 2010; E. Zhao et al., 2016)**.** ATF4 is found to be upregulated in solid tumors where it controls amino acid metabolism and consequently cell proliferation (Ye et al., 2010) as well as contributes to drug resistance (Tanabe et al., 2003). In esophageal squamous cell carcinoma ATF4 is upregulated which in turn controls the expression of serine synthesis genes (E. Zhao et al., 2016). In fibrosarcoma and colorectal adenocarcinoma cells, induction of ER stress and NEAA deprivation results in ATF4 upregulation, and addition of NEAA rescues cells deficient in ATF4 (Ye et al., 2010). ATF4 is also reported to be overexpressed in cancer associated stromal cells leading to the induction of asparagine synthesis which, in turn, is used as a nitrogen source by the surrounding cancer cells to combat glutamine deprivation (Linares et al., 2017). ATF4 is a known transcription factor of GPT2. Under conditions of stress, liver cells have been reported to upregulate GPT2 via stress response factor ATF4 (Salgado, Metón, Anemaet, & Baanante,

2014b). In colorectal cancer, *PIK3CA* mutations have been shown to make cells glutamine dependent by upregulating GPT2 via PDK1-RSK2-ATF4 signaling (Hao et al., 2016).

In this study, *ATF4* knockdown significantly reduced *GPT2* expression (Figure 37a). Conversely, ER stress induced *ATF4* upregulation via tunicamycin treatment and increased *GPT2* expression (Figure 37c), confirming previous reports(Salgado et al., 2014b). To test this association at clinical level the METABRIC dataset was analyzed which revealed a strong positive correlation exists between *ATF4* and *GPT2* in breast cancer patients (Figure 38). ATF4 has been previously linked to glutamine metabolism in breast cancer patients (van Geldermalsen et al., 2015a). In the cohort of 96 triple negative breast cancer cases *ATF4* gene expression significantly correlated with glutamine transporter *ASCT2* and glutamine metabolism related genes *GLS* and *GLUL.* Therefore, similar to c-Myc, ATF4 might play an important role in regulation of glutamine metabolism in cancer.

While c-Myc and ATF4 play important roles in cancer cell metabolism rewiring, in case of GPT2 and other genes as well, knockdown of the transcription factors does not induce complete elimination of gene expression. In the same way as cancer cells can compensate for blockage of one metabolic pathway by using another pathway, signaling pathways can also be switched according to the need of the cells(McCormick, 1999). Furthermore, gene expression can be controlled by multiple regulatory factors. Even though the afore-mentioned two transcription factors play a role in GPT2 expression, there could be other factors as well. The factors may also vary according to the subtype and genetic background of the cancer. It is interesting to note that MDA MB 468 cells, which have the highest expression of GPT2, are deficient of the tumor suppressor *RB1* (Retinoblastoma transcriptional corepressor 1), which is commonly mutated in cancers(Johnson et al., 2016). Loss of *RB1* in mouse embryonic fibroblasts, has been shown to increase glutamine consumption via upregulation of ASCT2 and consequent increase in glutamine breakdown via GLS1 activity (M. R. Reynolds et al., 2014). Therefore, it is reasonable to assume that lack of *RB1* in MDA MB 468 may have a function in regulating metabolism and it would be worth investigating if it plays a role in GPT2 expression as well. The expression of GPT2 could, however, be dependent on a many more factors, including, the genetic landscape

like mutations, amplifications, epigenetic regulation as well as the tumor microenvironment and all these factors have to be taken into consideration while investigating the regulation of GPT2.

6. Conclusions and Outlook

In conclusion, GPT2 plays a crucial role in connecting the glycolytic and glutaminolytic pathways as the GPT2 catalyzed reaction requires both to be functional. Warburg effect and glutaminolysis, the two pillars of cancer metabolism are, therefore, not independent of each other, rather they work in a concerted manner, via aminotransferases, to meet the energetic and biosynthetic demands of the cells. Finally, alanine secretion and alanine aminotransferase activity have the potential to be biomarkers as well as therapeutic targets.

While it is clear from this study that GPT2 is important for breast cancer cell growth and is also deregulated in patients, there is a need to prove that the effect it has on cell growth translates to tumorigenesis *in vivo*. In this regard, future experiments have been planned to study this aspect. While the RNAi approach and chemical inhibition are suitable for cell lines studies, *in vivo* experiments necessitate a different approach. Therefore, in the planned experiments, *GPT2* in MDA MB 468 cells will be knocked out using the CRISPR/Cas9 system and used to monitor tumor growth in xenograft mouse models. These experiments are currently on-going.

There is evidence that in the case of metabolism, the boundaries between the well-established molecular subtypes of breast cancer become indistinguishable. This gives rise to the need for different markers, possibly metabolic to identify the metabolic propensity of cell lines (and subsequently of patients). In this regard this study should be extended to more cell lines in order to represent a larger genetic and metabolic spectrum seen in patients. Furthermore, there is a need for larger cohorts of patient tissues and blood to be analyzed for both GPT2 expression and alanine levels. As an extension to this project, future studies have been planned to correlate *GPT2* and alanine levels in breast cancer patient cohorts. Associations seen in these analyses could help develop alanine as a biomarker.

While combinatorial effects of targeting GPT2 together with other factors involved in energy metabolism were observed, none of these effects substantial. This indicates that cells have yet other pathways that can compensate for these blockages and there is a need to discover what these are. It is clear that the cells reorganize their glucose carbon expenditure under GPT2

inhibition, therefore, dual targeting of GPT2 and glycolysis might lead to substantial decrease in cell growth. Furthermore, effects of GPT2 on other biosynthetic pathways that are fed by transaminase pathways need to be investigated to get a broader understanding of the role of GPT2 in cell growth.

This study, therefore, emphasizes the heterogeneity in the metabolic landscape of breast cancer, and the importance of glutamine driven anaplerosis in the cells. Effects of GPT2 on cell growth indicate that this is an important factor for cancer cells, however, combinatorial treatment with other compensatory pathways will hopefully ensure maximum success in combating tumor progression.

References

Al-Mashhadani, Z. I., Muk, A. J. A., & Al-Faraji, -Razaq. (2012). مجلة بنإ لهيثما مللعلو لصرفةا و لتطبيقيةا Estimation of ALP, GPT and GOT Activities in Iraqi Patients Female With Breast Cance r, *25*(1).

Alexandrov, L. B., Nik-Zainal, S., Wedge, D. C., Aparicio, S. A. J. R., Behjati, S., Biankin, A. V., … Stratton, M. R. (2013). Signatures of mutational processes in human cancer. *Nature*, *500*(7463), 415–421.

Alimova, I. N., Liu, B., Fan, Z., Edgerton, S. M., Dillon, T., Lind, S. E., & Thor, A. D. (2009). Metformin inhibits breast cancer cell growth, colony formation and induces cell cycle arrest in vitro. *Cell Cycle*, *8*(6), 909–915.

Anso, E., Mullen, A. R., Felsher, D. W., Matés, J. M., Deberardinis, R. J., & Chandel, N. S. (2013). Metabolic changes in cancer cells upon suppression of MYC. *Cancer & Metabolism*, *1*(1), 7.

Astuti, D., Douglas, F., Lennard, T. W., Aligianis, I. A., Woodward, E. R., Evans, D. G. R., … Maher, E. R. (2001). Germline SDHD mutation in familial phaeochromocytoma. *The Lancet*, *357*(9263), 1181–1182.

Atsumi, T., Chesney, J., Metz, C., Leng, L., Donnelly, S., Makita, Z., … Bucala, R. (2002). High expression of inducible 6-phosphofructo-2-kinase/fructose-2,6-bisphosphatase (iPFK-2; PFKFB3) in human cancers. *Cancer Research*, *62*(20), 5881–7.

Audet-Walsh, É., Papadopoli, D. J., Gravel, S.-P., Yee, T., Bridon, G., Caron, M., … al., et. (2016). The PGC-1α/ERRα Axis Represses One-Carbon Metabolism and Promotes Sensitivity to Anti-folate Therapy in Breast Cancer. *Cell Reports*, *14*(4), 920–931.

Avizienyte, E., Loukola, A., Roth, S., Hemminki, A., Tarkkanen, M., Salovaara, R., … Aaltonen, L. A. (1999). LKB1 somatic mutations in sporadic tumors. *The American Journal of Pathology*, *154*(3), 677–81.

Baek, S., Choi, C.-M., Ahn, S. H., Lee, J. W., Gong, G., Ryu, J.-S., … Moon, D. H. (2012). Exploratory Clinical Trial of (4S)-4-(3-[18F]fluoropropyl)-L-glutamate for Imaging xC- Transporter Using Positron Emission Tomography in Patients with Non-Small Cell Lung or Breast Cancer. *Clinical Cancer Research*, *18*(19), 5427–5437.

Bar-Shalom, R., Yefremov, N., Guralnik, L., Gaitini, D., Frenkel, A., Kuten, A., … Israel, O. (2003). Clinical performance of PET/CT in evaluation of cancer: additional value for diagnostic imaging and patient management. *Journal of Nuclear Medicine : Official Publication, Society of Nuclear Medicine*, *44*(8), 1200–9.

Baselga, J., Cortés, J., Kim, S.-B., Im, S.-A., Hegg, R., Im, Y.-H., … Swain, S. M. (2012). Pertuzumab plus Trastuzumab plus Docetaxel for Metastatic Breast Cancer. *New England Journal of Medicine*, *366*(2), 109–119.

Baysal, B. E., Ferrell, R. E., Willett-Brozick, J. E., Lawrence, E. C., Myssiorek, D., Bosch, A., … Devlin, B. (2000). Mutations in SDHD, a mitochondrial complex II gene, in hereditary paraganglioma. *Science (New York, N.Y.)*, *287*(5454), 848–51.

Bear, H. D., Tang, G., Rastogi, P., Geyer, C. E., Robidoux, A., Atkins, J. N., … Wolmark, N. (2012). Bevacizumab Added to Neoadjuvant Chemotherapy for Breast Cancer. *New England Journal of Medicine*, *366*(4), 310–320.

Benjamini, Y., & Hochberg, Y. (1995). Controlling the False Discovery Rate: A Practical and Powerful Approach to Multiple Testing. *Journal of the Royal Statistical Society. Series B (Methodological)*. WileyRoyal Statistical Society.

Bernhardt, S., Bayerlová, M., Vetter, M., Wachter, A., Mitra, D., Hanf, V., … Kantelhardt, E. J. (2017). Proteomic profiling of breast cancer metabolism identifies SHMT2 and ASCT2 as prognostic factors. *Breast Cancer Research*, *19*(1), 112.

Beuster, G., Zarse, K., Kaleta, C., Thierbach, R., Kiehntopf, M., Steinberg, P., … Ristow, M. (2011). Inhibition of alanine aminotransferase in silico and in vivo promotes mitochondrial metabolism to impair malignant growth. *The Journal of Biological Chemistry*, *286*(25), 22323–30. h

Biancur, D. E., Paulo, J. A., Małachowska, B., Quiles, M., Rey, D., Sousa, C. M., … Kimmelman, A. C. (2017). ARTICLE Compensatory metabolic networks in pancreatic cancers upon perturbation of glutamine metabolism. *Nature Communications*, *8*.

Birsoy, K., Possemato, R., Lorbeer, F. K., Bayraktar, E. C., Thiru, P., Yucel, B., … Sabatini, D. M. (2014). Metabolic determinants of cancer cell sensitivity to glucose limitation and biguanides. *Nature*, *508*(7494).

Blancato, J., Singh, B., Liu, A., Liao, D. J., & Dickson, R. B. (2004). Correlation of amplification and overexpression of the c-myc oncogene in high-grade breast cancer: FISH, in situ hybridisation and immunohistochemical analyses. *British Journal of Cancer*, *90*(8), 1612–9.

Budczies, J., Denkert, C., Müller, B. M., Brockmöller, S. F., Klauschen, F., Györffy, B., … Fiehn, O. (2012). Remodeling of central metabolism in invasive breast cancer compared to normal breast tissue – a GC-TOFMS based metabolomics study. *BMC Genomics*, *13*(1), 334.

Cairns, R. A., Harris, I. S., & Mak, T. W. (2011). Regulation of cancer cell metabolism. *Nature Publishing Group*, *11*.

Cancer Genome Atlas Network, T. (2012). Comprehensive molecular portraits of human breast tumours.

Carretero, J., Medina, P. P., Blanco, R., Smit, L., Tang, M., Roncador, G., … Sanchez-Cespedes, M. (2007). Dysfunctional AMPK activity, signalling through mTOR and survival in response to energetic stress in LKB1-deficient lung cancer. *Oncogene*, *26*(11), 1616–1625.

Carvalho, K. C., Cunha, I. W., Rocha, R. M., Ayala, F. R., Cajaíba, M. M., Begnami, M. D., … Soares, F. A. (2011). GLUT1 expression in malignant tumors and its use as an immunodiagnostic marker. *Clinics (Sao Paulo, Brazil)*, *66*(6), 965–72. h

Chakrabarti, G., Moore, Z. R., Luo, X., Ilcheva, M., Ali, A., Padanad, M., … Boothman, D. A. (2015). Targeting glutamine metabolism sensitizes pancreatic cancer to PARP-driven metabolic catastrophe induced by ß-lapachone. *Cancer & Metabolism*, *3*(1), 12.

Chan, K. W. Y., McMahon, M. T., Kato, Y., Liu, G., Bulte, J. W. M., Bhujwalla, Z. M., … van Zijl, P. C. M. (2012). Natural D -glucose as a biodegradable MRI contrast agent for detecting cancer. *Magnetic Resonance in Medicine*, *68*(6), 1764–1773.

Chen, J.-Q., & Russo, J. (2012). Dysregulation of glucose transport, glycolysis, TCA cycle and glutaminolysis by oncogenes and tumor suppressors in cancer cells. *Biochimica et Biophysica Acta*, *1826*(2), 370–84.

Cheng, K. W., Agarwal, R., Mitra, S., Lee, J.-S., Carey, M., Gray, J. W., & Mills, G. B. (2012). Rab25 increases cellular ATP and glycogen stores protecting cancer cells from bioenergetic stress. *EMBO Molecular Medicine*, *4*(2), 125–141.

Cheng, T., Sudderth, J., Yang, C., Mullen, A. R., Jin, E. S., Matés, J. M., & DeBerardinis, R. J. (2011). Pyruvate carboxylase is required for glutamine-independent growth of tumor cells. *Proceedings of the National Academy of Sciences of the United States of America*, *108*(21), 8674–9.

Chia, S., Gradishar, W., Mauriac, L., Bines, J., Amant, F., Federico, M., … Piccart, M. (2008). Double-blind, randomized placebo controlled trial of fulvestrant compared with exemestane after prior nonsteroidal aromatase inhibitor therapy in postmenopausal women with hormone receptor-positive, advanced breast cancer: results from EFECT. *Journal of Clinical Oncology : Official Journal of the American Society of Clinical Oncology*, *26*(10), 1664–70.

Choi, J., Jung, W.-H., & Koo, J. S. (2013). Metabolism-related proteins are differentially expressed according to the molecular subtype of invasive breast cancer defined by surrogate immunohistochemistry. *Pathobiology : Journal of Immunopathology, Molecular and Cellular Biology*, *80*(1), 41–52.

Chowdhury, S. K. R., Gemin, A., & Singh, G. (2005). High activity of mitochondrial glycerophosphate dehydrogenase and glycerophosphate-dependent ROS production in prostate cancer cell lines. *Biochemical and Biophysical Research Communications*, *333*(4), 1139–1145.

Christen, S., Lorendeau, D., Schmieder, R., Broekaert, D., Metzger, K., Veys, K., … Attwood, P. V. (2016). Breast Cancer-Derived Lung Metastases Show Increased Pyruvate Carboxylase-Dependent Anaplerosis. *Cell Reports*, *17*(3), 837–848.

Christofk, H. R., Vander Heiden, M. G., Harris, M. H., Ramanathan, A., Gerszten, R. E., Wei, R., … Cantley, L. C. (2008). The M2 splice isoform of pyruvate kinase is important for cancer metabolism and tumour growth. *Nature*, *452*(7184), 230–233.

Christofk, H. R., Vander Heiden, M. G., Wu, N., Asara, J. M., & Cantley, L. C. (2008). Pyruvate kinase M2 is a phosphotyrosine-binding protein. *Nature*, *452*(7184), 181–186.

Clark, A. R., & Toker, A. (2014). Signalling specificity in the Akt pathway in breast cancer. *Biochemical Society Transactions*, *42*(5), 1349–1355.

Clark, O., Yen, K., & Mellinghoff, I. K. (2016). Molecular Pathways: Isocitrate Dehydrogenase Mutations in Cancer. *Clinical Cancer Research*, *22*(8), 1837–1842.

Coloff, J. L., Murphy, J. P., Braun, C. R., Harris, I. S., Shelton, L. M., Kami, K., … Brugge, J. S. (2016). Differential Glutamate Metabolism in Proliferating and Quiescent Mammary Epithelial Cells. *Cell Metabolism*, *23*(5), 867–880.

Conde, V. R., Oliveira, P. F., Nunes, A. R., Rocha, C. S., Ramalhosa, E., Pereira, J. A., … Silva, B. M. (2015). The progression from a lower to a higher invasive stage of bladder cancer is associated with severe alterations in glucose and pyruvate metabolism. *Experimental Cell Research*, *335*(1), 91–98.

Cotte-Rodriguez, I., Miao, Z., Zhang, Y., & Chen, H. (2013). Introduction to protein mass spectrometry. In *Characterization of Protein Therapeutics using Mass Spectrometry*.

Cullinan, S. B., & Diehl, J. A. (2006). Coordination of ER and oxidative stress signaling: The PERK/Nrf2 signaling pathway. *The International Journal of Biochemistry & Cell Biology*, *38*, 317–332.

Curtis, C., Shah, S. P., Chin, S.-F., Turashvili, G., Rueda, O. M., Dunning, M. J., … Aparicio, S. (2012). The genomic and transcriptomic architecture of 2,000 breast tumours reveals novel subgroups. *Nature*, *486*.

Dai, X., Li, T., Bai, Z., Yang, Y., Liu, X., Zhan, J., & Shi, B. (2015). Breast cancer intrinsic subtype classification, clinical use and future trends. *Am J Cancer Res*, *5*(10), 2929–2943.

Dang, L., White, D. W., Gross, S., Bennett, B. D., Bittinger, M. A., Driggers, E. M., … Su, S. M. (2009). Cancer-associated IDH1 mutations produce 2-hydroxyglutarate. *Nature*, *462*(7274), 739–744.

Dang, C. V. (2013). MYC, Metabolism, Cell Growth, and Tumorigenesis. *Cold Spring Harbor Perspectives in Medicine*, *3*(8), a014217–a014217.

Dang, C. V, Le, A., & Gao, P. (2009). MYC-induced cancer cell energy metabolism and therapeutic opportunities. *Clinical Cancer Research : An Official Journal of the American Association for Cancer Research*, *15*(21), 6479–83.

Davidson, S. M., Papagiannakopoulos, T., Olenchock, B. A., Heyman, J. E., Keibler, M. A., Luengo, A., … Vander Heiden, M. G. (2016). Environment Impacts the Metabolic Dependencies of Ras-Driven Non-Small Cell Lung Cancer. *Cell Metabolism*, *23*(3), 517–528.

Deberardinis, R., & Cheng, T. (2009). Q's next: the diverse functions of glutamine in metabolism, cell biology and cancer. *Oncogene*, *29*, 313–324.

DeBerardinis, R. J. (2011). Serine metabolism: some tumors take the road less traveled. *Cell Metabolism*, *14*(3), 285–6.

Deberardinis, R. J., & Chandel, N. S. (n.d.). Fundamentals of cancer metabolism INTRODUCTION AND OVERARCHING PRINCIPLES.

DeBerardinis, R. J., & Chandel, N. S. (2016). Fundamentals of cancer metabolism. *Science Advances*, *2*(5).

DeBerardinis, R. J., Lum, J. J., Hatzivassiliou, G., & Thompson, C. B. (2008). The Biology of Cancer: Metabolic Reprogramming Fuels Cell Growth and Proliferation. *Cell Metabolism*, *7*(1), 11–20.

DeBerardinis, R. J., Mancuso, A., Daikhin, E., Nissim, I., Yudkoff, M., Wehrli, S., & Thompson, C. B. (2007). Beyond aerobic glycolysis: Transformed cells can engage in glutamine metabolism that exceeds the requirement for protein and nucleotide synthesis. *Proceedings of the National Academy of Sciences*, *104*(49), 19345–19350.

Deming, S. L., Nass, S. J., Dickson, R. B., & Trock, B. J. (2000). C-myc amplification in breast cancer: a meta-analysis of its occurrence and prognostic relevance. *British Journal of Cancer*, *83*(12), 1688–1695.

Deng, Y.-T., Huang, H.-C., & Lin, J.-K. (2009). Rotenone induces apoptosis in MCF-7 human breast cancer cell-mediated ROS through JNK and p38 signaling. *Molecular Carcinogenesis*, *49*(2),

Dilshara, M. G., Jeong, J.-W., Prasad Tharanga Jayasooriya, R. G., Neelaka Molagoda, I. M., Lee, S., Park, S. R., … Kim, G.-Y. (2017). Glutamine deprivation sensitizes human breast cancer MDA-MB-231 cells to TRIAL-mediated apoptosis. *Biochemical and Biophysical Research Communications*, *485*(2), 440–445.

Dimmer, K. S., Friedrich, B., Lang, F., Deitmer, J. W., & Bröer, S. (2000). The low-affinity monocarboxylate transporter MCT4 is adapted to the export of lactate in highly glycolytic cells. *The Biochemical Journal*, *350 Pt 1*, 219–27.

Eagle, H. (1955). Nutrition Needs of Mammalian Cells in Tissue Culture. *Science*, *122*(3168), 501–504.

Evans, J. M. M., Donnelly, L. A., Emslie-Smith, A. M., Alessi, D. R., & Morris, A. D. (2005). Metformin and reduced risk of cancer in diabetic patients. *BMJ (Clinical Research Ed.)*, *330*(7503), 1304–5.

Farmer, H., McCabe, N., Lord, C. J., Tutt, A. N. J., Johnson, D. A., Richardson, T. B., … Ashworth, A. (2005). Targeting the DNA repair defect in BRCA mutant cells as a therapeutic strategy. *Nature*, *434*(7035), 917–921.

Fendt, S.-M., Bell, E. L., Keibler, M. A., Davidson, S. M., Wirth, G. J., Fiske, B., … Stephanopoulos, G. (2013). Metformin decreases glucose oxidation and increases the dependency of prostate cancer cells on reductive glutamine metabolism. *Cancer Research*, *73*(14), 4429–38.

Fendt, S.-M., Bell, E. L., Keibler, M. A., Olenchock, B. A., Mayers, J. R., Wasylenko, T. M., … Li, P.-L. (2013). Reductive glutamine metabolism is a function of the α-ketoglutarate to citrate ratio in cells. *Nature Communications*, *4*, 441–464.

Figueroa, M. E., Abdel-Wahab, O., Lu, C., Ward, P. S., Patel, J., Shih, A., … Melnick, A. (2010). Leukemic IDH1 and IDH2 Mutations Result in a Hypermethylation Phenotype, Disrupt TET2 Function, and Impair Hematopoietic Differentiation. *Cancer Cell*, *18*(6), 553–567.

FOULDS, L. (1954). The experimental study of tumor progression: a review. *Cancer Research*, *14*(5), 327–39.

Fu, X., Osborne, C. K., & Schiff, R. (2013). Biology and therapeutic potential of PI3K signaling in ER+/HER2-negative breast cancer. *Breast (Edinburgh, Scotland)*, *22 Suppl 2*(0 2), S12-8.

Fumarola, C., Caffarra, C., La Monica, S., Galetti, M., Alfieri, R. R., Cavazzoni, A., … Bonelli, M. A. (2013). Effects of sorafenib on energy metabolism in breast cancer cells: role of AMPK–mTORC1 signaling. *Breast Cancer Research and Treatment*, *141*(1), 67–78.

Galdieri, L., Gatla, H., Vancurova, I., & Vancura, A. (2016). Activation of AMP-Activated Protein Kinase by Metformin Induces Protein Acetylation in Prostate and Ovarian Cancer Cells. *The Journal of Biological Chemistry*.

Gao, P., Tchernyshyov, I., Chang, T.-C., Lee, Y.-S., Kita, K., Ochi, T., … Dang, C. V. (2009). c-Myc suppression of miR-23a/b enhances mitochondrial glutaminase expression and glutamine metabolism. *Nature*, *458*(7239), 762–765.

Gatenby, R. A., & Gillies, R. J. (2004). Why do cancers have high aerobic glycolysis? *Nature Reviews Cancer*, *4*(11), 891–899.

Geyer, C. E., Forster, J., Lindquist, D., Chan, S., Romieu, C. G., Pienkowski, T., … Cameron, D. (2006). Lapatinib plus Capecitabine for HER2-Positive Advanced Breast Cancer. *New England Journal of Medicine*, *355*(26), 2733–2743.

Gimenez-Roqueplo, A.-P., Favier, J., Rustin, P., Rieubland, C., Kerlan, V., Plouin, P.-F., … Jeunemaitre, X. (2002). Functional Consequences of a *SDHB* Gene Mutation in an Apparently Sporadic Pheochromocytoma. *The Journal of Clinical Endocrinology & Metabolism*, *87*(10), 4771–4774.

Glaudemans, A. W. J. M., Enting, R. H., Heesters, M. A. A. M., Dierckx, R. A. J. O., van Rheenen, R. W. J., Walenkamp, A. M. E., & Slart, R. H. J. A. (2013). Value of 11C-methionine PET in imaging brain tumours and metastases. *European Journal of Nuclear Medicine and Molecular Imaging*, *40*(4), 615–635.

Gross, M. I., Demo, S. D., Dennison, J. B., Chen, L., Chernov-Rogan, T., Goyal, B., … Bennett, M. K. (2014). Antitumor Activity of the Glutaminase Inhibitor CB-839 in Triple-Negative Breast Cancer. *Molecular Cancer Therapeutics*, *13*(4), 890–901.

Gross, S., Cairns, R. A., Minden, M. D., Driggers, E. M., Bittinger, M. A., Jang, H. G., … Mak, T. W. (2010). Cancer-associated metabolite 2-hydroxyglutarate accumulates in acute myelogenous leukemia with isocitrate dehydrogenase 1 and 2 mutations. *The Journal of Experimental Medicine*, *207*(2), 339–44.

GUPPY, M., GREINER, E., & BRAND, K. (1993). The role of the Crabtree effect and an endogenous fuel in the energy metabolism of resting and proliferating thymocytes. *European Journal of Biochemistry*, *212*(1), 95–99.

Hanahan, D., & Weinberg, R. A. (2000). The Hallmarks of Cancer. *Cell*, *100*(1), 57–70.

Hanahan, D., & Weinberg, R. A. (2011). Hallmarks of Cancer: The Next Generation. *Cell*, *144*(5), 646–674.

Hao, Y., Samuels, Y., Li, Q., Krokowski, D., Guan, B.-J., Wang, C., … Wang, Z. (2016). Oncogenic PIK3CA mutations reprogram glutamine metabolism in colorectal cancer. *Nature Communications*, *7*, 11971.

Harding, H. P., Zhang, Y., Zeng, H., Novoa, I., Lu, P. D., Calfon, M., … Ron, D. (2003). An Integrated Stress Response Regulates Amino Acid Metabolism and Resistance to Oxidative Stress. *Molecular Cell*, *11*(3), 619–633.

Hassanein, M., Hoeksema, M. D., Shiota, M., Qian, J., Harris, B. K., Chen, H., … Massion, P. P. (2013). SLC1A5 mediates glutamine transport required for lung cancer cell growth and survival. *Clinical Cancer Research : An Official Journal of the American Association for Cancer Research*, *19*(3), 560–70.

Hay, N. (2016). Reprogramming glucose metabolism in cancer: can it be exploited for cancer therapy? *Nature Reviews Cancer*, *16*(10).

Hennipman, A., van Oirschot, B. A., Smits, J., Rijksen, G., & Staal, G. E. (1988). Glycolytic enzyme activities in breast cancer metastases. *Tumour Biology : The Journal of the International Society for Oncodevelopmental Biology and Medicine*, *9*(5), 241–8.

Hoekstra, A. S., Graaff, M. A. de, Bruijn, I. H. B., Ras, C., Seifar, R. M., Minderhout, I. van, … Bovée, J. V. M. G. (2015). Inactivation of <i>SDH</i> and <i>FH</i> cause loss of 5hmC and increased H3K9me3 in paraganglioma/pheochromocytoma and smooth muscle tumors. *Oncotarget*, *6*(36), 38777–38788.

Hou, P., Kuo, C.-Y., Cheng, C.-T., Liou, J.-P., Ann, D. K., & Chen, Q. (2014). Intermediary Metabolite Precursor Dimethyl-2-Ketoglutarate Stabilizes Hypoxia-Inducible Factor-1α by Inhibiting Prolyl-4-Hydroxylase PHD2. *PLoS ONE*, *9*(11), e113865.

Hsieh, A. L., Walton, Z. E., Altman, B. J., Stine, Z. E., & Dang, C. V. (2015). MYC and Metabolism on the Path to Cancer. *Seminars in Cell & Developmental Biology*.

Hu, S., Balakrishnan, A., Bok, R. A., Anderton, B., Larson, P. E. Z., Nelson, S. J., … Goga, A. (2011). 13C-pyruvate imaging reveals alterations in glycolysis that precede c-Myc-induced tumor formation and regression. *Cell Metabolism*, *14*(1), 131–42.

Hu, S., Balakrishnan, A., Bok, R. A., Anderton, B., Larson, P. E. Z., Nelson, S. J., … Thompson, C. B. (2011). 13C-pyruvate imaging reveals alterations in glycolysis that precede c-Myc-induced tumor formation and regression. *Cell Metabolism*, *14*(1), 131–42.

Hu, W., Tian, H., Yue, W., Li, L., Li, S., Gao, C., … Shan, S. (2016). Rotenone induces apoptosis in human lung cancer cells by regulating autophagic flux. *IUBMB Life*, *68*(5), 388–393.

Hu, Z., Fan, C., Oh, D. S., Marron, J., He, X., Qaqish, B. F., … Perou, C. M. (2006). The molecular portraits of breast tumors are conserved across microarray platforms. *BMC Genomics*, *7*(1), 96.

Huang, K. T., Dobrovic, A., Fox, S. B., Huang -KatieHuang, K. T., & Dobrovic -AlexanderDobrovic, A. (n.d.). No evidence for promoter region methylation of the succinate dehydrogenase and fumarate hydratase tumour suppressor genes in breast cancer.

Huang, X., Wullschleger, S., Shpiro, N., McGuire, V. A., Sakamoto, K., Woods, Y. L., … Alessi, D. R. (2008). Important role of the LKB1-AMPK pathway in suppressing tumorigenesis in PTEN-deficient mice. *The Biochemical Journal*, *412*(2), 211–21.

Isaacs, J. S., Jung, Y. J., Mole, D. R., Lee, S., Torres-Cabala, C., Chung, Y.-L., … Neckers, L. (2005). HIF overexpression correlates with biallelic loss of fumarate hydratase in renal cancer: Novel role of fumarate in regulation of HIF stability. *Cancer Cell*, *8*(2), 143–153.

Israelsen, W. J., Dayton, T. L., Davidson, S. M., Fiske, B. P., Hosios, A. M., Bellinger, G., … Vander Heiden, M. G. (2013). PKM2 Isoform-Specific Deletion Reveals a Differential Requirement for Pyruvate Kinase in Tumor Cells. *Cell*, *155*(2), 397–409.

Iurlaro, R., León-Annicchiarico, C. L., & Muñoz-Pinedo, C. (2014). Regulation of Cancer Metabolism by Oncogenes and Tumor Suppressors (pp. 59–80).

Jadvar, H. (2011). Prostate Cancer: PET with 18F-FDG, 18F- or 11C-Acetate, and 18F- or 11C-Choline. *Journal of Nuclear Medicine*, *52*(1), 81–89.

Ji, H., Ramsey, M. R., Hayes, D. N., Fan, C., McNamara, K., Kozlowski, P., … Wong, K.-K. (2007). LKB1 modulates lung cancer differentiation and metastasis. *Nature*, *448*(7155), 807–810.

Johnson, J., Thijssen, B., McDermott, U., Garnett, M., Wessels, L. F. A., & Bernards, R. (2016). Targeting the RB-E2F pathway in breast cancer. *Oncogene*, *35*(37), 4829–4835.

Kaplan, E. L., & Meier, P. (n.d.). Nonparametric Estimation from Incomplete Observations.

Keith, B., Johnson, R. S., & Simon, M. C. (2011). HIF1α and HIF2α: sibling rivalry in hypoxic tumour growth and progression. *Nature Reviews. Cancer*, *12*(1), 9–22.

Killian, J. K., Kim, S. Y., Miettinen, M., Smith, C., Merino, M., Tsokos, M., … Meltzer, P. S. (2013). Succinate Dehydrogenase Mutation Underlies Global Epigenomic Divergence in Gastrointestinal Stromal Tumor. *Cancer Discovery*, *3*(6), 648–657.

Kim, J. -w., Gao, P., Liu, Y.-C., Semenza, G. L., & Dang, C. V. (2007). Hypoxia-Inducible Factor 1 and Dysregulated c-Myc Cooperatively Induce Vascular Endothelial Growth Factor and Metabolic Switches Hexokinase 2 and Pyruvate Dehydrogenase Kinase 1. *Molecular and Cellular Biology*, *27*(21), 7381–7393.

Kim, S., Kim, D. H., Jung, W.-H., & Koo, J. S. (2013). Succinate dehydrogenase expression in breast cancer. *SpringerPlus*, *2*(1), 299.

Kiuru, M., Lehtonen, R., Eerola, H., Aittomäki, K., Blomqvist, C., Nevanlinna, H., … Launonen, V. (2005). No germline FH mutations in familial breast cancer patients. *European Journal of Human Genetics*, *13*(4), 506–509.

Korangath, P., Teo, W. W., Sadik, H., Han, L., Mori, N., Huijts, C. M., … Sukumar, S. (2015). Targeting Glutamine Metabolism in Breast Cancer with Aminooxyacetate. *Clinical Cancer Research : An Official Journal of the American Association for Cancer Research*.

Krall, A. S., Xu, S., Graeber, T. G., Braas, D., & Christofk, H. R. (2016). Asparagine promotes cancer cell proliferation through use as an amino acid exchange factor. *Nature Communications*, *7*, 11457.

Kruskal, W. H., & Wallis, W. A. (1952). Use of Ranks in One-Criterion Variance Analysis. *Journal of the American Statistical Association*, *47*(260), 583–621.

Kunutsor, S. K., Apekey, T. A., Hemelrijck, M. Van, Calori, G., & Perseghin, G. (2014). Gamma glutamyltransferase, alanine aminotransferase and risk of cancer: Systematic review and meta-analysis. *International Journal of Cancer. Journal International Du Cancer*.

Lampa, M., Arlt, H., He, T., Ospina, B., Reeves, J., Zhang, B., … Srinivasan, L. (2017). Glutaminase is essential for the growth of triple-negative breast cancer cells with a deregulated glutamine metabolism pathway and its suppression synergizes with mTOR inhibition. *PloS One*, *12*(9), e0185092.

Lanning, N. J., Castle, J. P., Singh, S. J., Leon, A. N., Tovar, E. A., Sanghera, A., … Graveel, C. R. (2017). Metabolic profiling of triple-negative breast cancer cells reveals metabolic vulnerabilities. *Cancer & Metabolism*, *5*(1), 6.

Le, A., Lane, A. N., Hamaker, M., Bose, S., Gouw, A., Barbi, J., … Dang, C. V. (2012). Glucose-Independent Glutamine Metabolism via TCA Cycling for Proliferation and Survival in B Cells.

Lehmann, B. D., Bauer, J. A., Chen, X., Sanders, M. E., Chakravarthy, A. B., Shyr, Y., & Pietenpol, J. A. (2011). Identification of human triple-negative breast cancer subtypes and preclinical models for selection of targeted therapies. *The Journal of Clinical Investigation*, *121*(7), 2750–67.

Lehmann, B. D., Jovanovi?, B., Chen, X., Estrada, M. V., Johnson, K. N., Shyr, Y., … Pietenpol, J. A. (2016). Refinement of Triple-Negative Breast Cancer Molecular Subtypes: Implications for Neoadjuvant Chemotherapy Selection. *PLOS ONE*, *11*(6), e0157368.

Lehmann, B. D., Jovanović, B., Chen, X., Estrada, M. V., Johnson, K. N., Shyr, Y., … Pietenpol, J. A. (2016). Refinement of Triple-Negative Breast Cancer Molecular Subtypes: Implications for Neoadjuvant Chemotherapy Selection. *PLOS ONE*, *11*(6), e0157368.

Letouzé, E., Martinelli, C., Loriot, C., Burnichon, N., Abermil, N., Ottolenghi, C., … Favier, J. (2013). SDH Mutations Establish a Hypermethylator Phenotype in Paraganglioma. *Cancer Cell*, *23*(6), 739–752.

Li, C., Xue, Y., Xi, Y.-R., & Xie, K. (2017). Progress in the application and mechanism of metformin in treating non-small cell lung cancer. *Oncology Letters*, *13*(5), 2873–2880.

Lieberman, B. P., Ploessl, K., Wang, L., Qu, W., Zha, Z., Wise, D. R., … Kung, H. F. (2011). PET imaging of glutaminolysis in tumors by 18F-(2S,4R)4-fluoroglutamine. *Journal of Nuclear Medicine : Official Publication, Society of Nuclear Medicine*, *52*(12), 1947–55.

Liedtke, C., & Kolberg, H.-C. (2016). Systemic Therapy of Advanced/Metastatic Breast Cancer - Current Evidence and Future Concepts. *Breast Care (Basel, Switzerland)*, *11*(4), 275–281.

Lim, S.-O., Li, C.-W., Xia, W., Lee, H.-H., Chang, S.-S., Shen, J., … Hung, M.-C. (2016). EGFR signaling enhances aerobic glycolysis in triple negative breast cancer cells to promote tumor growth and immune escape. *Cancer Research*.

Linares, J. F., Cordes, T., Duran, A., Reina-Campos, M., Valencia, T., Ahn, C. S., … Diaz-Meco, M. T. (2017). ATF4-Induced Metabolic Reprograming Is a Synthetic Vulnerability of the p62-Deficient Tumor Stroma. *Cell Metabolism*, *0*(0).

Liu, B., Fan, Z., Edgerton, S. M., Deng, X.-S., Alimova, I. N., Lind, S. E., & Thor, A. D. (2009). Metformin induces unique biological and molecular responses in triple negative breast cancer cells. *Cell Cycle*, *8*(13), 2031–2040.

Lloyd, S. M., Arnold, J., & Sreekumar, A. (2015). Metabolomic profiling of hormone-dependent cancers: a bird's eye view. *Trends in Endocrinology & Metabolism*, *26*(9), 477–485.

Locasale, J. W., Grassian, A. R., Melman, T., Lyssiotis, C. A., Mattaini, K. R., Bass, A. J., … Vander Heiden, M. G. (2011). Phosphoglycerate dehydrogenase diverts glycolytic flux and contributes to oncogenesis. *Nature Genetics*, *43*(9), 869–874.

Lorenzi, P. L., & Weinstein, J. N. (2009). Asparagine synthetase: a new potential biomarker in ovarian cancer. *Drug News & Perspectives*, *22*(1), 61–4.

Lukey, M. J., Greene, K. S., Erickson, J. W., Wilson, K. F., & Cerione, R. A. The oncogenic transcription factor c-Jun regulates glutaminase expression and sensitizes cells to glutaminase-targeted therapy. *Nature Communications*, *7*, 11321.

Lukey, M. J., Greene, K. S., Erickson, J. W., Wilson, K. F., & Cerione, R. A. (2016). The oncogenic transcription factor c-Jun regulates glutaminase expression and sensitizes cells to glutaminase-targeted therapy. *Nature Communications*, *7*, 11321.

Lunt, S. Y., & Vander Heiden, M. G. (2011). Aerobic Glycolysis: Meeting the Metabolic Requirements of Cell Proliferation. *Annual Review of Cell and Developmental Biology*, *27*(1), 441–464.

Luo, Z., Zang, M., & Guo, W. (2010). AMPK as a metabolic tumor suppressor: control of metabolism and cell growth. *Future Oncology*, *6*(3), 457–470.

Madiraju, A. K., Erion, D. M., Rahimi, Y., Zhang, X.-M., Braddock, D. T., Albright, R. A., … Shulman, G. I. (2014). Metformin suppresses gluconeogenesis by inhibiting mitochondrial glycerophosphate dehydrogenase. *Nature*, *510*(7506), 542–546.

Maiti, B., Kundranda, M. N., Spiro, T. P., & Daw, H. A. (2010). The association of metabolic syndrome with triple-negative breast cancer. *Breast Cancer Research and Treatment*, *121*(2), 479–83.

Mannsperger, H. A., Gade, S., Henjes, F., Beissbarth, T., & Korf, U. (2010). RPPanalyzer: Analysis of reverse-phase protein array data. *Bioinformatics (Oxford, England)*, *26*(17), 2202–2203.

Márquez, J., Sánchez-Jiménez, F., Medina, M. A., Quesada, A. R., & de Castro, I. N. (1989). Nitrogen metabolism in tumor bearing mice. *Archives of Biochemistry and Biophysics*, *268*(2), 667–675.

Martín-Rufián, M., Nascimento-Gomes, R., Higuero, A., Crisma, A. R., Campos-Sandoval, J. A., Gómez-García, M. C., … Matés, J. M. (2014). Both GLS silencing and GLS2 overexpression synergize with oxidative stress against proliferation of glioma cells. *Journal of Molecular Medicine (Berlin, Germany)*, *92*(3), 277–90.

Martinez-Outschoorn, U. E., Peiris-Pagés, M., Pestell, R. G., Sotgia, F., & Lisanti, M. P. (2016). Cancer metabolism: a therapeutic perspective. *Nature Reviews. Clinical Oncology*.

Matthiesen, R., & Bunkenborg, J. (2013). Introduction to mass spectrometry-based proteomics. In *Mass spectrometry data analysis in proteomics*.

Maximos, M., Bril, F., Portillo Sanchez, P., Lomonaco, R., Orsak, B., Biernacki, D., … Cusi, K. (2015). The role of liver fat and insulin resistance as determinants of plasma aminotransferase elevation in nonalcoholic fatty liver disease. *Hepatology*, *61*(1), 153–160.

McCarthy, N. (2015). Metabolism: MYC clocks on. *Nature Reviews Cancer*.

McCormick, F. (1999). Signalling networks that cause cancer. *Trends in Cell Biology*, *9*(12), M53-6.

Metallo, C. M., Gameiro, P. A., Bell, E. L., Mattaini, K. R., Yang, J., Hiller, K., … Stephanopoulos, G. (2011). Reductive glutamine metabolism by IDH1 mediates lipogenesis under hypoxia. *Nature*, *481*(7381), 380–4.

Miao, P., Sheng, S., Sun, X., Liu, J., & Huang, G. (2013). Lactate dehydrogenase a in cancer: A promising target for diagnosis and therapy. *IUBMB Life*, *65*(11), 904–910.

Miller, D. M., Thomas, S. D., Islam, A., Muench, D., & Sedoris, K. (2012). c-Myc and cancer metabolism. *Clinical Cancer Research : An Official Journal of the American Association for Cancer Research*, *18*(20), 5546–53.

Mishra, P., & Ambs, S. Metabolic Signatures of Human Breast Cancer. *Molecular & Cellular Oncology*, *2*(3).

Momcilovic, M., Bailey, S. T., Lee, J. T., Fishbein, M. C., Magyar, C., Braas, D., … Shackelford, D. B. (2017). *Targeted Inhibition of EGFR and Glutaminase Induces Metabolic Crisis in EGFR Mutant Lung Cancer*. *Cell Reports* (Vol. 18).

Morin, A., Letouzé, E., Gimenez-Roqueplo, A.-P., & Favier, J. (2014). Oncometabolites-driven tumorigenesis: From genetics to targeted therapy. *International Journal of Cancer. Journal International Du Cancer*.

Mullen, A. R., Wheaton, W. W., Jin, E. S., Chen, P.-H., Sullivan, L. B., Cheng, T., … DeBerardinis, R. J. (2011). Reductive carboxylation supports growth in tumour cells with defective mitochondria. *Nature*, *481*(7381), 385–8.

Müller, U., & Niemann, S. (2000). Mutations in SDHC cause autosomal dominant paraganglioma, type 3. *Nature Genetics*, *26*(3), 268–270.

Nanda, R., Chow, L. Q. M., Dees, E. C., Berger, R., Gupta, S., Geva, R., … Buisseret, L. (2016). Pembrolizumab in Patients With Advanced Triple-Negative Breast Cancer: Phase Ib KEYNOTE-012 Study. *Journal of Clinical Oncology : Official Journal of the American Society of Clinical Oncology*, *34*(21), 2460–7.

Nelson, S. J., Kurhanewicz, J., Vigneron, D. B., Larson, P. E. Z., Harzstark, A. L., Ferrone, M., … Murray, J. A. (2013). Metabolic Imaging of Patients with Prostate Cancer Using Hyperpolarized [1-13C]Pyruvate. *Science Translational Medicine*, *5*(198). Retrieved from

Nicklin, P., Bergman, P., Zhang, B., Triantafellow, E., Wang, H., Nyfeler, B., … Murphy, L. O. (2009). Bidirectional transport of amino acids regulates mTOR and autophagy. *Cell*, *136*(3), 521–34.

Nicolay, B. N., & Dyson, N. J. (2013). The multiple connections between pRB and cell metabolism. *Current Opinion in Cell Biology*, *25*(6), 735–40. 2

Nikiforov, M. A., Chandriani, S., O'Connell, B., Petrenko, O., Kotenko, I., Beavis, A., … Cole, M. D. (2002). A functional screen for Myc-responsive genes reveals serine hydroxymethyltransferase, a major source of the one-carbon unit for cell metabolism. *Molecular and Cellular Biology*, *22*(16), 5793–800.

Noble, W. S., & MacCoss, M. J. (2012). Computational and statistical analysis of protein mass spectrometry data. *PLoS Computational Biology*.

Nowell, P. C. (1976). The clonal evolution of tumor cell populations. *Science (New York, N.Y.)*, *194*(4260), 23–8.

Osthus, R. C., Shim, H., Kim, S., Li, Q., Reddy, R., Mukherjee, M., … Dang, C. V. (2000). Deregulation of Glucose Transporter 1 and Glycolytic Gene Expression by c-Myc. *Journal of Biological Chemistry*, *275*(29), 21797–21800.

Pacold, M. E., Brimacombe, K. R., Chan, S. H., Rohde, J. M., Lewis, C. A., Swier, L. J. Y. M., … Sabatini, D. M. (2016). A PHGDH inhibitor reveals coordination of serine synthesis and one-carbon unit fate. *Nature Chemical Biology*, *12*(6), 452–458.

Pang, B., Cheng, S., Sun, S.-P., An, C., Liu, Z.-Y., Feng, X., & Liu, G.-J. (2014). Prognostic role of PIK3CA mutations and their association with hormone receptor expression in breast cancer: a meta-analysis. *Scientific Reports*, *4*, 6255.

Park, J. H., Vithayathil, S., Kumar, S., Sung, P.-L., Dobrolecki, L. E., Putluri, V., … al., et. (2016). Fatty Acid Oxidation-Driven Src Links Mitochondrial Energy Reprogramming and Oncogenic Properties in Triple-Negative Breast Cancer. *Cell Reports*, *14*(9), 2154–2165.

Park, S., Chang, C.-Y., Safi, R., Liu, X., Baldi, R., Jasper, J. S., … McDonnell, D. P. (2016). ERRα Regulated Lactate Metabolism Contributes to Resistance to Targeted Therapies in Breast Cancer. *Cell Reports*, *15*(2), 323–335.

Parker, J. S., Mullins, M., Cheang, M. C. U., Leung, S., Voduc, D., Vickery, T., … Bernard, P. S. (2009). Supervised risk predictor of breast cancer based on intrinsic subtypes. *Journal of Clinical Oncology : Official Journal of the American Society of Clinical Oncology*, *27*(8), 1160–7.

Pavlova, N. N., & Thompson, C. B. (2016). The Emerging Hallmarks of Cancer Metabolism. *Cell Metabolism*.

Paweletz, C. P., Charboneau, L., Bichsel, V. E., Simone, N. L., Chen, T., Gillespie, J. W., … Liotta, L. A. (2001). Reverse phase protein microarrays which capture disease progression show activation of pro-survival pathways at the cancer invasion front. *Oncogene*, *20*(16), 1981–1989.

Pelicano, H., Zhang, W., Liu, J., Hammoudi, N., Dai, J., Xu, R.-H., … Huang, P. (2014). Mitochondrial dysfunction in some triple-negative breast cancer cell lines: role of mTOR pathway and therapeutic potential. *Breast Cancer Research*, *16*(5), 434.

Penkert, J., Ripperger, T., Schieck, M., Schlegelberger, B., Steinemann, D., Illig, T., … Illig, T. (2015). On metabolic reprogramming and tumor biology: A comprehensive survey of metabolism in breast cancer. *Oncotarget*, *7*(41), 67626–67649.

Peterson, A. L., Walker, A. K., Sloan, E. K., & Creek, D. J. (2016). Optimized Method for Untargeted Metabolomics Analysis of MDA-MB-231 Breast Cancer Cells. *Metabolites*, *6*(4).

Pietzke, M., & Kempa, S. (2014). Pulsed stable isotope-resolved metabolomic studies of cancer cells. *Methods in Enzymology*, *543*, 179–98.

Pinheiro, C., Sousa, B., Albergaria, A., Paredes, J., Dufloth, R., Vieira, D., … Baltazar, F. (2011). GLUT1 and CAIX expression profiles in breast cancer correlate with adverse prognostic factors and MCT1 overexpression. *Histology and Histopathology*, *26*(10), 1279–86.

Pollard, P. J., Brière, J. J., Alam, N. A., Barwell, J., Barclay, E., Wortham, N. C., … Tomlinson, I. P. M. (2005). Accumulation of Krebs cycle intermediates and over-expression of HIF1 in tumours which result from germline FH and SDH mutations. *Human Molecular Genetics*, *14*(15), 2231–2239.

Poschke, I., Mao, Y., Kiessling, R., & de Boniface, J. (2013). Tumor-dependent increase of serum amino acid levels in breast cancer patients has diagnostic potential and correlates with molecular tumor subtypes. *Journal of Translational Medicine*, *11*, 290.

Possemato, R., Marks, K. M., Shaul, Y. D., Pacold, M. E., Kim, D., Birsoy, K., … Sabatini, D. M. (2011a). Functional genomics reveal that the serine synthesis pathway is essential in breast cancer. *Nature*, *476*(7360), 346–350.

Possemato, R., Marks, K. M., Shaul, Y. D., Pacold, M. E., Kim, D., Birsoy, K., … Sabatini, D. M. (2011b). Functional genomics reveal that the serine synthesis pathway is essential in breast cancer. *Nature*, *476*(7360), 346–350.

Quirós, P. M., Prado, M. A., Zamboni, N., D'Amico, D., Williams, R. W., Finley, D., … Auwerx, J. (2017). Multi-omics analysis identifies ATF4 as a key regulator of the mitochondrial stress response in mammals. *The Journal of Cell Biology*, *216*(7).

Reynolds, M., Lane, A., Robertson, B., Kemp, S., Liu, Y., Hill, B., … Clem, B. (2013). Control of glutamine metabolism by the tumor suppressor Rb. *Oncogene*, *33*, 556–566.

Reynolds, M. R., Lane, A. N., Robertson, B., Kemp, S., Liu, Y., Hill, B. G., … Clem, B. F. (2014). Control of glutamine metabolism by the tumor suppressor Rb. *Oncogene*, *33*(5), 556–66.

Rizwan, A., Serganova, I., Khanin, R., Karabeber, H., Ni, X., Thakur, S., … Koutcher, J. A. (2013). Relationships between LDH-A, lactate, and metastases in 4T1 breast tumors. *Clinical Cancer Research : An Official Journal of the American Association for Cancer Research*, *19*(18), 5158–69.

Rodrigues, T. B., Serrao, E. M., Kennedy, B. W. C., Hu, D.-E., Kettunen, M. I., & Brindle, K. M. (2013). Magnetic resonance imaging of tumor glycolysis using hyperpolarized 13C-labeled glucose. *Nature Medicine*, *20*(1), 93–97.

Sacco, F., Silvestri, A., Posca, D., Castagnoli, L., Mann, M., Cesareni, G., … Gherardini, P. F. (2016). Deep Proteomics of Breast Cancer Cells Reveals that Metformin Rewires Signaling Networks Away from a Pro-growth State. *Cell Systems*, *2*, 1–13.

Salgado, M. C., Metón, I., Anemaet, I. G., & Baanante, I. V. (2014a). Activating transcription factor 4 mediates up-regulation of alanine aminotransferase 2 gene expression under metabolic stress. *Biochimica et Biophysica Acta*, *1839*(4), 288–96.

Salgado, M. C., Metón, I., Anemaet, I. G., & Baanante, I. V. (2014b). Activating transcription factor 4 mediates up-regulation of alanine aminotransferase 2 gene expression under metabolic stress. *Biochimica et Biophysica Acta*, *1839*(4), 288–96.

Sauer, L. A., Stayman, J. W., & Dauchy, R. T. (1982). Amino acid, glucose, and lactic acid utilization in vivo by rat tumors. *Cancer Research*, *42*(10), 4090–7.

Schirrmeister, H., Kühn, T., Guhlmann, A., Santjohanser, C., Hörster, T., Nüssle, K., … Reske, S. N. (2001). Fluorine-18 2-deoxy-2-fluoro-D-glucose PET in the preoperative staging of breast cancer: comparison with the standard staging procedures. *European Journal of Nuclear Medicine*, *28*(3), 351–8.

Sellers, K., Fox, M. P., Bousamra, M., Slone, S. P., Higashi, R. M., Miller, D. M., … Fan, T. W.-M. (2015). Pyruvate carboxylase is critical for non–small-cell lung cancer proliferation. *Journal of Clinical Investigation*, *125*(2), 687–698.

Shajahan-Haq, A. N., Cook, K. L., Schwartz-Roberts, J. L., Eltayeb, A. E., Demas, D. M., Warri, A. M., … Clarke, R. (2014). MYC regulates the unfolded protein response and glucose and glutamine uptake in endocrine resistant breast cancer. *Molecular Cancer*, *13*(1), 239.

Sharma, A. K., Eils, R., & König, R. (2016). Copy Number Alterations in Enzyme-Coding and Cancer-Causing Genes Reprogram Tumor Metabolism. *Cancer Research*, *76*(14), 4058–67.

Shen, L., O'Shea, J. M., Kaadige, M. R., Cunha, S., Wilde, B. R., Cohen, A. L., … Ayer, D. E. (2015). Metabolic reprogramming in triple-negative breast cancer through Myc suppression of TXNIP. *Proceedings of the National Academy of Sciences of the United States of America*, *112*(17), 5425–30.

Shi, W., Oshlack, A., & Smyth, G. K. (2010). Optimizing the noise versus bias trade-off for Illumina whole genome expression BeadChips. *Nucleic Acids Research*, *38*(22), e204–e204.

Shim, H., Dolde, C., Lewis, B. C., Wu, C. S., Dang, G., Jungmann, R. A., … Dang, C. V. (1997). c-Myc transactivation of LDH-A: implications for tumor metabolism and growth. *Proceedings of the National Academy of Sciences of the United States of America*, *94*(13), 6658–63.

Siegel, R. L., Miller, K. D., & Jemal, A. (2017a). Cancer statistics, 2017. *CA: A Cancer Journal for Clinicians*, *67*(1), 7–30.

Siegel, R. L., Miller, K. D., & Jemal, A. (2017b). Cancer statistics, 2017. *CA: A Cancer Journal for Clinicians*, *67*(1), 7–30.

Singh, R., Pervin, S., Karimi, A., Cederbaum, S., & Chaudhuri, G. (2000). Arginase Activity in Human Breast Cancer Cell Lines: N{{omega}}-Hydroxy-L-arginine Selectively Inhibits Cell Proliferation and Induces Apoptosis in MDA-MB-468 Cells. *Cancer Res.*, *60*(12), 3305–3312.

Slamon, D. J., Leyland-Jones, B., Shak, S., Fuchs, H., Paton, V., Bajamonde, A., … Norton, L. (2001). Use of Chemotherapy plus a Monoclonal Antibody against HER2 for Metastatic Breast Cancer That Overexpresses HER2. *New England Journal of Medicine*, *344*(11), 783–792.

Smith, B., Schafer, X. L., Ambeskovic, A., Spencer, C. M., Land, H., Munger, J., … Feng, Z. (2016a). Addiction to Coupling of the Warburg Effect with Glutamine Catabolism in Cancer Cells. *Cell Reports*, *17*(3), 821–836.

Smith, B., Schafer, X. L., Ambeskovic, A., Spencer, C. M., Land, H., Munger, J., … Feng, Z. (2016b). Addiction to Coupling of the Warburg Effect with Glutamine Catabolism in Cancer Cells. *Cell Reports*, *17*(3), 821–836.

Smyth, G. (2005). limma: Linear Models for Microarray Data. In R. Gentleman, V. Carey, W. Huber, R. Irizarry, & S. Dudoit (Eds.), *Bioinformatics and Computational Biology Solutions Using R and Bioconductor* (pp. 397–420). Springer-Verlag.

Smyth, G. K. (2004). Linear Models and Empirical Bayes Methods for Assessing Differential Expression in Microarray Experiments. *Statistical Applications in Genetics and Molecular Biology*, *3*(1), 1–25.

Som, P., Atkins, H. L., Bandoypadhyay, D., Fowler, J. S., MacGregor, R. R., Matsui, K., … Zabinski, S. V. (1980). A fluorinated glucose analog, 2-fluoro-2-deoxy-D-glucose (F-18): nontoxic tracer for rapid tumor detection. *Journal of Nuclear Medicine : Official Publication, Society of Nuclear Medicine*, *21*(7), 670–5.

Son, J., Lyssiotis, C. A., Ying, H., Wang, X., Hua, S., Ligorio, M., … Kimmelman, A. C. (2013a). Glutamine supports pancreatic cancer growth through a KRAS-regulated metabolic pathway. *Nature*, *496*(7443), 101–105.

Son, J., Lyssiotis, C. A., Ying, H., Wang, X., Hua, S., Ligorio, M., … Kimmelman, A. C. (2013b). Glutamine supports pancreatic cancer growth through a KRAS-regulated metabolic pathway. *Nature*, *496*(7443), 101–5.

Sørlie, T., Perou, C. M., Tibshirani, R., Aas, T., Geisler, S., Johnsen, H., … Børresen-Dale, A. L. (2001). Gene expression patterns of breast carcinomas distinguish tumor subclasses with clinical implications. *Proceedings of the National Academy of Sciences of the United States of America*, *98*(19), 10869–74.

Sotgia, F., Martinez-Outschoorn, U. E., & Lisanti, M. P. (2013). Cancer Metabolism: New Validated Targets for Drug Discovery. *Oncotarget*, *4*, 1309–1316.

Souba, W. W. (1993). Glutamine and cancer. *Annals of Surgery*, *218*(6), 715–28.

Sousa, C. M., Biancur, D. E., Wang, X., Halbrook, C. J., Sherman, M. H., Zhang, L., … Kimmelman, A. C. (2016). Pancreatic stellate cells support tumour metabolism through autophagic alanine secretion. *Nature*, *536*(7617), 479–483.

Sullivan, L. B., Gui, D. Y., & Heiden, M. G. Vander. (2016). Altered metabolite levels in cancer: implications for tumour biology and cancer therapy. *Nature Reviews. Cancer*.

Sullivan, L. B., Gui, D. Y., Hosios, A. M., Bush, L. N., Freinkman, E., & Vander Heiden, M. G. (2015). Supporting Aspartate Biosynthesis Is an Essential Function of Respiration in Proliferating Cells. *Cell*, *162*(3).

Sun, L., Song, L., Wan, Q., Wu, G., Li, X., Wang, Y., … Zhang, H. (2015). cMyc-mediated activation of serine biosynthesis pathway is critical for cancer progression under nutrient deprivation conditions. *Cell Research*, *25*(4), 429–444.

Tan, A. S., Baty, J. W., Dong, L.-F., Bezawork-Geleta, A., Endaya, B., Goodwin, J., … Berridge, M. V. (2015). Mitochondrial Genome Acquisition Restores Respiratory Function and Tumorigenic Potential of Cancer Cells without Mitochondrial DNA. *Cell Metabolism*, *21*(1), 81–94.

Tanabe, M., Izumi, H., Ise, T., Higuchi, S., Yamori, T., Yasumoto, K., & Kohno, K. (2003). Activating transcription factor 4 increases the cisplatin resistance of human cancer cell lines. *Cancer Research*, *63*(24), 8592–5.

Tateishi, K., Wakimoto, H., Iafrate, A. J., Tanaka, S., Loebel, F., Lelic, N., … Cahill, D. P. (2015). Extreme Vulnerability of IDH1 Mutant Cancers to NAD+ Depletion. *Cancer Cell*, *28*(6), 773–784.

Teicher, B. A., Linehan, W. M., & Helman, L. J. (2012). Targeting cancer metabolism. *Clinical Cancer Research : An Official Journal of the American Association for Cancer Research*, *18*(20), 5537–45.

Telang, S., Yalcin, A., Clem, A. L., Bucala, R., Lane, A. N., Eaton, J. W., & Chesney, J. (2006). Ras transformation requires metabolic control by 6-phosphofructo-2-kinase. *Oncogene*, *25*(55), 7225–7234.

Tennant, D. A., Durán, R. V, & Gottlieb, E. (2010). Targeting metabolic transformation for cancer therapy. *Nature Reviews. Cancer*, *10*(4), 267–77.

Terunuma, A., Putluri, N., Mishra, P., Mathé, E. A., Dorsey, T. H., Yi, M., … Ambs, S. (2014). MYC-driven accumulation of 2-hydroxyglutarate is associated with breast cancer prognosis. *The Journal of Clinical Investigation*, *124*(1), 398–412.

Thornburg, J. M., Nelson, K. K., Clem, B. F., Lane, A. N., Arumugam, S., Simmons, A., … Chesney, J. (2008). Targeting aspartate aminotransferase in breast cancer. *Breast Cancer Research : BCR*, *10*(5), R84.

Timmerman, L. A., Holton, T., Yuneva, M., Louie, R. J., Padró, M., Daemen, A., … Gray, J. W. (2013). Glutamine Sensitivity Analysis Identifies the xCT Antiporter as a Common Triple-Negative Breast Tumor Therapeutic Target. *Cancer Cell*, *24*(4), 450–465.

Tomlinson, I. P. M., Alam, N. A., Rowan, A. J., Barclay, E., Jaeger, E. E. M., Kelsell, D., … Multiple Leiomyoma Consortium. (2002). Germline mutations in FH predispose to dominantly inherited uterine fibroids, skin leiomyomata and papillary renal cell cancer. *Nature Genetics*, *30*(4), 406–410.

Vacanti, N. M., Divakaruni, A. S., Green, C. R., Parker, S. J., Henry, R. R., Ciaraldi, T. P., … Metallo, C. M. (2014). Regulation of Substrate Utilization by the Mitochondrial Pyruvate Carrier. *Molecular Cell*, *56*(3), 425–435.

van Geldermalsen, M., Wang, Q., Nagarajah, R., Marshall, A. D., Thoeng, A., Gao, D., … Holst, J. (2015a). ASCT2/SLC1A5 controls glutamine uptake and tumour growth in triple-negative basal-like breast cancer. *Oncogene*.

van Geldermalsen, M., Wang, Q., Nagarajah, R., Marshall, A. D., Thoeng, A., Gao, D., … Holst, J. (2015b). ASCT2/SLC1A5 controls glutamine uptake and tumour growth in triple-negative basal-like breast cancer. *Oncogene*.

Vander Heiden, M. G., Cantley, L. C., & Thompson, C. B. (2009). Understanding the Warburg Effect: The Metabolic Requirements of Cell Proliferation. *Science*, *324*(5930), 1029–1033.

Vander Heiden, M. G., & DeBerardinis, R. J. (2017). Understanding the Intersections between Metabolism and Cancer Biology. *Cell*, *168*(4).

Vegran, F., Boidot, R., Michiels, C., Sonveaux, P., & Feron, O. (2011). Lactate Influx through the Endothelial Cell Monocarboxylate Transporter MCT1 Supports an NF- B/IL-8 Pathway that Drives Tumor Angiogenesis. *Cancer Research*, *71*(7), 2550–2560.

Venneti, S., Dunphy, M. P., Zhang, H., Pitter, K. L., Zanzonico, P., Campos, C., … Thompson, C. B. (2015). Glutamine-based PET imaging facilitates enhanced metabolic evaluation of gliomas in vivo. *Science Translational Medicine*, *7*(274), 274ra17-274ra17.

Verma, S., Miles, D., Gianni, L., Krop, I. E., Welslau, M., Baselga, J., … Blackwell, K. (2012). Trastuzumab Emtansine for HER2-Positive Advanced Breast Cancer. *New England Journal of Medicine*, *367*(19), 1783–1791.

Wahlström, T., & Henriksson, M. A. (2014). Impact of MYC in regulation of tumor cell metabolism. *Biochimica et Biophysica Acta*.

Wang, G. L., Jiang, B. H., Rue, E. A., & Semenza, G. L. (1995). Hypoxia-inducible factor 1 is a basic-helix-loop-helix-PAS heterodimer regulated by cellular O2 tension. *Proceedings of the National Academy of Sciences of the United States of America*, *92*(12), 5510–4.

Warburg, O. (1927). THE METABOLISM OF TUMORS IN THE BODY. *The Journal of General Physiology*, *8*(6), 519–530.

Warburg, O. (1956). On the Origin of Cancer Cells. *Science*, *123*(3191), 309–314.

Weinberg, R. A. (1995). The retinoblastoma protein and cell cycle control. *Cell*, *81*(3), 323–330.

Wheaton, W. W., Weinberg, S. E., Hamanaka, R. B., Soberanes, S., Sullivan, L. B., Anso, E., … Chandel, N. S. (2014). Metformin inhibits mitochondrial complex I of cancer cells to reduce tumorigenesis. *eLife*, *3*, e02242.

Wise, D. R., DeBerardinis, R. J., Mancuso, A., Sayed, N., Zhang, X.-Y., Pfeiffer, H. K., … Thompson, C. B. (2008). Myc regulates a transcriptional program that stimulates mitochondrial glutaminolysis and leads to glutamine addiction. *Proceedings of the National Academy of Sciences of the United States of America*, *105*(48), 18782–7.

Wise, D. R., & Thompson, C. B. (2010). Glutamine addiction: a new therapeutic target in cancer.

Wise, D. R., Ward, P. S., Shay, J. E. S., Cross, J. R., Gruber, J. J., Sachdeva, U. M., … Thompson, C. B. (2011). Hypoxia promotes isocitrate dehydrogenase-dependent carboxylation of -ketoglutarate to citrate to support cell growth and viability. *Proceedings of the National Academy of Sciences*, *108*(49), 19611–19616.

Wood, A. J. J., Smith, I. E., & Dowsett, M. (2003). Aromatase Inhibitors in Breast Cancer. *New England Journal of Medicine*, *348*(24), 2431–2442.

Xiang, X., Saha, A. K., Wen, R., Ruderman, N. B., & Luo, Z. (2004). AMP-activated protein kinase activators can inhibit the growth of prostate cancer cells by multiple mechanisms. *Biochemical and Biophysical Research Communications*, *321*(1), 161–167.

Xie, H., Hanai, J.-I., Ren, J.-G., Kats, L., Burgess, K., Bhargava, P., … Seth, P. (2014). Targeting lactate dehydrogenase-a inhibits tumorigenesis and tumor progression in mouse models of lung cancer and impacts tumor-initiating cells. *Cell Metabolism*, *19*(5), 795–809.

Yan, H., Parsons, D. W., Jin, G., McLendon, R., Rasheed, B. A., Yuan, W., … Bigner, D. D. (2009). *IDH1* and *IDH2* Mutations in Gliomas. *New England Journal of Medicine*, *360*(8), 765–773.

Yang, Roong-Ze; Blaileanu, Greorche; Hansen, Barbara C;Shuldiner, Alan R; Gong, D.-W. (2002). cDNA Cloning, Genomic Structure, Chromosomal Mapping, and Functional Expression of a Novel Human Alanine Aminotransferase. *Genomics*, *79*(3), 445–450.

Yang, C., Ko, B., Hensley, C. T., Jiang, L., Wasti, A. T., Kim, J., … DeBerardinis, R. J. (2014a). Glutamine oxidation maintains the TCA cycle and cell survival during impaired mitochondrial pyruvate transport. *Molecular Cell*, *56*(3).

Yang, C., Ko, B., Hensley, C. T., Jiang, L., Wasti, A. T., Kim, J., … DeBerardinis, R. J. (2014b). Glutamine Oxidation Maintains the TCA Cycle and Cell Survival during Impaired Mitochondrial Pyruvate Transport. *Molecular Cell*, *56*(3), 414–424.

Yang, L., Venneti, S., & Nagrath, D. (2017). Glutaminolysis: A Hallmark of Cancer Metabolism. *Annu. Rev. Biomed. Eng*, *19*, 163–94.

Yang, M., & Vousden, K. H. (2016). Serine and one-carbon metabolism in cancer. *Nature Reviews Cancer*, *16*(10), 650–662.

Yates, L. R., Knappskog, S., Wedge, D., Farmery, J. H. R., Gonzalez, S., Martincorena, I., … Campbell, P. J. (2017). Genomic Evolution of Breast Cancer Metastasis and Relapse. *Cancer Cell*, *32*(2), 169–184.e7. http://doi.org/10.1016/j.ccell.2017.07.005

Ye, J., Kumanova, M., Hart, L. S., Sloane, K., Zhang, H., De Panis, D. N., … Koumenis, C. (2010). The GCN2-ATF4 pathway is critical for tumour cell survival and proliferation in response to nutrient deprivation. *The EMBO Journal*, *29*(12), 2082–96.

Ying, H., Kimmelman, A. C., Lyssiotis, C. A., Hua, S., Chu, G. C., Fletcher-Sananikone, E., … DePinho, R. A. (2012). Oncogenic Kras maintains pancreatic tumors through regulation of anabolic glucose metabolism. *Cell*, *149*(3), 656–70.

Yoo, H., Antoniewicz, M. R., Stephanopoulos, G., & Kelleher, J. K. (2008). Quantifying reductive carboxylation flux of glutamine to lipid in a brown adipocyte cell line. *The Journal of Biological Chemistry*, *283*(30), 20621–7.

Yuan, J., Reed, A., Chen, F., & Stewart, C. N. (2006). Statistical analysis of real-time PCR data. *BMC Bioinformatics*, *7*(1), 85.

Yuneva, M. O., Fan, T. W. M., Allen, T. D., Higashi, R. M., Ferraris, D. V., Tsukamoto, T., … Bishop, J. M. (2012). The Metabolic Profile of Tumors Depends on Both the Responsible Genetic Lesion and Tissue Type. *Cell Metabolism*, *15*(2), 157–170.

Zaidi, N., Swinnen, J. V., & Smans, K. (2012). ATP-Citrate Lyase: A Key Player in Cancer Metabolism. *Cancer Research*, *72*(15), 3709–3714.

Zdzisińska, B., Żurek, A., & Kandefer-Szerszeń, M. (2017). Alpha-Ketoglutarate as a Molecule with Pleiotropic Activity: Well-Known and Novel Possibilities of Therapeutic Use. *Archivum Immunologiae et Therapiae Experimentalis*, *65*(1), 21–36.

Zhang, J., Li, G., Chen, Y., Fang, L., Guan, C., Bai, F., … Meng, Q. H. (2017). Metformin Inhibits Tumorigenesis and Tumor Growth of Breast Cancer Cells by Upregulating miR-200c but Downregulating AKT2 Expression. *Journal of Cancer*, *8*(10), 1849–1864.

Zhang, X., Zhu, X., Wang, C., Zhang, H., Cai, Z., Zhang, X., … Cai, Z. (2016). Non-targeted and targeted metabolomics approaches to diagnosing lung cancer and predicting patient prognosis. *Oncotarget*, *5*(0).

Zhao, E., Ding, J., Xia, Y., Liu, M., Ye, B., Choi, J.-H., … Thompson, C. B. (2016). KDM4C and ATF4 Cooperate in Transcriptional Control of Amino Acid Metabolism. *Cell Reports*, *14*(3), 506–19.

Zhao, Y. H., Zhou, M., Liu, H., Ding, Y., Khong, H. T., Yu, D., … Tan, M. (2009). Upregulation of lactate dehydrogenase A by ErbB2 through heat shock factor 1 promotes breast cancer cell glycolysis and growth. *Oncogene*, *28*(42), 3689–3701.

Appendix

Supplementary Table 1

MDA MB 468, MDA MB 231, MCF7 were grown under normal growth conditions in 10cm dishes in triplicates. Following day, media was changed and after 4h polar metabolites were extracted and quantified via GC-MS.

Please refer to the supplementary CD due to the length of the table.

Supplementary Table 2

MDA MB 468, MDA MB 231, MCF7 were grown under normal growth conditions in 6 well dishes in triplicates. After 48h RNA was harvested and mRNA expression was measured via microarray. Data was then normalized and differential gene analysis was performed by Khalid Abnaof.

Please refer to the supplementary CD due to the length of the table.

Supplementary Table 3

MDA MB 468, MDA MB 231, MCF7 were grown under normal growth conditions in 6 well plates in triplicates. Cell pellets were collected and lysates were harvested for mass spectrometry analysis after 48h. Harvesting of lysates, mass spectrometry, raw data extraction and initial analysis was done by Nadine Royla. Differential expression analysis and heatmaps were prepared by Khalid Abnaof.

Please refer to the supplementary CD due to the length of the table.

Supplementary Table 4

MDA MB 468, MDA MB 231, MCF7 were grown under normal growth conditions in 10cm dishes in triplicates. Spent media was collected after 48h and cell numbers were counted with CASY and used for normalization. Amino acids were derivatized, measured and initial analysis was done by Gernot Poschet.

Please refer to the supplementary CD due to the length of the table.

Abbreviations

α-KG	α-ketoglutarate
AKT	Serine/Threonine Kinase 1
AMPK	Adenosine monophosphate-activated kinase
ARG2	Arginase 2
ASCT2	Solute-linked carrier family A1 member 5 (SLC1A5)
ASS1	Argininosuccinate Synthase 1
ATF4	Activating transcription factor 4
ATP	Adenosine triphosphate
BAX	BCL2 Associated X, Apoptosis Regulator
BCA	Bicinchoninic acid protein assay
BCLA	β-chloro-L-alanine
BL	Basal-like
BRCA	Breast Cancer
CDK	Cycling dependent kinase
CEST	Chemical exchange saturation transfer
CO_2	Carbon dioxide
CRISPR	Clustered Regularly Interspaced Short Palindromic Repeat
cDNA	Complementary deoxyribonucleic acid
DNA	Deoxyribonucleic acid
DMSO	Dimethyl sulfoxide
ECM	Extracellular matrix
EDTA	Ethylenediaminetetraacetic acid
EGFR	Epidermal growth factor receptor
ER	Endoplasmic reticulum
ER+	Estrogen positive
ER-	Estrogen negative
ERBB2	Erb-B2 Receptor Tyrosine Kinase 2

ESR1	Estrogen Receptor 1
ETC	Electron transport chain
FBS	Fetal Bovine Serum
FCCP	Carbonyl cyanide-4 (trifluoromethoxy) phenylhydrazone
FDG	Fluorodeoxyglucose
FISH	Fluorescence in situ hybridisation
FGFR	Fibroblast growth factor receptor
FH	Fumarate hydratase
FOX	Forkhead Box
FSPG	(S)-4-(3-[18F]Fluoropropyl)-L-glutamic acid
GC-MS	Gas chromatography-mass spectrometry
GLS	Glutaminase
GLUL	Glutamate-ammonia ligase
GLUD	Glutamate dehydrogenase
GLUT	Glucose transporter
GOT	Glutamic-oxaloacetic transaminase
GPT	Glutamate pyruvate transaminase
GSH	Glutathione
HER2	Human Epidermal Growth Factor Receptor 2
HIF1α	Hypoxia inducible factor 1α
HK2	Hexokinase 2
HPLC	High pressure liquid chromatography
IDH	Isocitrate dehydrogenase
IM	Immunomodulatory
LAR	Luminal androgen receptor
LAT1	Solute Carrier Family 7 Member 5 (SL7A5)
LDH	Lactate dehydrogenase
LKB1	Serine/Threonine Kinase 11
KRAS	Kirsten Rat Sarcoma Viral Oncogene Homolog

M	Mesenchymal
MAPK	Mitogen-Activated Protein Kinase
MCT	Monocarboxylate transporters
MPER	Mammalian Protein Extraction Reagent
mRNA	Messenger ribonucleic acid
MRSI	Magnetic resonance spectroscopic imaging
MSL	Mesenchymal-like
mTOR	Mechanistic Target Of Rapamycin Kinase
NAD	Nicotinamide adenine dinucleotide
NADH	Nicotinamide adenine dinucleotide + hydrogen
NaF	Sodium Fluoride
NEAA	Non-essential amino acids
NTC	Non targeting control
OAA	Oxaloacetic acid
OCR	Oxygen consumption rate
OXPHOS	Oxidative phosphorylation
TP53	Tumor protein 53
PARP	Poly(ADP-Ribose) Polymerase
PBS	Phosphate buffered saline
PC	Pyruvate carboxylase
PD-1	Programmed cell death protein
PD-L	Programmed cell death protein ligand
PDH	Pyruvate dehydrogenase
PDK1	Pyruvate dehydrogenase kinase 1
PET	Positron emission tomography
PHGDH	Phosphoglycerate dehydrogenase
PI3K	Phosphatidylinositol-4,5-Bisphosphate 3-Kinase
PI3KCA	Phosphatidylinositol-4,5-Bisphosphate 3-Kinase Catalytic Subunit Alpha
PKM	Pyruvate Kinase, muscle

pRb	Retinoblastoma-associated protein
pRPS6	Phospho ribosomal protein S6
PTEN	Phosphatase and Tensin Homolog
PVDF	Polyvinylidene fluoride
PUM1	Pumilio RNA Binding Family Member 1
qRT-PCR	Quantitative reverse transcriptase polymerase chain reaction
RB1	Retinoblastoma Transcriptional Corepressor 1
RNA	Ribonucleic acid
RNAi	Ribonucleic acid interference
ROS	Reactive oxygen species
RPPA	Reverse phase protein array
RT	Room temperature
RTCA	Real time cell analyzer
SD	Standard deviation
SDHA	Succinate dehydrogenase A
SDS PAGE	Sodium dodecyl sulfate polyacrylamide gel electrophoresis
siRNA	Small interfering ribonucleic acid
TBST	Tris buffered saline with Tween 20
TCA cycle	Tricarboxylic acid (citric acid) cycle
TCGA	The cancer genome atlas
TEMED	Tetramethylethylenediamine
TNBC	Triple negative breast cancer
WST-1	Water-soluble tetrazolium salt 1
XBP1	X-Box Binding Protein 1
2-HG	2-hydroxyglutarate

Acknowledgements

It is good to have an end to journey toward, but it is the journey that matters in the end.

— Ursula K. Le Guin

This dissertation is a summation of work that would not have been possible without the contribution of all the people who accompanied me on this journey and I am deeply grateful for the opportunity to have worked and interacted with all of them. I would like to start by thanking my supervisor, Prof. Dr. Stefan Wiemann, for giving me the opportunity to work in the Division of Molecular Genome Analysis and for giving me the freedom to pursue my own ideas while being a constant source of support and motivation.

I would also like to thank my Thesis Advisory Committee members, Prof. Dr. Rüdiger Hell and Prof. Dr. Aurelio Teleman for guiding and advising me through my PhD even beyond the TAC meetings. I am thankful to Prof. Dr. Stefan Fringes for agreeing to chair my defense.

This project was a result of collaborations that extended beyond my lab. I would like to thank Dr. Gernot Poschet from the University of Heidelberg, who performed metabolic measurements, for always being so enthusiastic and helpful. I would also like to extend my gratitude to Dr. Stefan Kempa and Nadine Royla at the BIMSB, Berlin for kindly hosting me and helping me to perform labeling experiments and for all the discussions we had. I would like to thank Dr. Zita Soons and Dr. Rainer König for the initial analyses and meetings. I would also like to thank Stephan for the in-house collaborations with RPPA experiments and our “metabolism meetings” in the early days. I would like to thank Khalid for his help with the data analysis.

I would like to thank every member of the division of Molecular Genome Analysis for providing me with a vibrant and interactive environment during my PhD. I would especially like to thank Heike for contributing so enthusiastically to this project. I would also like to thank Cindy for always willing to help. I am grateful to Angelika, Ewald, Rita, Corinna, Daniela, Sara and Sabine, each of whom has helped me along the way. I would also like to thank Christian who interviewed me for this position and welcomed me so warmly to Heidelberg and to the group. I am deeply grateful to all the Post Docs, PhDs, masters and bachelors students, past and present, who made this experience fruitful and enjoyable, also beyond the confines of the work space. My time here was greatly enriched by our lunch and coffee sessions. Special mention to the expendables, without whom this journey

would have been a very different one. Alex, thank you for being a constant support from my first day in the division, for always finding cake in the kitchen for us to eat and for bearing with my English corrections, I hope we can have a long conversation in German eventually. Chiara, thank you for so enthusiastically organizing just about everything, for always patiently explaining things and for letting me hitchhike with you and Gideon whenever I needed it. Simone, “Jesus boy”, thank you for teaching me to make the perfect carbonara and for always agreeing to join me for dessert. I would like to thank my office mates, Nese, for being the voice of reason that I sometimes did not want to hear, for being my shopping companion and for all conversations we’ve had about anything and everything and Emre, my “CRISPR guru”, for helping me design my primers as well as my office wall with equal excitement and for his laughter. Thank you for making our office the most entertaining and fun place to be, despite your singing!

My time in DKFZ also gave me the opportunity to meet different people outside my lab. Being in the student council and in different student teams allowed me to get to know different administrative members as well as other Postdocs and PhDs from around campus. These interactions and experiences greatly enriched my time as a PhD student and taught me skills I will carry with me in the future. I would also like to thank Patrizia for being there to talk to and share each other’s experiences.

I would like to thank my friends all around the world for their moral support even from afar. I am especially grateful to Enakshi, who has always been a phone call away, thank you for your constant words of encouragement and for understanding me.

I am grateful to my family members who have been so supportive, my grandmother for her encouragement and my sister for always believing the best in me. I am grateful to my parents, without whom I could not have come this far, I thank them for encouraging me to always aim higher and for giving me unconditional love and support all through my life. I would like to thank, Adi, for patiently being by my side through this entire journey, for even taking an interest in molecular biology to understand what I talked about and for providing me with the love and strength that I needed during my PhD and beyond.

Thank you all for this wonderful experience!